CHEMICAL REVIEWS

Review

pubs.acs.org/CR

Modeling Polymorphic Molecular Crystals with Electronic Structure Theory

Gregory J. O. Beran*

Department of Chemistry, University of California, Riverside, California 92521, United States

ABSTRACT: Interest in molecular crystals has grown thanks to their relevance to pharmaceuticals, organic semiconductor materials, foods, and many other applications. Electronic structure methods have become an increasingly important tool for modeling molecular crystals and polymorphism. This article reviews electronic structure techniques used to model molecular crystals, including periodic density functional theory, periodic second-order Møller−Plesset perturbation theory, fragment-based electronic structure methods, and diffusion Monte Carlo. It also discusses the use of these models for predicting a variety of crystal properties that are relevant to the study of polymorphism, including lattice energies, structures, crystal structure prediction, polymorphism, phase diagrams, vibrational spectroscopies, and nuclear magnetic resonance spectroscopy. Finally, tools for analyzing crystal structures and intermolecular interactions are briefly discussed.

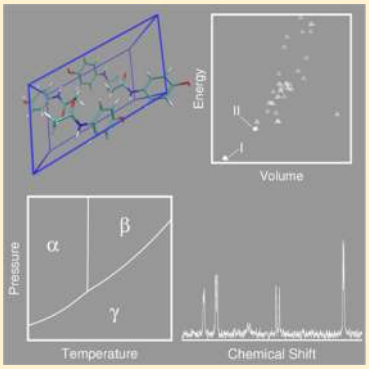

CONTENTS

Special Issue: Noncovalent Interactions

Received: November 2, 2015
Published: March 23, 2016

DOI: 10.1021/acs.chemrev.5b00648
Chem. Rev. 2016, 116, 5567−5613

1. INTRODUCTION

A given organic molecule can often adopt different crystal packing motifs, or polymorphs. It has been estimated that at least half of organic molecules exhibit polymorphism.[1] Many species exhibit multiple polymorphs: Flufenamic acid forms at least nine polymorphs.[2] The substance 5-methyl-2-[(2-nitrophenyl)amino]-3-thiophenecarbonitrile, also known has ROY, has seven well-characterized forms (and three others with unknown structures) that form brilliant red, orange, and yellow crystals.[3] Notably, all ten ROY polymorphs can be formed near ambient conditions. The explosive triacetone-triperoxide (TATP) has at least six polymorphs.[4] Indeed, McCrone quipped that "the number of forms known for each compound is proportional to the time and money spent in research on that compound."[5]

Including cocrystals, solvates, and salts can dramatically increase the number of crystal structures observed for a given compound. Gallic acid exhibits at least three anhydrate polymorphs, five monohydrates, and over 20 solvates.[6] Even a small molecule can exhibit a surprising diversity of distinct crystal structures, particularly if one moves beyond ambient conditions and examines the high-pressure region of the phase diagram. The 15th phase of ice was discovered in 2009,[7] and a dozen phases of nitrogen have been suggested.[8]

The crystal packing of an organic molecule can have a significant impact on its properties. In the pharmaceutical industry, different polymorphs can exhibit substantially different solubilities and therefore bioavailabilities. Widely used drugs such as aspirin, acetaminophen, Lipitor (cholesterol reduction), Plavix (blood thinner), and Zantac (heartburn) are all known to be polymorphic. The surprise appearance of a stable, insoluble polymorph can force the temporary removal of a drug from the market. The most famous case of this is the drug ritonavir, whose year-long absence from the market denied HIV patients a much-needed treatment and cost its maker an estimated $250 million in lost sales.[9,10] Other drugs with polymorphism-related recalls include the antiseizure drug carbamazepine[11] and the Parkinson's disease rotigotine.[12] Individual polymorphs can be patented, creating a host of intellectual property and legal issues.[13] Polymorphism also factors in organic semiconductor materials, foods, and explosives.

The energy differences between polymorphs are typically small. A recent survey[14] of 508 polymorphic species (and 1061 crystals) found that over half of all polymorph pairs were separated by less than 2 kJ/mol in lattice energy, and only 5% of cases exceeded 7.2 kJ/mol. This makes reliable polymorph prediction challenging. Tremendous progress in polymorph prediction has been made using high-quality multipolar force field descriptions of intermolecular interactions, sometimes with a quantum mechanical (QM) description of the intramolecular interactions.[15,16] Indeed, such models have led to many successful predictions, as exemplified in some of the more recent blind tests of crystal structure prediction.[17−21]

Over the past decade or two, however, electronic structure methods have demonstrated a powerful ability to handle the subtle balances between intra- and intermolecular interactions and among the various types of intermolecular interactions (e.g., electrostatics, polarization, hydrogen bonding, and van der Waals dispersion) that occur in molecular crystals, all of which can be challenging to model reliably in force field approaches. As will be discussed later, dispersion-corrected density functional theory (DFT) methods have had an incredible success rate in crystal structure prediction and many other problems surrounding polymorphic molecular crystals. At the same time, periodic second-order Møller−Plesset perturbation theory (MP2) and even diffusion Monte Carlo (DMC) can now be applied to molecular crystal problems. There has also been a flurry of development in fragment-based electronic structure methods which greatly expand the reach of correlated wave function methods like MP2, coupled cluster methods, and symmetry adapted perturbation theory (SAPT) into pharmaceutical and other chemically relevant molecular crystals. This wide variety of tools increasingly allows one to address theoretically challenging questions in organic materials with high accuracy.

This review is divided into two main parts. Section 2 describes electronic structure methods which are regularly used in molecular crystal modeling. It highlights the current state-of-the-art for predicting noncovalent interactions and discusses some of the practical factors that should be considered when using such methods.

Section 3 then reviews a range of crystal properties related to crystal polymorphism that one can predict with electronic structure theory. These include not only basic structure optimizations and lattice energy calculations, but also ab initio crystal structure prediction and the prediction of meaningful polymorphic energy differences. Given a set of known and/or predicted polymorphs, the next step is to construct a phase diagram that maps out the most stable polymorphs as a function of temperature and pressure.

In addition, both vibrational (infrared, Raman, terahertz, and inelastic neutron scattering) and nuclear magnetic resonance (NMR) spectroscopies provide powerful tools for characterizing crystal structures. Predicting these spectroscopic properties is often critical to interpreting them. Finally, a handful of analysis tools used to interpret crystal structure and intermolecular interactions are discussed.

Many other interesting problems in molecular crystals are not covered here. For example, solid-state chemical reactions driven by light, heat, or mechanical forces can occur with extremely high efficiency and selectivity thanks to the fixed arrangements of the molecules in the crystal lattice. Theoretical modeling of such reactions is in its infancy compared to the modeling of reactions in the gas or solution phases. Nor does this review address the broad range of work involving organic semiconductor materials, band gaps, excited states, or the mechanical properties of crystals. Of course, many of the electronic structure modeling techniques and lessons learned here are equally relevant to those problems. Finally, given the emphasis on electronic structure methods here, force field techniques are largely omitted from discussion here. Other reviews in the literature highlight developments in some of these areas.[15,16,22]

2. THEORETICAL MODELS

Electronic structure methods for predicting molecular crystal energetics and optimizing structures have progressed tremendously over the past decade. Advances in three key areas are largely responsible for these improvements: (1) the development of density functional models that include van der Waals dispersion, (2) significant progress in periodic MP2 algorithms, and (3) fragment-based electronic structure methods that dramatically reduce the costs of performing correlated electronic structure calculations in large systems such as

DOI: 10.1021/acs.chemrev.5b00648
Chem. Rev. 2016, 116, 5567−5613

molecular crystals. The following sections describe each of these advances in turn.

2.1. Periodic Density Functional Theory

Van der Waals dispersion interactions arise from correlated fluctuations among different regions of electron density, and they contribute substantially to the stability of densely packed organic molecular crystals. In principle, density functional theory with the exact density functional would describe such interactions readily. However, as noted many years ago,[23] widely used semilocal density functional approximations cannot describe these inherently nonlocal interactions. Much effort has gone into the development of dispersion-including DFT models in recent years. These fall into two major categories: nonlocal functionals that inherently include van der Waals dispersion, and posthoc corrections.

Nonlocal density functionals include the van der Waals density functionals vdW-DF1[24−26] and vdW-DF2[27] of Langreth and co-workers, the related functionals developed by Vydrov and Van Voorhis,[28,29] and many others (see review in ref 30). Unlike typical posthoc dispersion correction schemes, nonlocal density functionals include van der Waals interactions self-consistently in the density. On the other hand, nonlocal van der Waals density functionals are typically more computationally demanding than traditional semilocal density functionals.

Nonlocal functionals perform well for noncovalent interactions in dimer benchmark tests[31−33] In molecular crystals, current evidence suggests that structures obtained with vdW-DF2 are quite good, for instance, but that lattice energies may be less reliable.[34,35] See sections 3.1 and 3.2 for more details. Other molecular crystal applications include ices,[36,37] benzene,[38] aspirin,[38] fullerenes,[39] hexamine,[39] and energetic materials.

Nonlocal density functionals continue to be improved, of course, and newer ones may perform better. The LC-VV10 functional,[29] which uses the long-range corrected hybrid ωPBE exchange functional and the VV10 correlation functional, reduces the mean absolute error for the binding energies in the S66 test set[40,41] from 2.0 kJ/mol for vdW-DF2 to 0.6 kJ/mol, for instance.[32] Another study found that VV10-type functionals performed on par with the popular DFT-D3 method (discussed below).[31]

Posthoc dispersion corrections range from relatively simple empirical force field-like schemes such as Grimme's earliest DFT-D1[42] and DFT-D2 models,[43] to more elaborate approaches in which the dispersion coefficients depend on the chemical environment.[44−49] Refitting empirical dispersion parameters for solid state applications was common in first-generation corrections,[50−53] but this is becoming less necessary as the dispersion models improve in their ability to reflect the specific chemical environment of an atom in a particular molecule.

State-of-the-art dispersion corrections with minimal empirical fitting include DFT-D3,[44,45] the Tkatchenko-Scheffler (TS) correction,[46] the many-body dispersion model (MBD),[47−49] and the exchange-dipole moment (XDM) model.[54−57] The performance of different dispersion corrections has been reviewed extensively elsewhere.[30,58−63] At present, there is no broad consensus that any one of the recent models (D3, MBD, or XDM) performs notably better than the others.

The D3 correction is clearly superior to D1 and D2, and it has demonstrated excellent performance in a variety of small-molecule[31,64−68] and supramolecular benchmarks.[33,69,70] It also behaves well in molecular crystals,[71−73] and a version has even been applied to density functional tight binding (DFTB).[74]

Similarly good results are found using the MBD correction.[61,62] Many studies have demonstrated the importance of going beyond the pairwise TS model to include many-body effects.[61,62,75−82] Tkatchenko and co-workers have shown that the MBD model works "seamlessly" across many different system sizes,[81] from small molecule noncovalent interactions to supramolecular systems,[75,76] materials,[78,83−85] and molecular crystals.[77,79,80,82]

Benchmarks of the XDM model also demonstrate good performance across a variety of small[67,86−88] and large systems.[89] In the supramolecular S12L set,[33] XDM outperformed (5.0 kJ/mol mean absolute error) all other dispersion corrections, including PBE-D3 (9.6 kJ/mol) and PBE-MBD (7.5 kJ/mol).[89] It has also been used in crystal benchmarks[34,57] and to predict the enantiomeric excess in chiral crystals.[90]

Many other dispersion-including models exist, such as the popular ωB97X-D functional,[91] periodic double-hybrid density functionals,[92] density-dependent dispersion corrections,[93] and dispersion-corrected atom-centered pseudopotentials.[94−96]

2.1.1. Many-Body Dispersion. The importance of many-body dispersion has been the subject of some debate. As noted above, Tkatchenko, DiStasio, and co-workers have provided numerous examples where their MBD model, which includes self-consistently screened many-body dispersion interactions, performs substantially better than the pairwise only TS correction.[61,62,75−82] On the other hand, inclusion of the Axilrod−Teller−Muto (ATM) three-body intermolecular dispersion contribution[97,98] in models like D3,[44] XDM,[99] and others[100] produces variable results. Sometimes the ATM contributions improve the quality of the predictions, but not always.[69,72,100−102]

Some of this apparent disagreement actually arises from differences in the definition of many-body dispersion. The MBD model defines the three-body and higher terms in terms of triplets of atoms, whereas some other authors refer to many-body interactions as involving three or more distinct molecules. Both definitions are useful, but they describe somewhat different phenomena. Much of the important correlation energy captured by a model like MBD actually corresponds to, for example, density fluctuations involving a pair of atoms in one molecule and a third atom in a neighboring molecule. In the molecular definition, those contributions would be called a pairwise interaction rather than a many-body one.

Recent benchmark CCSD(T) and DFT calculations[102] on many-body intermolecular interactions shed some light on the seemingly ambiguous performance of ATM type dispersion corrections. The benchmarks consisted of three-body intermolecular interactions for 69 trimers extracted from molecular crystals (the 3B-69 test set), and they showed that a broad range of density functionals performed poorly compared to wave function methods, often providing three-body energies which were no better than Hartree−Fock (HF). More significantly, the errors observed with DFT seemed to stem mostly from delocalization/self-interaction error[88,102,103] and problems with the many-body contributions in widely used exchange functionals.[104] Hybrid functionals like BHLYP and PBE0 exhibit less delocalization error and perform better. Interestingly, problems with a given exchange functional often appear to exhibit opposite signs in the two- and three-body

DOI: 10.1021/acs.chemrev.5b00648
Chem. Rev. 2016, 116, 5567−5613

terms, which leads to fortuitous error cancellation in the full system calculation.[104]

A second potential issue with the inclusion of many-body dispersion involves the turning off the interactions at short-range. In the MBD model, this is handled via range-separation between the semilocal density functional at short-range and the MBD model at long-range.[49] In ATM-type dispersion correction models, an empirical damping function is typically used.

Unfortunately, considerable ambiguity surrounds the proper form of the ATM damping function[99] and attempts to fit the damping function parameters are hindered by the fact that the dispersion contribution is conflated with the delocalization and exchange errors noted above. In the 3B-69 benchmark set, adding an ATM term improves B3LYP, but any nonzero ATM correction actually makes PBE0 worse, which is clearly unphysical.[102] Accordingly, simple empirical fitting of the ATM damping function on a training set is unlikely to provide physically meaningful results. Research in these areas is ongoing.

2.2. Periodic MP2

MP2 for periodic systems was first developed several decades ago for polymers and other one-dimensional systems.[105−107] Development in 1-D models continues with logarithmic-scaling down-sampling of the k vectors in reciprocal space,[108] Monte Carlo evaluation of the MP2 energy expression,[109] and other advances.[110,111]

More pertinent to molecular crystals, however, have been the recent advances in efficient methods for periodic MP2 in three dimensions. The combination of these lower-cost algorithms and modern computer hardware improvements makes periodic MP2 an increasingly viable tool for studying molecular crystals. Note too that many of the periodic MP2 algorithms described below can also be utilized in double-hybrid density functionals[92,112] and in methods based on the random phase approximation (RPA).[113,114]

The era of efficient 3-D periodic MP2 algorithms began when the Scuseria group implemented atomic orbital-based algorithms using Laplace transform techniques, which they have demonstrated on polymers.[115−117] Subsequently, the CRYSCOR group implemented a density-fitted local MP2 algorithm[118−122] that employs a direct space approach and a Pulay/Werner-style local correlation scheme based on projected atomic orbital domains. This implementation was the first to demonstrate the general feasibility of periodic MP2 in chemically interesting molecular crystals. The parallel version scales to dozens of processor cores, and calculations have been reported for unit cells containing more than 100 atoms.

The developers of periodic local MP2 have demonstrated its performance on a variety of small-molecule crystals, including carbon dioxide,[123] ammonia,[123] acetylene,[124] hydrogen cyanide,[124] formic acid,[124] and ice XI.[124] They have explored the high-pressure phases of nitrogen,[125] the Compton profiles of urea,[126] and the polymorphic energetics of oxalyl dihydrazide.[127]

Several studies explore the basis set convergence of periodic MP2 in systems like lithium hydride,[128,129] ammonia,[123] and carbon dioxide.[123] Others examine the performance of spin-component-scaled MP2 algorithms (see section 2.5.1)[123,124] for lattice energies or benchmark DFT lattice energies against MP2 results.[130] For solid argon, periodic local MP2 compares very well with the incremental approach (see section 2.4.2) using MP2.[131] One can also use periodic local MP2 as the base level for subsequent incremental corrections to achieve very high accuracy.[132]

Very recently, a new variant of the LMP2 algorithm has been developed which replaces the projected atomic orbitals with orbital specific virtuals (OSVs).[133] The OSV approximation eliminates the need to carefully choose domains, largely removes any discontinuities from the potential energy surface, and decreases the computational cost.

A few other periodic MP2 algorithms have been developed in recent years. Kresse and co-workers[134,135] implemented a plane wave periodic MP2 approach using the projector augmented wave approach which has been tested on bulk and rare gas solids such as Ne, Ar, C, Si, SiC, MgO, BN, AlN, LiH, and others. Using MP2 natural orbitals obtained from a plane wave calculation, one can even compute periodic CCSD(T),[136] as has been done for the high-pressure phase transition in LiH, for instance.[137] Katouda and Nagase[138] implemented canonical MP2 using the resolution of the identity approximation. Scheffler and co-workers[113,139] have developed efficient periodic MP2 and RPA algorithms based on the resolution of the identity approximation and numerical atomic orbitals.

Most recently, Del Ben and co-workers[112,114] developed the massively parallel Gaussian and plane wave MP2 (GPW-MP2) model. GPW-MP2 uses an auxiliary basis set of plane waves to represent the pair density when evaluating the two-electron integrals. Analytical gradients of GPW-MP2 have also been demonstrated recently.[140] The algorithm scales up to a hundred thousand processors with 80% parallel efficiency, allowing it to be applied to systems with hundreds of atoms. The current implementation of GPW-MP2 calculations are Γ point only, which means that supercells are typically required for molecular crystal calculations, and it requires pseudopotentials to provide the smooth densities needed for the plane wave representation.

GPW-MP2 has been used to predict lattice constants and lattice energies in crystals such as urea, formic acid, benzene, pyromellitic dianhydride, succinic anhydride, and cyclotrimethylene-trinitramine.[112,114,140] Another GPW-MP2 study explored the proton ordering in ice XV.[37] RPA methods have also been applied to ices[37,141] and a few other crystals.[114]

Large basis sets can present a challenge for periodic MP2. First, the HF self-consistent field equations are sometimes difficult to converge in large Gaussian basis sets due to quasi linear-dependencies in the atomic orbitals that arise in densely packed crystalline systems. This difficulty can often be addressed through well-designed algorithms and careful numerical treatments.[142,143] Alternatively, dual-basis schemes, in which a smaller basis set is used for the HF portion of the calculation, while a larger basis set is used for the LMP2 calculation, are sometimes employed.[128]

Second, MP2 exhibits steep computational scaling with respect to the number of basis functions. Using large basis sets dramatically increases the computational cost of the calculations. Explicitly correlated periodic MP2 methods,[110,129,144] which allow one to achieve well-converged results using only modest (e.g., double- or triple-ζ) basis sets, are becoming increasingly available. See section 2.6 for additional discussion of explicitly correlated methods.

Finally, MP2 suffers from its own problems in treating van der Waals dispersion. These can be corrected via spin-component scaling (section 2.5.1), an MP2C-style correction (section 2.5.1), or through an incremental-style method (section 2.4.2) in which periodic MP2 serves as the base-level

DOI: 10.1021/acs.chemrev.5b00648
Chem. Rev. 2016, 116, 5567−5613

upon which refinements for pairwise interactions using coupled cluster or other high-quality calculations are performed.

2.3. Diffusion Monte Carlo

Diffusion Monte Carlo algorithms have made substantial advances in recent years, and they are now increasingly applied to large and condensed phase systems for benchmarking purposes. For example, DMC has been used to obtain reliable energetics for supramolecular interactions, which can then be used to assess a variety of electronic structure models for describing noncovalent interactions.[75,76,145−148]

DMC has also been applied directly to some molecular crystals. For instance, DMC has been used to compare the lattice energies of ice Ih, II, VIII, and XV[146,149] with dispersion-corrected DFT[77,149] and an embedded many-body expansion model.[150] Another study explored the viability of two potential new ice phases, ice 0 and ice i with DFT and performed DMC calculations to validate the DFT energetics for these unusual phases.[151] Methane clathrates, which involve cages of water molecules encapsulating methane molecules, have also been the subject of DMC studies, both using model cages[148] and in the full crystal.[152] MP2 predicts the energetics of the methane-water interactions and the binding energy of the cage well thanks to cancellation of errors in the 2-body and 3-body terms,[153] while several common dispersion corrected DFT models exhibit somewhat larger discrepancies.[148,152]

Another set of studies have examined the high-pressure phases of hydrogen, particularly phase IV which occurs at several hundred GPa of pressure. While this phase appears to be insulating in experiments, several DFT studies predicted a metallic phase. However, the combination of DMC calculations and the treatment of nuclear quantum effects predicts a structure in much better agreement with the experiments.[154,155]

In what are probably the largest DMC molecular crystal calculations to date, the energy difference between the two polymorphs of diiodobenzene has been computed with DMC.[156,157] This study revealed that DFT predicts an incorrect stability ordering in the absence of a dispersion correction. Adding a dispersion correction[158,159] or using an incremental scheme to correct the 1- and 2-body terms[160] (section 2.4.2) allows one to obtain the correct stability ordering (section 3.4.3).

While DMC energy benchmarks have proved helpful in the examples mentioned above, DMC calculations on molecular crystals continue to be hindered by finite size effects and the dependency of polymorph energies on the choice of the trial nodal surface. A recent paper on diiodobenzene examined a number of these issues in detail.[157] They found that a $1 \times 1 \times 1$ simulation cell calculation using fixed nodes obtained from LDA gives the correct energy ordering, while using PBE to define the nodal surface reverses the ordering. However, if a larger $1 \times 3 \times 3$ simulation cell is employed, DMC calculations using either the LDA or PBE nodal surfaces correctly predict the α polymorph to be more stable. Unfortunately, single-point energy calculations in the larger simulation cell required 640 000 supercomputer processor hours per polymorph.

Changes in the treatment of finite size effects, particularly for the kinetic energy, also had a large impact on the diiodobenzene polymorphic energy difference. The best current refinement suggests that the α form is preferred by 8.6 ± 5.3 kJ/mol.[157] However, tighter convergence in the statistical error bars would be needed to discriminate among closely separated polymorphs in other crystals, and further technical advances will be required before DMC calculations on molecular crystals become routine.

Finally, the full configuration interaction quantum Monte Carlo (FCIQMC) method has recently been demonstrated for simple solids, including rare gases and LiH.[161] Such calculations provide another powerful means for benchmarking electronic structure methods in periodic systems.

2.4. Fragment Methods

Fragment-based electronic structure methods have exploded in popularity over the past decade. These methods decompose a calculation on a large system into many smaller subsystem ("fragment") calculations, whose results are then pieced together to obtain the energy or other property for the full system. Many schemes have been developed for defining how the fragments should be formed (overlapping versus non-overlapping fragments, for instance) and how to account for the interactions among fragments while avoiding any possible double-counting. However, most existing models can be viewed within a unified framework,[162,163] and several reviews have been written on the subject,[164−166] including one focused on molecular crystals.[167]

For molecular crystals, typical fragmentation schemes treat each individual molecule as a distinct, nonoverlapping fragment. Interactions between the fragments are then handled via a many-body expansion such that the total energy E of the system is expressed in terms of 1-body, 2-body, 3-body, and higher-order terms

$$E = \sum_i E_i + \sum_{i>j} \Delta^2 E_{ij} + \sum_{i>j>k} \Delta^3 E_{ijk} + \cdots \quad (1)$$

The first term on the right-hand side sums over the energy E_i of each molecule in the central unit cell. The second term sums over 2-body interaction energies for each pair of molecules i and j

$$\Delta^2 E_{ij} = E_{ij} - E_i - E_j \quad (2)$$

The third term sums over the nonadditive 3-body contributions involving molecules i, j, and k

$$\Delta^3 E_{ijk} = E_{ijk} - \Delta^2 E_{ij} - \Delta^2 E_{ik} - \Delta^2 E_{jk} - E_i - E_j - E_k \quad (3)$$

Note that the 2-body and higher terms all involve contributions between molecules in the central unit cell and periodic image molecules.

One- and two-body terms are obviously important. The former capture differences in the molecular geometry/conformation between the gas and crystalline phases or across different crystal polymorphs (conformational polymorphism). The pairwise interactions often account for 80−90% of the lattice energy.[168] The primary differentiation among different fragment methods comes from how they handle the many-body (three-body and higher) terms.

The simplest possibility is to sum the many-body expansion until it converges. Indeed, this strategy has been used successfully in calculations of the benzene crystal lattice energy (section 3.1.1), including the recent sub-kJ/mol accuracy prediction of Yang et al.[169] In that case, summing up through four-body contributions (tetramers) proved sufficient to converge the lattice energy.

More generally, however, the many-body expansion will not necessarily converge so rapidly, as is the case for crystals exhibiting strong hydrogen-bonding cooperativity. In such

DOI: 10.1021/acs.chemrev.5b00648
Chem. Rev. 2016, 116, 5567−5613

cases, explicit summation of the many-body expansion to higher orders has a number of pitfalls. First, the number of n-body contributions grows combinatorially with n (though distance-based screening can reduce the scaling). Second, the cost of evaluating an n-body fragment also grows rapidly with n. MP2 scales $O(N^5)$ with the number of basis functions N in the n-body fragment, for example. Third, the magnitude of each individual n-body energy contribution shrinks, which can lead to numerical precision difficulties.[170] Fourth, basis set superposition errors (BSSE) can become particularly problematic in the higher-order terms of the many-body expansion.[171,172]

Instead, one can either truncate the expansion and neglect the higher-order terms, or one can approximately sum the higher-order terms through all orders using a lower level of theory. In the former case, one typically truncates terms beyond 2-body and employs embedding to incorporate aspects of the missing many-body effects into the lower-order terms. In the latter case, the higher order terms are summed implicitly by performing a full periodic calculation on the system and subtracting out the 1- and 2-body terms which will be replaced with calculations from a higher-quality electronic structure method.

Not all models rely on the many-body expansion, however. The hierarchical method,[173−175] for instance, performs a series of calculations to investigate how the energy changes as a cluster of atoms/molecules grows and relates those changes to the contributions from bulk and surface atoms. While accurate, broader use of the hierarchical method has been hindered by its requirement for large cluster calculations that are generally more computationally demanding than those required in other fragment methods.

The next sections describe several fragment-based methods that have been developed for molecular crystal problems in detail.

2.4.1. Binary Interaction and Other Embedding Methods. The binary interaction method of Hirata and co-workers was first developed for molecular systems[176,177] and was subsequently extended to periodic crystalline systems.[178] Binary interaction includes 1-body and 2-body terms only, neglecting all higher-order contributions in the many-body expansion. Each monomer and dimer calculation is electrostatically embedded in a series of point charges (at shorter distances) and unit cell dipoles (at longer ranges). The electrostatic embedding incorporates long-range pairwise electrostatics/polarization and many-body polarization effects. This model can be viewed as a simple approximation to the fragment molecular orbital (FMO) model[179−181] in which the embedding densities are approximated using point charges/dipoles. The ternary interaction variant of the model augments binary interaction to include explicit three-body terms,[176,177] but this increases the computational cost substantially and has not been used in many practical crystalline applications.

The atomic point charges which define the embedding potential are determined self-consistently for each monomer in the unit cell based on Hartree−Fock and Momany's[182] atomic charge calculation scheme. Initial atomic charges are calculated for each isolated monomer and used to construct the embedding potential. Each monomer calculation is then repeated in the embedding potential constructed from these charges, which provides a new set of atomic charges. The process is repeated until self-consistency is achieved. The longer-range electrostatic embedding potential is modeled via computed unit cell dipole moments, which are similarly optimized to self-consistency.

Binary interaction has been extended to the calculation of energies, analytical gradients and Hessians,[178] normal mode phonon analysis,[183] and the exploitation of space group symmetry.[183] It has been successfully applied to a number of problems involving energies, vibrational spectroscopy, high-phase transitions, and other properties in crystals such as ice,[184] carbon dioxide,[185−189] formic acid,[178] hydrogen fluoride,[190,191] and even liquid water.[192] Many of these applications are discussed in a recent review article[193] and in sections 3.5 and 3.6 below.

Other embedding methods also exist. For example, the embedded many-body expansion of Bygrave, Allan, and Manby[194] goes beyond electrostatic embedding to include exchange-repulsion contributions in the embedding potential. This model has been shown to predict energies and structures in good agreement with experiment for crystals like carbon dioxide,[194] ices,[194,195] clathrate hydrates,[153] and hydrogen fluoride,[194] with low computational cost. Hartman et al.[196−198] have used an embedded 1- and 2-body model to compute NMR chemical shifts accurately (section 3.7). Very recently, Fang and co-workers[199] have adapted the generalized energy-based fragmentation (GEBF) scheme to periodic systems via electrostatic embedding. Embedding continues to be an active area of research,[200−205] and it is likely that significant advances in embedding methods for molecular crystal problems will be made in the near future.

2.4.2. Incremental Methods. Whereas the methods described in the previous section truncate the many-body expansion, incremental methods[206−209] retain all many-body terms but approximate the higher-order terms using a lower level of theory. The higher-order many-body terms are summed implicitly by performing an energy calculation on the entire system and subsequently replacing the energies of the low-order terms in the expansion with values computed using a higher level of theory. For example, to treat the 1- and 2-body terms at a high level and approximate the remaining terms at a low level, one would compute the energy as,

$$E^{\text{high}} \approx E^{\text{low}} + \sum_i (E_i^{\text{high}} - E_i^{\text{low}}) + \sum_{i>j} (\Delta^2 E_{ij}^{\text{high}} - \Delta^2 E_{ij}^{\text{low}}) \quad (4)$$

where E^{low} and E^{high} refer to the energy of the entire system at the low and high levels of theory, respectively. Note that this approach is similar to multilayer ONIOM schemes[210,211] used in nonperiodic systems, particularly ones that have been designed for treating multiple centers.[212,213] Dahlke and Truhlar's fragment model that combines electrostatically embedded 1- and 2-body terms with a many-body HF calculation is essentially an incremental method as well.[214]

The additive form of eq 4 makes analytical differentiation straightforward, and there are typically no contributions from embedding potentials to complicate the derivatives. This means that properties such as crystal structures (section 3.2), phonons (section 3.6), and chemical shifts (section 3.7) can be computed with minimal modifications to existing electronic structure codes.

Most applications of incremental methods have been to bulk solids and inorganic materials,[209,215] but there have been a number of demonstrations that these models can work well for

DOI: 10.1021/acs.chemrev.5b00648
Chem. Rev. 2016, 116, 5567−5613

molecular crystals as well. Traditionally, HF is used as the low level of theory, while the increments are treated with some correlated level of theory. For molecular crystals, the correlation energy included via the increments converges rapidly—only 2-body and perhaps 3-body increments are generally needed. This basic approach has been used to obtain accurate lattice energies for rare gas crystals[216,217] and ice Ih,[218] for instance.

Of course, one can also use a better model than HF for the low level. A number of researchers have used the incremental approach to improve upon DFT. This offers the advantage that the many-body terms are treated using a model that includes electron−electron correlation, unlike HF. This has been applied to the lattice energies of benzene,[219] urea,[220] and hexamine.[220] It also performs well for predicting the energy differences between the two polymorphs of diiodobenzene.[160] Another interesting variant uses machine learning to correct the 1- and 2-body terms in DFT.[221]

However, there is evidence that DFT does not always predict many-body contributions accurately. Standard functionals omit many-body dispersion, but this can potentially be restored by the Axilrod−Teller term in the D3 dispersion correction or the MBD model (see section 2.1). Beyond dispersion, however, widely used density functionals exhibit problems with many-body polarization (via delocalization or self-interaction error)[102] and exchange.[104] In a normal DFT calculation on the entire supersystem, some of the many-body errors seems to cancel with the systematic errors in the 1- and 2-body terms. In contrast, incremental schemes that combine DFT and correlated wave function methods do not benefit from such cancellation.

The advent of efficient periodic MP2 algorithms means that one can now use MP2 for the low level of theory and correct to near coupled cluster quality using only small, relatively affordable coupled cluster calculations (e.g., local coupled cluster models) for the increments.[132] Because MP2 captures a sizable fraction of the correlation energy, this can offer substantial advantages over HF-based incremental methods. MP2 provides a reasonable approximation for the many-body polarization and exchange effects found in coupled cluster models, for instance, though care is needed when many-body dispersion becomes significant.[102,222]

2.4.3. Hybrid Many-Body Interaction. Instead of using electronic structure methods for the many-body terms as in the incremental approach, one can use a force field. The hybrid many-body interaction (HMBI) model[168,223−225] combines 1-body and short-range 2-body QM contributions with long-range and many-body MM terms evaluated using a polarizable force field:

$$E^{\mathrm{HMBI}} \approx E^{\mathrm{MM}} + \sum_i (E_i^{\mathrm{QM}} - E_i^{\mathrm{MM}}) + \sum_{i>j} d_{ij}(\Delta^2 E_{ij}^{\mathrm{QM}} - \Delta^2 E_{ij}^{\mathrm{MM}}) \quad (5)$$

where d_{ij} is a damping function that heads toward zero as the intermolecular separation increases, thereby transitioning from QM to MM treatment of the pairwise interactions at longer ranges.

Polarizable force fields are needed to capture the many-body effects which are omitted in the simple pairwise-additive electrostatics models used in traditional force fields. The force field can also include other terms, such as exchange[226] or many-body dispersion[168] terms. One can use existing force fields,[223] such as Amoeba,[227−229] or the force field parameters can be calculated on the fly.[168,226,230] Electrostatics can be particularly sensitive to the specific molecular geometries,[230] and on-the-fly force field generation allows one to achieve higher accuracy than fixed parameter force fields.[168]

The HMBI model has been implemented for the calculation of nuclear gradients and Hessians[231] with full exploitation of space group symmetry.[232] It has been tested for lattice energies,[168,224] and structure optimizations.[231] It has been combined with the quasiharmonic approximation to predict finite temperature structures, thermochemistry, and mechanical properties in carbon dioxide[233] and other small molecule crystals.[234] HMBI has also been used to study molecular crystal polymorphism in aspirin,[235] oxalyl dihydrazide,[236] and ice XV.[237]

2.4.4. Summary. In the end, all of the aforementioned fragment methods have proved successful for modeling molecular crystals. There is no clear consensus that any particular fragment approach is superior to the others, though they each have their advantages. For instance, charge-embedding schemes are extremely easy to implement for energy calculations, and they perform very well. On the other hand, extra care must be taken in the energy gradients and Hessians, since the contribution to a single gradient or Hessian element now depends on the positions of all other atoms through the embedding potential.[178] In addition, polarization effects are not the only important many-body effects. One might also incorporate many-body exchange and dispersion effects in embedding models, though this is not widely done at present.

Incremental methods and the hybrid many-body interaction model can potentially capture the broad range of many-body interactions and exhibit gradients that are formally simpler. On the other hand, performing a periodic HF, DFT, or MP2 calculation on the entire system in an incremental model adds to the computational expense. In the case of HMBI, the accuracy depends on obtaining a good-quality polarizable force field to describe the many-body terms.

It is interesting to observe that several different fragment approximations described above have proved successful in molecular crystals. Indeed, a study by Pruitt et al.[238] demonstrated that two different fragment methods (the FMO and systematic molecular fragmentation by annihilation models) perform similarly for water clusters, despite differences such as the treatment of embedding/many-body effects. Such results speak to the general validity of fragment approaches for these types of systems.

2.5. Appropriate Electronic Structure Models for Fragment Methods

Most of the fragment-based methods described above allow the user to choose an appropriate electronic structure method for use in evaluating the individual fragment contributions to the energy (or other property). In practice, this choice is governed by the computational requirements of the method and the desired accuracy. The steep computational scaling of methods like MP2 ($O(N^5)$ with system size N) or CCSD(T) ($O(N^7)$) is well-known. Fragment methods usually require expensive QM calculations only on monomers and dimers, but dimer calculations on pharmaceuticals or organic semiconductor species can still be computationally demanding.

DOI: 10.1021/acs.chemrev.5b00648
Chem. Rev. 2016, 116, 5567−5613

In practical crystal structure prediction or polymorphism applications, one seeks to assess the relative stability of two competing crystal structures. The energy differences between the structures are usually less than 10 kJ/mol, and they are often closer to ∼1−2 kJ/mol.[14] Achieving such high accuracy represents a stiff challenge for electronic structure methods. So-called chemical accuracy of 1 kcal/mol (4 kJ/mol) is the "gold standard" for predicting chemical reaction energetics, and obtaining kJ/mol accuracy for a property like molecular atomization energy is feasible only for the smallest molecules.[239] Fortunately, noncovalent interactions are much weaker than the energies associated with breaking and forming covalent chemical bonds. In this context, kJ/mol accuracy is merely challenging to obtain, rather than nearly impossible.

Though the net energy differences between crystal structures are often small, the relevant individual energy contributions are often much larger. For example, conformational polymorphism, where different intramolecular conformations of a flexible molecule adopt different intermolecular packing, occurs in many polymorphic crystals. In such cases, molecules often achieve more favorable intermolecular packing by adopting a strained intramolecular conformation. Even an unfavorable 20 kJ/mol intramolecular distortion of a molecule can sometimes produce a crystal structure that is more stable overall.[240]

For these reasons, one must treat both intra- and intermolecular interactions accurately.[16] Neither the systematic overestimation of van der Waals dispersion in MP2 nor the omission of dispersion in traditional semilocal DFT functionals (without dispersion corrections) is conducive to achieving a balanced descriptions of the various interactions, for instance. Given the small net energy differences that result from these balances, obtaining chemically meaningful predictions also requires ensuring that the predictions are well-converged with respect to the electronic structure method/basis set. BSSE can be particularly problematic (section 2.6).

The next several sections discuss the advantages and disadvantages of various wave function-based electronic structure methods. Note that for most purposes, the use of standard DFT to describe 1- and 2-body terms is not recommended. As noted in section 2.1, individual *n*-body contributions obtained from conventional DFT models often behave somewhat worse than the whole. Fully periodic DFT models often provide more accurate results than their fragmented counterparts. On the other hand, fragment-based NMR chemical shift calculations represent a case where fragmenting DFT can work well (section 3.7.2).

2.5.1. MP2 and Related Methods. After DFT, MP2-based methods are the most popular electronic structure methods used to model molecular crystals, especially in the context of fragment methods. With modern density-fitting algorithms,[241−244] MP2 requires only moderately more computational effort than HF or hybrid density functionals, at least for the size of molecules for which crystalline MP2 calculations are feasible.

Unlike traditional semilocal density functional approximations, MP2 naturally includes two-body van der Waals dispersion. This formal property has limited value, though, and the poor performance of MP2 for describing dispersion interactions is well-known.[63] MP2 overestimates the binding energy of the parallel displaced benzene dimer stack geometry by almost a factor of 2,[245] for instance. On the other hand, MP2 underestimates the dispersion in weakly polarizable systems such as the helium or neon dimers.[246] In selected systems like carbon dioxide which are intermediately polarizable, MP2 actually predicts the interaction energies fairly well.[247]

The dispersion problem with MP2 can be understood from the perspective of intermolecular perturbation theory.[248,249] The dispersion energy occurs at second-order and is given by the following sum-over-states expression:

$$E_{\mathrm{disp}}^{(2)} = -\sum_{m,n\neq 0} \frac{|\langle \phi_0^{\mathrm{A}} \phi_0^{\mathrm{B}} | \hat{V}^{\mathrm{AB}} | \phi_m^{\mathrm{A}} \phi_n^{\mathrm{B}} \rangle|^2}{E_m^{\mathrm{A}} - E_0^{\mathrm{A}} + E_n^{\mathrm{B}} - E_0^{\mathrm{B}}} \tag{6}$$

where ϕ_0^{A} and ϕ_m^{A} represent ground and *m*th excited state wave function on molecule A, and the energy denominator involves the energy difference between the ground (E_0^{A}) and excited state (E_m^{A}) on each molecule. The analogous terms for molecule B are also present, and $\hat{V}^{\mathrm{AB}}$ represents the interaction operator between the two molecules (the perturbation).

At the MP2 level, the excited state wave functions are treated at the uncoupled Hartree−Fock (UCHF) level, which effectively amounts to a Koopmans' theorem-style approximation for the excited states: generate the excited states by simply replacing a given occupied orbital with a virtual one, and compute the excitation energy in the denominator as the difference between the unrelaxed HF orbital energies. This simplistic approximation for the excitation energies and excited state wave functions leads to the aforementioned poor treatment of dispersion at the MP2 level.

A number of approaches seek to improve the behavior of MP2. Spin-component scaling (SCS) reduces errors in MP2 by reweighting the same spin and opposite spin contributions to the correlation energy.[250,251] This can be particularly effective when using parameters determined specifically for intermolecular interactions (SCS(MI)-MP2).[252] SCS(MI)-MP2 performs well on small-molecule, equilibrium geometry dimer benchmarks[63,253] similar to those in the S22 test set[254] against which the scaling parameters were fitted.[252]

In larger systems, however, SCS(MI)-MP2 performs no better than SCS-MP2.[33,70] SCS(MI)-MP2 is also less effective in cases like the oxalyl dihydrazide crystal, where both intra- and intermolecular interactions are important.[236] More recent work combining spin-component scaling and range-separation[255] may help with some imbalances between inter- and intramolecular interactions in crystals, though it remains to be demonstrated. Dispersion-weighted MP2 represents another approach for adjusting spin-component scaled models based on the types of interactions involved which also performs well in many dimer interaction benchmark studies.[256]

Instead of scaling the MP2 correlation components, a different and very successful strategy is to remove the problematic UCHF dispersion from MP2 and replace it with a better description. Multiple approaches for doing this have been explored. Some utilize high-quality dispersion coefficients,[257] while others utilize SAPT dispersion computed from coupled Hartree−Fock[258] or coupled Kohn−Sham (CKS) theory. The most successful and widely used of these approaches is MP2C, where the "C" indicates the CKS dispersion correction.[246,259] The MP2C energy is given by

$$E_{\mathrm{MP2C}} = E_{\mathrm{MP2}} - E_{\mathrm{disp}}^{\mathrm{UCHF}} + E_{\mathrm{disp}}^{\mathrm{CKS}} \tag{7}$$

In other words, one computes the MP2 energy, then removes the UCHF dispersion which is already present in MP2 (as computed from SAPT), and replaces it with CKS dispersion. In the context of eq 6, this amounts to replacing the simple

DOI: 10.1021/acs.chemrev.5b00648
Chem. Rev. 2016, 116, 5567−5613

Koopmans' theorem approximation for the dispersion energy with one in which the excited states and excitation energies are computed from time-dependent density functional theory.

In benchmark calculations, MP2C consistently performs among the best of any $O(N^5)$ MP2-based models, earning the "bronze standard" label after CCSD(T) ("gold") and dispersion-weighted CCSD (DW-CCSD, "silver") in ref 253. MP2C provides a well-balanced description of a variety of intermolecular interactions, though it exhibits larger errors than usual in very strongly electrostatic or charged systems.[253] It also performs very well on the S22 test set,[259,260] the S66 test set,[41] and other noncovalent systems.[70,148,261−265]

The computational performance of MP2C can be enhanced in a couple ways. First, the periodic symmetry found in molecular crystals means that only a handful of unique monomers typically exist. Therefore, when calculating the UCHF and CKS dispersion terms, one need only calculate the frequency-frequency response functions for each unique monomer in the central unit cell. The response functions for monomers outside the central unit cell are identical to the central unit cell ones. Accordingly, one can compute the dispersion correction for all pairs of molecules in the crystal with only trivial effort beyond that of the central unit cell.[266] In the end, this reduces the computational cost of computing the MP2C dispersion correction for a crystal by up to 2 orders of magnitude, making it essentially free on top of the underlying MP2 calculation.

Second, it is computationally wasteful to compute the full MP2 energy, only to discard most of the long-range intermolecular correlation when subtracting out the UCHF dispersion. Attenuated MP2C[267] addresses this issue by attenuating the Coulomb operator in MP2[255,268−270] in order to eliminate long-range correlation. Any residual UCHF dispersion can be subtracted by computing the similarly attenuated UCHF dispersion, and then one can add in the CKS dispersion to capture long-range correlation more accurately. Interestingly, one can also use this sort of approach to help compensate for finite basis set errors, which allows one to use smaller basis sets for substantial computational savings.[267]

The biggest weakness of MP2C is that the dispersion energy correction is defined only for intermolecular interactions. For example, one might use MP2C to correct the interactions between phenyl rings in two different models, but it would not help with the intramolecular interactions between two phenyl rings connected by a covalent linker. Similarly, attenuated MP2C performs poorly for peptide conformers.[267] This could prove potentially problematic in some cases of conformational polymorphism.

One possible solution to the challenge of describing both intra- and intermolecular interactions is to exploit the many-body expansion by treating the intramolecular (1-body) terms with a more advanced method like coupled cluster theory, and only using MP2C for the intermolecular interactions. Coupled cluster calculations on monomers are much less computationally demanding than those on dimers. Some local coupled cluster approaches can also provide mixed-level treatment where CCSD(T) is used for strong local molecular orbital pairs (predominantly intramolecular), while weak pairs are treated with MP2 or better models.[271,272]

Alternatively, the recently developed combination of MP2+VV10,[273] which combines short-range MP2 with long-range DFT correlation using the VV10 functional may also suggest a path forward. Intramolecular variants of SAPT are also being developed[274−276] and might prove useful in this context. Future work will determine if methods like these can provide a true, all-purpose method for achieving near coupled cluster accuracy with only MP2-like computational cost.

MP2.5, which averages the MP2 and MP3 energies, is an alternative approach that substantially improves upon MP2 at the $O(N^6)$ computational cost of a single CCSD iteration.[277,278] The decision to average these energies was made based on empirical observation; the 50:50 mixture of MP2 and MP3 appears to be nearly optimal over a wide range of systems and basis sets. Though the computational cost of MP2.5 is high compared to MP2, it costs far less than CCSD(T) despite providing near coupled cluster accuracy.[63,102,278] MP2.5 has rarely been applied to molecular crystals thus far,[160] but it does provide a viable intermediate between MP2 and CCSD(T).

For three-body and higher interactions, it is important to note that MP2 includes many-body polarization and exchange effects, but it lacks many-body dispersion. Three-body dispersion terms do not appear until third order in perturbation theory. This means that MP2 is ill-suited for cases like the benzene crystal where the three-body dispersion contributions account for ∼10% of the lattice energy.[279]

Benchmark calculations on the 3B-69 test set of three-body interactions provide insights.[102] MP2 performs fairly well for a water trimer, for instance, because the many-body effects stem almost entirely from polarization and exchange effects, which MP2 includes. The absence of three-body dispersion terms in MP2 means, however, that it performs increasingly poorly as the magnitude of the dispersion energy contribution to the three-body interaction grows.

One can attempt to correct these deficiencies by adding corrections to MP2. This requires some care, however, since the third-order terms should typically be canceled somewhat by terms that arise in fourth-order perturbation theory and beyond. MP2.5 largely rectifies the problems with MP2 and 3-body dispersion,[102] though with noniterative $O(N^6)$ computational cost. Including only half the MP3 contribution in MP2.5 effectively accounts for much of the cancellation that would occur at MP4 and beyond.

Alternatively, one can simply augment MP2 with the missing three-body dispersion terms. One can do this with a symmetry-adapted perturbation theory (SAPT)-style 3-body dispersion correction[280] or with an Axilrod−Teller-Muto form using atom-centered dispersion coefficients (and empirical short-range damping). In practice, the more rigorous SAPT dispersion correction substantially overestimates the size of the three-body dispersion, while the ATM model performs very well (using a damping model fitted only to rare gases).[222] The combination of damping and neglect of terms beyond the triple-dipole dispersion in the ATM model appears to effectively compensate for the missing higher-order terms to produce a model that is fortuitously (but consistently) more balanced.

2.5.2. Coupled Cluster Methods. Coupled-cluster singles, doubles, and perturbative triples (CCSD(T)) provides the gold standard for many problems, including the description of noncovalent interactions. Its $O(N^7)$ scaling has long-prevented its widespread application in molecular crystal calculations. However, recent algorithmic improvements and approximations are making large-scale coupled cluster calculations much more feasible. In particular, the combination of density fitting, truncation of the virtual space, and local correlation

DOI: 10.1021/acs.chemrev.5b00648
Chem. Rev. 2016, 116, 5567−5613

approximations all substantially improve the realm of applicability of these methods.

Methods such as the pair natural orbital (PNO),[281,282] frozen natural orbital (FNO),[283,284] and orbital-specific virtual (OSV) space[285] approximation significantly reduce the effective size of the virtual space. In the FNO approximation, for instance, MP2 natural orbitals with low occupation numbers are discarded. For a typical closely packed trimer, the FNO approximation reduces the virtual space by a modest 15−20%. However, when performing calculations involving ghost atoms (as are used in a counterpoise correction), the savings can be dramatic. Applying the FNO approximation to a dimer or monomer job in the trimer basis set reduces the virtual space by ∼80−85% and ∼99%, respectively, with no appreciable loss in accuracy. Combining the FNO approximation with density fitting or Cholesky decomposition techniques produces a 4-fold speed-up over a conventional CCSD(T) counterpoise-corrected benzene trimer calculation. The total error introduced into the three-body energy by these approximations is only 0.007 kJ/mol.[284]

Methods like PNO and OSV use tensor factorizations and rank reductions to prune the set of virtual orbitals retained for a given occupied orbital (OSV) or orbital pair (PNO). Combining these methods with localized occupied orbitals makes them particularly cost-effective and allows them to be applied to systems containing hundreds of atoms.[282] In the context of molecular crystals, where many weak, long-range interactions are present, care should of course be taken with respect to how aggressively the long-range interactions are approximated or neglected.

Nevertheless, it is clear that coupled cluster methods will play an increasingly important role in fragment-based molecular crystal modeling. The recent use of such techniques to achieve accuracy rivaling experiment in benzene crystal is particularly impressive (see section 3.1 for details).[169,286]

2.5.3. Symmetry-Adapted Perturbation Theory. Symmetry adapted perturbation theory (SAPT) treats the wave functions of isolated molecules as a zeroth-order state, and it models the interactions between those molecules as a perturbation. The standard case involves a perturbative expansion for a pair of molecules,[287,288] though SAPT expressions for three interacting molecules have also been derived.[280,289]

Traditionally, most SAPT calculations in the literature employ either the SAPT0 or SAPT2 approximations from a monomer HF starting point. SAPT0 can roughly be viewed as a Hartree−Fock treatment of intermolecular electrostatics, exchange, and induction coupled with dispersion and exchange-dispersion terms from second-order perturbation theory. When using density fitting, the computational effort required to evaluate SAPT0 is similar to that of MP2. SAPT2 includes all terms from SAPT0 and adds terms that couple inter- and intramolecular correlation up to second order in perturbation theory, and it produces intermolecular interaction energies similar in quality to those of MP2. Higher accuracy is obtainable by including higher-order terms in the perturbation series, albeit with ever-increasing computational cost.

More recently, the closely related SAPT(DFT) and DFT-SAPT models have been developed.[290,291] SAPT(DFT) is analogous to SAPT0, except the zeroth-order monomer states are computed at the DFT level, which means that they include intramolecular correlation automatically. In practice, SAPT(DFT) provides a nice balance between accuracy and computational affordability.[63] Tests of many different SAPT models and basis sets found that SAPT(DFT) was one of the best for practical applications.[292] Efficient implementations allow SAPT(DFT) to be applied to systems with ∼200 atoms and 5000 basis functions.[293] Notably, however, SAPT(DFT) tends to underestimate the strength of hydrogen bonded interactions.[265,292]

SAPT(DFT) was used to compute both 2- and 3-body terms for the benzene lattice energy.[279] Additionally, SAPT(DFT) was used to parametrize a potential for the energetic material RDX.[294] In turn, crystal structure prediction based on this potential correctly identified the experimental structure as the lowest-energy one.[279,295]

Recently, Herbert and co-workers have been developing a class of methods that combine explicit polarization to capture many-body polarization effects with a SAPT treatment of dispersion of exchange repulsion and dispersion.[296−298] This method appears promising for future molecular crystal applications.

2.6. Basis Sets

The choice of basis set is extremely important when modeling the noncovalent interactions that occur in molecular crystals. Given the small, kJ/mol energy differences which often separate different crystal polymorphs, it is critical to ensure that one's predictions are well-converged with respect to basis set. Due to the generally slow convergence of the correlation energy in wave function methods and basis set superposition error (BSSE), very large basis sets are often required to achieve accurate, well-converged lattice energies in molecular crystals. Triple-zeta quality basis sets augmented with diffuse functions (e.g., aug-cc-pVTZ) appear to be the minimum useful basis set size, though extrapolating to the complete basis set limit (CBS) is often important (see section 3.1)

When comparing the relative stability of different crystal polymorphs, one sometimes obtains reliable results in modest basis sets thanks to error cancellation, but not always. As discussed in section 3.4, excellent error cancellation allows one to predict the energy difference between the two polymorphs of aspirin reliably even in a double-ζ basis set. On the other hand, BSSE causes the relative energies of the oxalyl dihydrazide polymorphs to change dramatically with increasing basis set size.

The need for large basis sets is a major factor for why MP2-like lattice energy calculations can be much more expensive than DFT ones. For an organic molecule containing tens of atoms, the computational cost of a density-fitted MP2 calculation in a given basis set is fairly similar to that of a hybrid functional in the same basis set. However, the MP2 calculation requires a larger basis set to achieve reasonably converged results, which makes MP2 somewhat more expensive than DFT in practice.

2.6.1. Explicitly Correlated Approaches. While one can (any many do) use conventional correlation methods and large basis sets, explicitly correlated F12 methods offer an effective alternative for achieving basis set convergence in correlation energies. F12 methodologies have been reviewed elsewhere,[299−301] so the focus here lies on their performance for noncovalent interaction energies and in molecular crystals.

Early tests on the S22 benchmark set by Marchetti et al.[302] showed that MP2-F12/aug-cc-pVTZ gives results that are on par with MP2/CBS. Subsequent calculations with CCSD(T*)-F12a/aug-cc-pVTZ (the asterix refers to the fact that the triples

DOI: 10.1021/acs.chemrev.5b00648
Chem. Rev. 2016, 116, 5567−5613

were scaled instead of being explicitly correlated) found similarly good convergence.[256] Several other studies examining the performance of explicitly correlated models for noncovalent interactions echo these results.[303−305]

In a recent benchmark study[253] on a wide variety of dimer interactions involving 49 dimer complexes and 345 interaction energies using nearly 400 method/basis set combinations, Burns et al. argue that MP2C-F12/aug-cc-pVDZ provides a very cost-effective level of theory for all but the most challenging electrostatics-dominated systems such as multiple hydrogen bonds or ionic complexes. Due to fortuitous error cancellation between the HF and correlation energies, MP2C-F12/aug-cc-pVDZ even performs slightly better than MP2C-F12/aug-cc-pVTZ, and they identified it as their "bronze standard" for noncovalent interactions, with an accuracy of 0.67 kJ/mol relative to "gold-standard" complete-basis CCSD(T) benchmark interaction energies. Even better results (0.21 kJ/mol errors)[253] were obtained using the "silver standard" dispersion-weighted CCSD(T*)-F12/aug-cc-pVDZ model defined in ref 256.

Although the basis set convergence of HF is much more rapid than that of the correlation energy, the finite basis set errors in HF are often larger than those in the explicitly correlated correlation energy. In explicitly correlated calculations, the finite basis set error in the HF reference is often corrected using the complementary auxiliary basis set (CABS) correction,[306,307] which computes the correction due to singles excitations into the larger complementary auxiliary basis space using second-order perturbation theory.

Explicitly correlated calculations have been used in a number of molecular crystal studies. For example, Manby and various co-workers have employed MP2-F12 in their studies of lattice energies for ices[150,194] and in methane clathrate hydrates.[153] Explicitly correlated coupled cluster models played a critical role in computing the benzene lattice energy with sub-kJ/mol accuracy (section 3.1.1)[169] Very recently, Fang et al.[199] employed MP2-F12 and CCSD(T)-F12 in their PBC-GEBF lattice energy benchmarks.

2.6.2. Counterpoise Corrections. Employing a counterpoise correction[308] for BSSE is usually beneficial to achieving useful crystal lattice energies, especially with correlated wave function methods. BSSE effects are most pronounced in small basis sets and can lead to poor convergence of the many-body expansion.[172] However, computing a counterpoise correction in the context of a many-body expansion is not entirely trivial. Several BSSE-correction schemes exist for groups of interacting molecules.[171,177,309−312] The most straightforward approach would be to perform each fragment calculation in the basis of the entire system. For a trimer *ABC*, this would amount to

$$\begin{aligned} E_{ABC}^{\mathrm{CP}} = {} & E_A^{abc} + E_B^{abc} + E_C^{abc} + (E_{AB}^{abc} - E_A^{abc} - E_B^{abc}) \\ & + (E_{AC}^{abc} - E_A^{abc} - E_C^{abc}) + (E_{BC}^{abc} - E_B^{abc} - E_C^{abc}) \\ & + (E_{ABC}^{abc} - E_{AB}^{abc} - E_{AC}^{abc} - E_{BC}^{abc} + E_A^{abc} + E_B^{abc} \\ & + E_C^{abc}) \end{aligned} \tag{8}$$

where the superscripts *a*, *b*, and *c* refer to the use of basis functions from the corresponding monomers *A*, *B*, and *C*. The first three terms represent the 1-body contributions, the next three sets of terms are 2-body contributions, and the final group of terms is the three-body contribution.

In systems containing many fragments, like a crystal, using the full system basis is impractical. The many-body counterpoise correction approach[171] approximates this correction by treating the ghost basis functions according to a truncated many-body expansion. For example, when correcting a two-body term in a tetramer, one would approximate the counterpoise correction using an isolated monomer and a set of three monomer calculations that each include ghost functions from one of the other molecules.

Another common approach is the Valiron-Mayer one, which performs each set of *k*-mer fragment calculations in the full basis of that *k*-mer.[177] For example, the energy of a trimer *ABC* in the Valiron-Mayer approach[311] is given as

$$\begin{aligned} E_{ABC}^{\mathrm{VM}} = {} & E_A^a + E_B^b + E_C^c + (E_{AB}^{ab} - E_A^{ab} - E_B^{ab}) \\ & + (E_{AC}^{ac} - E_A^{ac} - E_C^{ac}) + (E_{BC}^{bc} - E_B^{ac} - E_C^{bc}) \\ & + (E_{ABC}^{abc} - E_{AB}^{abc} - E_{AC}^{abc} - E_{BC}^{abc} + E_A^{abc} + E_B^{abc} \\ & + E_C^{abc}) \end{aligned} \tag{9}$$

Compared to eq 8, this equation uses smaller groups of basis functions for the 1- and 2-body terms, making those calculations less expensive. However, it requires many more fragment calculations, since one must compute each monomer in the monomer, dimer, and trimer basis sets, for instance. Unfortunately, the exponential growth in the number of fragment calculations makes this approach costly for large clusters, since different cluster basis sets are used at each order in the many-body expansion. However, one can approximate it by including only the low-order terms in the many-body expansion.[177]

Note that for two-body fragment terms, the approximation to eq 8 from ref 171 and the approximation to eq 9 from ref 177 lead to identical models—differences first arise with the three-body terms. Finally, it is always prudent to use the largest basis sets practical (ideally aug-cc-pVTZ or better) to reduce the size of any BSSE effects and the sensitivity of one's results to the particular form of the counterpoise correction adopted.

2.7. General Recommendations

In the end, what electronic structure methods should one use to model molecular crystals? Dispersion-corrected density functionals provide an excellent balance between accuracy and computational efficiency. The structures optimized with DFT are typically within good agreement with experiment. While it is certainly possible that higher-quality structures could be obtained from wave function methods/fragment methods, no clear evidence to this effect has yet been presented in the literature.

For lattice energies, dispersion-corrected DFT often performs well and provides a very good starting point for most applications. However, problem cases can arise where two different but generally reliable density functionals predict conflicting energetic orderings for a set of potential polymorphs (see section 3.4). In these cases, one should consider wave function based models like MP2C or (if feasible) coupled cluster calculations. Basis sets of triple-ζ quality provide reasonable quality results with conventional MP2C, though one should strive for the CBS limit if more reliable results are needed. Alternatively, explicitly correlated methods like MP2C−F12 are particularly effective, as discussed in section 2.6.1. The use of large basis sets/explicit correlation also helps reduce the BSSE, minimizing some of the problems discussed in section 2.6.

DOI: 10.1021/acs.chemrev.5b00648
Chem. Rev. 2016, 116, 5567−5613

Finally, substantial insight can often be gained by examining how the crystal energetics converge with respect to both the method and basis set. Performing a series of calculations that explore the convergence and sensitivity of the predictions to the choice of model parameters can be critical to deciding, for example, whether a predicted ∼1 kJ/mol preference for a given structure is potentially meaningful, or simply an artifact of the model chemistry.

3. CRYSTAL PROPERTY PREDICTION

3.1. Lattice Energies

The lattice energy, or the energy required per molecule to break a crystal apart into noninteracting molecules, represents one of the most basic and difficult molecular crystal properties to predict. The lattice energy is typically dominated by energy required to overcome the intermolecular attractions, but it can also include contributions arising from changes in the intramolecular conformation between the crystal and gas phases.

In molecules, computing molecular atomization energies often reveals problems in the treatment of electron−electron correlation, since one cannot rely on the error cancellations in the description of chemical bonding that frequently occur when modeling other types of chemical reactions. Similarly, the comparison of gas and crystalline phase energetics in a lattice energy exposes deficiencies in the theoretical description of the intermolecular interactions in the crystal and/or the intramolecular conformational energetics. This contrasts the calculation of polymorph energy differences, for instance, where errors in the treatment of intermolecular interactions may cancel somewhat (see section 3.4).

The next section discusses performance of various methods on the widely studied benzene crystal. The subsequent sections provide a broader perspective on the accuracy of different models for lattice energy prediction.

3.1.1. Benzene Crystal. Benzene crystal represents a canonical test case for lattice energy prediction. Its molecular size is small enough to allow high-level electronic structure calculations, and its rigidity means that intramolecular contributions to the lattice energy are small (and sometimes neglected entirely). The intermolecular interactions arise primarily from a mixture of van der Waals dispersion and quadrupolar interactions. On the one hand, the difficulty of describing van der Waals dispersion makes benzene crystal a challenging test case for many electronic structure methods. On the other hand, it lacks the strong polarization and/or cooperative hydrogen bonding effects found in many other crystals. Accordingly, the many-body effects in benzene are somewhat unusual in that they are dominated by many-body dispersion.

Recently, Yang and co-workers[169] achieved a new milestone in the field[313,314] when they obtained sub-kJ/mol accuracy for the benzene crystal lattice energy, predicting 55.9 ± 0.76 ± 0.1 versus 55.3 ± 2.2 kJ/mol derived from experiment. In the predicted lattice energy, the first stated uncertainty corresponds to the estimated error in the electronic structure treatment, while the second uncertainty corresponds to the estimated error arising from the crystal geometry. Note that the estimated error bars on the prediction are only half the size of those for the reference value of the lattice energy derived from experiment (see Figure 1).

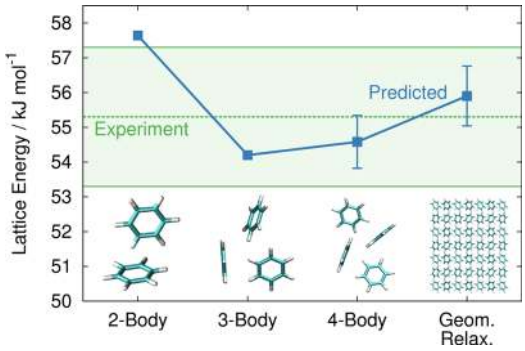

Figure 1. Convergence of the benzene lattice energy at the coupled cluster level (from Yang et al.[169]). Reprinted with permission from ref 313. Copyright 2015 John Wiley & Sons.

This feat was achieved by summing a many-body expansion up through 4-body terms, with each contribution computed as accurately as possible using coupled cluster theory. Dimers out to 11 Å were treated using canonical CCSD(T)-F12/aug-cc-pVTZ. Quadruples contributions to the dimer interactions were estimated to contribute 0.4 kJ/mol to the lattice energy based on small double-ζ basis set calculations which were rescaled to compensate for basis set incompleteness. Trimers out to 9 Å and nearest-neighbor tetramers were modeled using the OSV local CCSD(T0)-F12 method and triple-ζ basis sets. Figure 1 shows that the 3- and 4-body terms contribute up to several kJ/mol to the lattice energy, but that their sum cancels somewhat in this crystal. Other estimates of basis-set incompleteness were included. A final contribution of an estimated 1.3 kJ/mol arises from the relaxation of the experimental 138 K structure down to 0 K.

These benchmark benzene calculations provide a nice reference for comparison with other predictions found in the literature. A collection of results reported by many investigators is reported in Table 1. The computational details such as structure and basis set vary across these different studies, so the comparison is imperfect. Nevertheless, Table 1 provides an instructive and representative set of the accuracy one can achieve for lattice energies with various models.

To begin, several large-basis CCSD(T) benchmark calculations have been reported by other investigators: Lattice energy calculations by the Sherrill group[286,315] reiterate the importance of beyond pairwise interactions in benzene—three-body interactions destabilize it by nearly 4 kJ/mol (see also Figure 1. Most of this destabilization stems from 3-body dispersion. Note that the Sherrill group values are a couple kJ/mol smaller than the corresponding values from Yang et al.,[169] even though both used the same unrelaxed experimental 138 K neutron diffraction structure (though the Yang et al. values reported here also include the estimated 1.3 kJ/mol geometric relaxation). Most of that difference arises in the pairwise interaction terms, with Yang and co-workers summing to larger distances and estimating longer-range contributions. Differences in basis set and correlation beyond triples also contribute to a smaller extent.

Several other coupled cluster studies with more approximate treatments of long-range and many-body interactions predict the lattice energy in the similar range. An HMBI calculation which combines 1- and 2-body CCSD(T) with a polarizable force field for long-range and many-body interactions predicts 53.0 kJ/mol (including geometric relaxation).[168,231] A GEBF study at the CCSD(T) level[199] and an incremental method

DOI: 10.1021/acs.chemrev.5b00648
Chem. Rev. 2016, 116, 5567−5613

Table 1. Predicted Benzene Lattice Energies (in kJ/mol) Taken from Various Studies Found in the Literature[a]

type	method	lattice energy	source
experiment		55.3 ± 2.2	Yang et al.[169]
fragment	coupled cluster 2 + 3 + 4-body	55.9 ± 0.76 ± 0.1	Yang et al.[169]
fragment	CCSD(T) 2 + 3-body	51.6	Kennedy et al.[286]
fragment	CCSD(T) 2-body	55.3	Ringer and Sherrill[286,315]
fragment	HMBI CCSD(T)	53.0	Wen and Beran[168,231]
fragment	GEBF CCSD(T)	50.7	Fang, Li, Gu, and Li[199]
fragment	CCSD(T) 2-body + PBE	50.5	Bludsky, Rubes, and Soldan[219]
periodic MP2	local MP2	56.6	Maschio et al.[130]
periodic MP2	GPW-MP2 (fixed cell)	58.8	Del Ben et al.[140]
periodic MP2	GPW-MP2	63.0	Del Ben et al.[140]
fragment	GEBF MP2-F12	65.0	Fang, Li, Gu, and Li[199]
fragment	HMBI MP2	60.6	Wen and Beran[168,231]
fragment	HMBI MP2C	49.0	Huang, Shao, and Beran[266,316]
fragment	SAPT 2 + 3-body	50.3	Podeszwa, Rice, and Szalewicz[279]
periodic DFT	B3LYP	15.9	Civalleri et al.[53]
periodic DFT	B3LYP-D*	48.5	Civalleri et al.[53]
periodic DFT	B3YLP+C6 disp	49.8	Feng and Li[51]
periodic DFT	AC-FDT	47.0	Lu, Li, Rocca, and Galli[317]
periodic DFT	B86b-XDM	51.2	Otero-dela-Roza and Johnson[34]
periodic DFT	PBE-D2	56.3	Otero-dela-Roza and Johnson[34]
periodic DFT	PBE-D3	54.8	Moellmann and Grimme[72]
periodic DFT	PBE-D3 (3-body)	51.0	Moellmann and Grimme[72]
periodic DFT	PBE-TS	66.5	Otero-dela-Roza and Johnson[34]
periodic DFT	PBE-XDM	49.5	Otero-dela-Roza and Johnson[34]
periodic DFT	PBE-MBD	55.0	Reilly and Tkatchenko[80]
periodic DFT	PBE0-D3	59.8	Moellmann and Grimme[72]
periodic DFT	PBE0-D3 (3-body)	56.1	Moellmann and Grimme[72]
periodic DFT	PBE0-TS	62.0	Reilly and Tkatchenko[80]
periodic DFT	PBE0-MBD	51.0	Reilly and Tkatchenko[80]
periodic DFT	vdW-DF1	59.9	Otero-dela-Roza and Johnson[34]
periodic DFT	vdW-DF2	55.9	Otero-dela-Roza and Johnson[34]
periodic DFT	DFTB-D3	56.0	Brandenburg and Grimme[74]

[a]Note that differences in basis sets and geometries used across the different studies accounts for some of the variation in the lattice energies. See original studies for details.

study which corrected PBE with CCSD(T) 1- and 2-body terms[219] both predicted lattice energies near 50.5 kJ/mol.

Of course, coupled cluster calculations are computationally demanding. MP2 provides much more reasonable costs, but its problems with van der Waals dispersion (section 2.5.1) cause MP2 to overestimate the benzene lattice energy by some 10 kJ/mol, with values around 60−65 kJ/mol. Interestingly, the periodic local MP2 value of Maschio and co-workers is much smaller at 56.6 kJ/mol.[130] This weaker binding probably stems in part from the smaller, double-ζ basis set used in that study. As indicated by the coupled cluster discussion above, care should also be taken to include the long-range correlation effects that have a nontrivial effect on the benzene lattice energy.

MP2C provides an inexpensive correction to MP2 that substantially improves agreement with CCSD(T). For benzene, MP2C HMBI calculations predict a lattice energy of 49.0.[266] While the dispersion correction in MP2C overcompensates relative to experiment correlation here, MP2C is in better agreement with the experimental value than MP2. A careful SAPT treatment that includes 2-body and 3-body terms also performs fairly well, with a lattice energy of 50.3 kJ/mol.[279]

Next, we turn to DFT methods. In the absence of van der Waals dispersion, a model like B3LYP predicts a lattice energy of only 15.9 kJ/mol, relative to the experimental value of 55.3 ± 2.2 kJ/mol. Adding an empirical dispersion correction on top of B3LYP increases the lattice energy to around 49 kJ/mol. More generally, most DFT methods which account for dispersion predict lattice energies in the range of 50−60 kJ/mol, in fairly good agreement with experiment.

The differences among the various dispersion corrections are particularly interesting. Coupling three different pairwise dispersion corrections to PBE gives somewhat different results: PBE-TS predicts 66.5 kJ/mol, PBE-D3 predicts 54.8 kJ/mol, and PBE-XDM predicts 49.5. Switching to the hybrid PBE0 functional decreases the lattice energy by several kJ/mol to 62.0 for PBE0-TS, but increases by several kJ/mol to 59.8 kJ/mol for PBE0-D3. Dispersion beyond 2-body is repulsive in the benzene crystal, and adding intermolecular three-body (D3) or interatomic many-body dispersion (MBD) reduces the lattice energy to 56.1 or 51.0 kJ/mol, respectively. Note too that vdW-DF2 performs very well here, though it performs less well on other species,[34] as discussed in section 3.1.2.

Taken together, these results demonstrate that dispersion-corrected DFT provides an effective tool for predicting molecular crystal lattice energies. However, it is clear that there remain nontrivial differences among different functionals and dispersion corrections. In some cases, the differences behave as one might expect, hybrid functionals perform better than GGA functionals, and accounting for higher-order dispersion contributions generally improves the agreement. On the other hand, differences between the D3, TS, and XDM corrections, for example, indicate the sensitivity of the models to the specific nature of the correction and the manner in which the short-range functional and long-range dispersion contributions are combined. A similar theme arises in the prediction of the relative energetics in crystal polymorphs (section 3.4).

3.1.2. Other Benchmarks. A broader perspective on the performance of various methods can be gained by examining their performance of a more diverse set of molecular crystals. The C21 test set,[34] and the subsequently slightly refined X23 test set,[80] provide useful lattice energy benchmarks. It is important to realize that the errors in the experimental lattice energies often approach the magnitude of the errors in the theoretical calculations. Experimentally reported sublimation

DOI: 10.1021/acs.chemrev.5b00648
Chem. Rev. 2016, 116, 5567−5613

Table 2. Mean Absolute Errors for Dispersion-Corrected DFT Models on the X23 (or C21 in Selected Cases) Benchmark Set, in kJ/mol

method	MAD	ref
DFTB-D3	10.4	74
PBE-D3	4.6	72
PBE-D3 (3-body)	5.0	72
PBE-XDM	5.4[a]	34
vdW-DF1	10.2[a]	34
vdW-DF2	10.1[a]	34
PBE-TS	13.4	80
PBE-MBD	5.9	80
PBE-LRD	11.5	318
revPBE-LRD	6.0	318
PBE0-D3	5.0	72
PBE0-D3 (3-body)	5.0	72
PBE0-TS	10.0	80
PBE0-MBD	3.9	80

[a]C21 test set instead of X23.

enthalpies often vary by up to a few kJ/mol,[319] and the conversion of finite temperature sublimation enthalpies to 0 K lattice energies adds additional error unless performed carefully.[34,80]

Consider first the performance of dispersion-corrected density functional models. While the results once again vary modestly with the specific functional and dispersion correction (Table 2), one generally can predict lattice energies with a mean absolute deviation of 4−5 kJ/mol.[34,51,72,80] The largest DFT errors are observed for PBE-TS (13.4 kJ/mol),[80] PBE0-TS (10.0 kJ/mol),[80] and vdW-DF2 (10.1 kJ/mol).[34] In the first two cases, going beyond the pairwise-only TS correction to include many-body dispersion using MBD dramatically improves the results, cutting the errors down to 5.9 kJ/mol (PBE-MBD) and 3.9 kJ/mol (PBE0-MBD).[80]

For a given functional and dispersion correction, larger DFT errors are typically observed for hydrogen-bonded crystals rather than those which are held together primarily through van der Waals interactions. This is consistent with the results of dimer[63,64,67,87,88] and trimer[102] benchmarks, for which delocalization (self-interaction) error that affects the description of polarization becomes more clearly significant once dispersion has been accounted for. Overall, despite potentially sizable differences in the lattice energies predicted by different density functionals and dispersion corrections for any particular crystal (e.g., benzene), several different dispersion corrections appear to perform statistically similarly on broader test sets.

To test the performance of various models in strongly polarized systems, Brandenburg and Grimme[320] recently constructed the ICE10 benchmark test set based on ten polymorphs of ice. They demonstrate that, even in ices, van der Waals dispersion is "mandatory for an accurate description of both the structures and energies". They observe particularly balanced performance for BLYP-D3 including Axilrod−Teller−Muto three-body dispersion: mean absolute errors below 1% in lattice parameters and 1 kcal/mol in the lattice energies. They also observe that hybrid functionals perform slightly better than GGAs for the lattice energies.

Brandenburg and Grimme[74] have also developed a dispersion-corrected version of DFTB, DFTB-D3, which performs impressively well for benzene (Table 1). In broader testing, DFTB-D3 predicts lattice energies within 8−12 kJ/mol, or 10−20%. Such errors are about a factor of 2 larger than the comparable DFT-D3 results, but DFTB-D3 energies can be computed up to 2 orders of magnitude faster than conventional DFT-D3. While ∼10 kJ/mol accuracy is probably insufficient for some applications, it might provide a useful tool for high-throughput (e.g., screening potential structures during crystal structure prediction) or large-molecules.

Various wave function benchmark lattice energy studies have also been performed. Periodic local MP2 calculations predicted the lattice energy of small-molecule crystals (like acetylene, ammonia, ice, formic acid, etc.) to within 3.1 kJ/mol in mean absolute deviation.[123,124] Rescaling the same- and opposite spin MP2 correlation components according to the SCS(MI)-MP2 approach reduces that error to 2.3 kJ/mol.[123,124] SCS(MI)-MP2 also helps in the benzene crystal.[286] On the other hand, it performs less well for the polymorph energetics in oxalyl dihydrazide.[236]

Note that these local MP2 tests do not include any dispersion-dominated crystals for which MP2 would be expected to perform poorly. Even for carbon dioxide, the difference between the MP2 and CCSD(T) lattice energy predictions is small.[168] Another set of periodic LMP2 benchmarks predicted lattice energies within 5−10 kJ/mol, though those calculations used small double-ζ basis sets.[130] The use of larger basis sets would likely affect the lattice energies[128,224] substantially (hopefully reducing the errors further).

Del Ben and co-workers[112,114] have compared GPW-MP2, GPW direct-RPA, and dispersion-corrected DFT results on seven small-molecule crystals. They report root-mean-square errors of 16.9 kJ/mol for MP2, ∼20 kJ/mol for direct RPA based on either PBE0 or B3LYP input orbitals, and 21.5 kJ/mol for B3LYP-D3. Note that these errors are somewhat larger than those discussed earlier because the current studies compare predicted lattice energies against finite-temperature sublimation enthalpies (i.e., no attempt was made to correct for finite-temperature effects). Nevertheless, the cohesive energy comparisons reported suggest that (a) GPW-MP2 and the local MP2 algorithms from CRYSCOR agree to within ∼2 kJ/mol,[112] (b) direct-RPA performs several kJ/mol worse than MP2,[114] and (c) both MP2 and direct-RPA perform slightly better than B3LYP-D3.[114]

One can also use periodic MP2 to implement double hybrid density functionals. While this area has not yet been explored thoroughly, a test of double-hybrid density functionals based on periodic LMP2 on a handful of small-molecule crystals (ammonia, carbon dioxide, formamide, and urea) found errors around 6 kJ/mol.[92] Double-hybrid functional calculations based on the GPW-MP2 formulation have also been reported by Del Ben et al.,[112] with performance similar to or slightly better than that noted for GPW-MP2 above. For instance, they obtained root-mean-square errors of 15.6 kJ/mol for B2PLYP-D3, versus 16.9 kJ/mol for MP2.

Fragment methods have been used to predict benchmark lattice energies at the MP2 and coupled cluster levels. In tests on simple molecular crystals, MP2-level fragment lattice energies agree with periodic local MP2 ones to within 1−2 kJ/mol.[123,168] Fragment method benchmarks[168,199,218,224] indicate that MP2 performs generally well in crystals where van der Waals dispersion is not too important, just as one would expect from its performance on dimer benchmark sets for noncovalent interactions.[63] Errors of ∼1−4 kJ/mol are achievable when MP2 and large basis sets are used for the 1-

DOI: 10.1021/acs.chemrev.5b00648
Chem. Rev. 2016, 116, 5567−5613

and 2-body terms, along with a more approximate treatment of many-body terms. However, MP2 overestimates the lattice energy of crystals like benzene or imidazole by 10−15 kJ/mol.

If one uses CCSD(T) instead of MP2 for the 1- and 2-body terms along with an effective many-body approximation (e.g., embedding, a polarizable force field, or an incremental scheme), one corrects many of the residual errors in MP2, particularly in cases where MP2 dramatically overestimates the dispersion. CCSD(T)-quality calculations approach a few kJ/mol accuracy in many cases.[168,199,218,224] Recent, systematic tests against thermodynamically consistent experimental values for 25 small molecule crystals found mean absolute deviations of 13% or 4.8 kJ/mol.[321] The same study also found that local, explicitly correlated coupled cluster methods were particularly effective for reproducing CCSD(T)/CBS benchmarks with lower computational cost.

Models like MP2C provide an effective approximation for CCSD(T) at much lower computational cost. MP2C maintains or slightly improves upon the high-accuracy MP2 provides for hydrogen bonded crystals, while dramatically reducing the large errors it exhibits in cases like benzene.[266,267]

3.1.3. Summary. In the end, a few general lessons regarding molecular crystal lattice energy prediction can be drawn from the benchmark studies found in the literature. First, small-molecule lattice energies can be predicted with accuracy that rivals experiment. However, doing so requires high-level electronic structure treatments (coupled cluster theory) and careful consideration of higher-order terms in the many-body expansion. Such results are unlikely to be routinely obtainable. Instead, the use of high-quality dispersion-corrected density functionals or fragment-based wave function methods allows one to obtain ∼2−5 kJ/mol accuracy, which corresponds to errors of ∼5% or less for the lattice energy of a typical small molecule crystal.

Second, while explicit summation of the many-body series through four-body terms worked well in benzene, the same rapid convergence of the many-body expansion may not occur in a case with highly cooperative hydrogen bonding, like ices. Furthermore, basis set superposition error and numerical precision issues can be particularly problematic for higher-order terms in the many-body expansion.[170−172] Third, polarization is not the only important many-body contribution. Three-body dispersion accounts for ∼10% of the benzene lattice energy,[279] for instance (see section 2.5.1).

Fourth, the use of sufficiently large basis sets is important, particularly for correlated wave function methods. The difference between a counterpoise-corrected aug-cc-pVDZ and the extrapolated CBS limit can be 10% or more of the lattice energy.[224] Basis sets of triple-ζ quality often provide useful accuracy for MP2 or CCSD(T), though sometimes larger basis sets (or explicit correlation) are needed to resolve subtle energetic contributions between different crystal polymorphs. Basis sets containing diffuse orbitals are particularly important for describing molecular polarizabilities and dispersion interactions correctly. The basis set requirements for DFT are less demanding, but care still should be taken to ensure good convergence with respect to basis set size.

Fifth, the crystal geometry matters when targeting kJ/mol accuracy. Yang and co-workers estimated that the benzene lattice energy increases by 1.3 kJ/mol due to changes in the crystal structure upon cooling from 138 to 0 K.[169] The effects of thermal expansion will be even larger between 0 K and room temperature. In other words, the geometry and thermal effects on the lattice energy can be of the same magnitude as the inherent electronic structure errors of ∼2−4 kJ/mol.[233,234] Since typical electronic structure calculations ignore temperature, they miss both these changes in the unit cell volume and thermal contributions to the enthalpy/entropy. Care must be taken when using predicted energetics to discuss properties of room temperature crystals. Section 3.2 will discuss the theoretical prediction of crystal geometries, while section 3.5 will discuss the prediction of crystal properties at finite temperatures and pressures.

3.2. Crystal Structures

To predict accurate lattice energies or other properties, one must obtain reliable crystal structures. This section focuses on how well an optimized structure reproduces an experimentally determined one. The more encompassing crystal structure prediction problem, which seeks to predict the most stable crystal structures starting from only a 2-D representation of the molecule, will be discussed in section 3.3.

Before examining the performance of specific methods, it is important to consider which experimental structures one wishes to compare against. First, the majority of experimental crystal structures found in the literature were solved using single-crystal X-ray diffraction, which has trouble identifying hydrogen atom positions. Therefore, most quantitative comparisons between predicted and experimental structures examine only the non-hydrogen atoms.

Second, the structure of a given crystal can expand significantly between 0 K and room temperature. In phase I carbon dioxide, for example, thermal expansion swells the unit cell volume by ∼8% between 6 and 195 K at atmospheric pressure.[322] On the other hand, the strong hydrogen bond network in ice Ih hinders thermal expansion: its unit cell volume swells by only 2% between 10 and 265 K at atmospheric pressure.[323] In any case, crystal properties are frequently measured near room temperature, but most predictions occur at 0 K (and usually neglect zero-point vibrations as well). In addition to altering the structure, thermal expansion can have nontrivial impacts on thermodynamic or mechanical properties, as discussed in section 3.5.

When optimizing a crystal, one typically optimizes both the atomic coordinates and the lattice parameters to obtain the structure that minimizes the electronic energy. To optimize structures at finite temperatures and pressures, one should minimize the free energy instead. This requires augmenting the electronic energy with the zero-point energy, thermal contributions (e.g., computed using the quasiharmonic approximation), and a pressure−volume term.

Alternatively, one sometimes has access to experimentally measured lattice parameters, which can be extracted from powder X-ray diffraction, even if the full single-crystal X-ray structure is unavailable. In those cases, one might optimize only the atomic positions, holding the lattice parameters fixed, to obtain a structure which approximates the one at finite temperatures and pressures.

Even if the full crystal structure is experimentally available, one still usually wants to relax the hydrogen positions assigned from the X-ray crystallography. Furthermore, evidence suggests that refining the crystallographic atomic coordinates with dispersion-corrected DFT often improves agreement with experimental NMR chemical shifts, for instance (see section 3.7).[324] Therefore, it is often worthwhile to relax all atomic

DOI: 10.1021/acs.chemrev.5b00648
Chem. Rev. 2016, 116, 5567−5613

coordinates, even when starting from an X-ray or neutron diffraction structure.

Space-group symmetry constraints can be employed during the optimization to accelerate convergence by both lowering the cost of each individual energy/gradient evaluation and by reducing the number of degrees of freedom which need to be optimized.[232] Molecular crystal potential energy surfaces appear to be fairly flat near the minimum in many cases, which can sometimes make converging the optimization difficult. Tight numerical tolerances for the integrals, grids, and any other relevant parameters can improve the convergence properties.

3.2.1. DFT Structures. The vast majority of quantum mechanical molecular crystal optimizations are performed with DFT, either using plane waves or Gaussian basis sets. Van der Waals dispersion can dramatically reshape the potential energy surface, and dispersion-corrected density functionals should always be used.

Civalleri and co-workers compared a set of crystal structures optimized with B3LYP with and without an empirical C_6/R^6 dispersion correction.[53] The D* correction is a rescaled version of Grimme's D2 correction[43] which was fitted on a series of molecular crystals. Even for a case like the ammonia crystal, which is dominated by polar and hydrogen bonding interactions, the cell volume is overestimated by 13% at the B3LYP/TZP level of theory. Adding the dispersion correction reduces the volume considerably, producing a unit cell that is only 4% too small. The effect is even more dramatic for benzene crystal, where neglecting dispersion produces a unit cell volume that is nearly 40% too large at the B3LYP/6-31G** level. Including the dispersion correction produces a volume which is off by only 4%. Increasing the basis to TZP reduces that volume error to 0.4%. Similar results are seen in energetic materials, where the inclusion of a dispersion correction reduces the lattice parameters errors from up to 10% to around 1%.[325]

It is sometimes argued that one can omit the dispersion correction during structure relaxation in special cases, such as when the lattice constants are held fixed or when the crystal is exposed to several GPa of external pressure. In the former case, the unit cell shape provides a constraint which often prevents the atoms from moving too far from their initial positions (e.g., if one started from an experimental structure). In the latter case, pressure pushes the nearest-neighbor intermolecular interactions toward the short-range, repulsive wall, and long-range dispersion becomes less significant in a relative sense. Byrd et al.[326] found that the importance of the dispersion correction diminished in energetic material crystals at pressures above 6−7 GPa.

Nevertheless, even if one can sometimes obtain plausible structures without a dispersion correction, such good results are clearly fortuitous. Indeed, even with fixed unit cell parameters, including the dispersion correction slightly improves the agreement of the predicted structures with experiment.[327] Given that many dispersion corrections provide an effective description of dispersion while adding only trivial additional computational cost, one should always include dispersion when modeling crystal structures (and energetics) with DFT.

Compared to lattice energies, molecular crystal structures are relatively easy to predict correctly. Benchmark studies have considered a wide range of functionals and dispersion corrections. Generally speaking, the structures obtained with various density functionals and pairwise-additive dispersion corrections typically agree with experiment to within a few percent. Small basis sets provide decent structures with DFT, but accurate work should use large plane wave basis sets or Gaussian basis sets of at least triple-ζ quality to obtain well-converged predictions.

In one impressively broad test, van de Streek and Neumann[327] fully optimized 241 experimental organic crystal structures taken from the August 2008 issue of *Acta Cryst. E* using their PW91-D (an empirical dispersion correction).[328] After including a simple, two-parameter empirical correction for thermal expansion, they found that the root-mean-square deviation in the unit cell volumes was 1.1%. The average root-mean-square displacement of the atomic positions was only 0.095 Å, and it drops to 0.084 Å if one discounts 16 disordered structures. Notably, one crystal for which the DFT-D errors were large turned out to undergo a low-temperature phase transition,[329] and the DFT predictions were in much better agreement with this low-temperature structure.

Subsequently, van de Streek et al.[330] used DFT-D to examine the reliability of 215 experimental crystal structures which were solved from powder X-ray diffraction (instead of the more conventional single cystal X-ray diffraction). Based on discrepancies with the DFT predictions, they found that 9% of the structures were in error. Most of the errors identified were minor errors in space group or the position of an atom, and in at least several cases, the authors of the original studies had noted ambiguities in their solution but had been unable to resolve them. This study both validates powder X-ray diffraction for structure determination and reiterates the power of electronic structure modeling for molecular crystal structures.

In addition to computing the lattice energies in their C21 test set, Otero-dela-Roza and Johnson[34] benchmarked the quality of the corresponding crystal structures. To compare against finite-temperature experimental structures, the DFT optimizations were performed under an appropriate "thermal pressure" to approximate the thermal expansion.

They found that PBE-D, PBE-TS, and B86b-XDM all predict excellent geometries, with errors around 0.05 Å (1−2%) and 0.1−0.2° (0.1−0.2%) for the lattice lengths and angles, respectively. Interestingly, PBE-XDM roughly doubles the mean absolute error relative to B86b-XDM. They argue that the repulsive wall in the B86b exchange functional is better suited for correction with the XDM model than the one in the PBE exchange functional. Finally, vdW-DF1 performs rather poorly, with a mean absolute error of 0.16 Å in the lattice lengths, but vdW-DF2 performs much better. On the same set of crystals, Moellmann and Grimme[72] find that PBE-D3 and TPSS-D3 predict unit cell volumes that are 2% and 3% too large, respectively. The same measure for B86b-XDM is 3.8%. Several studies[331−333] have compared the performance of the D3, TS, XDM, and DCACP dispersion corrections and van der Waals density functionals for predicting unit cell volumes. All methods predicted individual lattice parameters to within 1%, with optPBE-vdW giving the best performance.

Note that a method which produces good quality structures does not necessarily translate into accurate lattice energies.[34] Comparison of Tables 2 and 3 is instructive. PBE-TS produces the best lattice parameters here, but it predicts some of the worst energetics for these crystals. Similarly, while vdW-DF2 substantially improves upon vdW-DF1 for structures, both give similarly poor lattice energies.

Compared to PBE-TS, it has been demonstrated that PBE-MBD tends to shrink the unit cell volume modestly.[77,80] It

DOI: 10.1021/acs.chemrev.5b00648
Chem. Rev. 2016, 116, 5567−5613

Table 3. Errors in the Predicted Crystal Unit Cell Parameters for the Crystals Contained in the C21 Test Set[34]

	cell lengths (Å)	cell angles (degrees)
PBE-D2	0.06	0.19
PBE-TS	0.05	0.14
PBE-XDM	0.06	0.29
B86b-XDM	0.06	0.17
vdW-DF1	0.16	0.11
vdW-DF2	0.07	0.13

reduces the errors in the low-temperature unit cell volumes of three glycine polymorphs to a fraction of a percent.[79] On the other hand, the improvement offered for the volumes of various ice structures is less clear.[77] Analytical gradients of the MBD model have recently been implemented for nonperiodic systems.[334] The authors show improvements in the geometries optimized for the benzene dimer and short polypeptide chains when using the MBD correction instead of pairwise TS or D3 ones. Additional investigations of the role of MBD in periodic crystal geometry optimizations will likely be forthcoming.

3.2.2. MP2 Structures. While most studies optimize crystal structures at the DFT level, a few have used MP2 or even coupled cluster methods. An HMBI study compared the structures of five different crystals (ice, formamide, acetamide, benzene, and imidazole) obtained with B3LYP-D* (where D* is the aforementioned empirical DFT dispersion-correction of Civalleri et al.[53]) and with MP2/aug-cc-pVDZ (using the HMBI fragment model) to low-temperature experimental structures.[231] The MP2/aug-cc-pVDZ lattice parameters (root-means square error of 1.6%) improve upon the structures obtained with B3LYP-D*/6-31G** (3.4%), and they are similar to those obtained from B3LYP-D*/TZP (2.0%).

The rmsd15 metric[335] compares the positions of atoms in a 15-molecule cluster extracted from the crystal and encapsulates errors in both the positions of atoms in the unit cell and in the lattice parameters (section 3.8). For the five crystals noted above, the MP2 rmsd15 values are 0.06−0.16 Å. The B3LYP-D*/TZP values are similar, albeit with a slightly wider range of errors (rmsd15 of 0.02−0.22 Å).

Other studies have optimized crystal structures for small molecule crystals such as ices,[184,194,336] ammonia,[123] carbon dioxide,[123,194] hydrogen fluoride,[183,190,191,194] and formic acid[178] with MP2 using the binary interaction fragment method or the embedded many-body expansion model. Lattice parameters for these simple crystals are typically within a few hundredths of an angstrom or less. The choice of basis set is important. Using a triple-ζ quality basis set like aug-cc-pVTZ instead the small aug-cc-pVDZ basis set one often reduces errors in the predicted lattice parameters for these crystals by ∼0.1 Å.

Very recently, analytical gradients were implemented for the periodic GPW-MP2 algorithms.[140] Using a triple-ζ basis set, optimized lattice parameters for a handful of crystals were underestimated by 1−7%, and volumes were in error by up to 15%. At least some of this error stems from BSSE. Test calculations in a quadruple-ζ basis set on formic acid reduced the error from 8% to 4%.

Two recent studies[233,234] examined the temperature-dependent volume of carbon dioxide and other small molecule crystals with by combining large-basis MP2 or even CCSD(T) with a quasiharmonic contribution for thermal expansion evaluated at the MP2 level. As shown in Figure 2, MP2/aug-cc-pVDZ captures the correct thermal expansion trend, but it overestimates the cell volume by up to ∼10%. Increasing the basis set toward the CBS limit significantly reduces the errors in the predicted volume, with the best MP2/CBS and CCSD(T)/CBS structures underestimating the volume by 2−3%. Similarly good results were observed for a few other small molecule crystals.[234] In these crystals, zero-point expansion accounts for roughly a third to a half of the overall expansion between the structure obtained by minimizing the electronic energy and the room-temperature structure.[234]

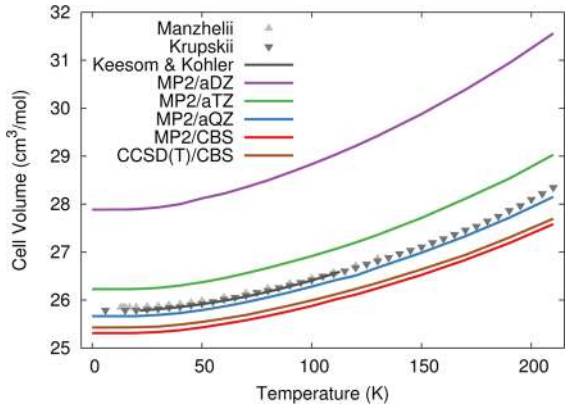

Figure 2. Comparison of the predicted and experimental volumes of carbon dioxide phase I (dry ice) as a function of temperature. Thermal effects were modeled using the quasiharmonic approximation. Experimental data was taken from refs 322 and 337−339. Reprinted with permission from ref 233. Published by The Royal Society of Chemistry.

In summary, wave function methods offer the potential for improving upon DFT crystal structures. However, the existing data on MP2 and coupled cluster crystal structure optimizations is currently too limited to demonstrate clear benefits in practice. Unfortunately, correlated wave function methods are both inherently more expensive and generally require larger basis sets than DFT, which makes such structural optimizations substantially more demanding than DFT ones. Accordingly, dispersion correctly DFT will likely continue to be used for the vast majority of crystal structure optimizations, and one can expect structures to agree with experimental structures observed at similar temperatures (for finite-temperature free-energy structure optimizations) or low temperatures (for electronic energy structure optimizations) to within a few percent.

3.3. Crystal Structure Prediction

If one can predict lattice energies and reproduce experimental structures reliably, the next step is to predict crystal structures entirely from first-principles, without any experimental data inputs. Successful crystal structure prediction (CSP) requires several key features. First, one must adequately search the space of possible crystal packing motifs. Crystal packing space is vast, with 230 space groups and differing numbers of molecules in the asymmetric unit cell. Fortunately, ∼90% of known organic crystals structures fall into only ten space groups,[340] and crystals with no more than a few molecules in the asymmetric unit are very common. Still, care must be taken: one polymorph of pyridine contains 4 molecules in the asymmetric unit, for instance.[341]

DOI: 10.1021/acs.chemrev.5b00648
Chem. Rev. 2016, 116, 5567−5613

Second, one must compute the lattice energies accurately. The energy differences between polymorphs are usually a few kJ/mol or less,[1,14,342] making reliable discrimination difficult. Third, one should consider temperature effects. Whereas lattice energies neglect tempearture, free energies indicate which phases are thermodynamically favored at finite temperatures and pressures. While one can sometimes obtain correct predictions despite neglecting temperature and/or entropic effects, many examples exist where the most stable crystal phases changes with temperature and/or pressure (see section 3.5). As discussed in section 3.5, an extensive survey by Nyman and Day[14] observed that switching from lattice energy to free energy reranked polymorphs at room temperature about 10% of the time. Finally, one should bear in mind that crystallization is often a kinetic process, rather than a thermodynamic one. Even a perfect prediction of the most stable crystal polymorphs may not match the observed crystal structures if a metastable phase has been crystallized experimentally.

Blind tests of crystal structure prediction have been organized by the Cambridge Crystallographic Data Center every few years.[17−21,343−345] These contests ask participants to predict the crystal structures of organic molecules starting from only the 2-D molecular structure. The crystal structures for the blind test species have been obtained experimentally, but they are not publicly released until the conclusion of the blind test.

The earliest blind tests involved small, rigid organic molecules. As the years have progressed, the molecules in the test have generally grown larger and more complicated, often including intramolecular conformational flexibility. Flexibility proves particularly challenging both because it increases the effective number of degrees of freedom that must be searched and because correctly balancing inter- and intramolecular interactions is difficult for many MM and QM models.[15,16,240,346]

Though the early blind tests resulted in many failed predictions, recent years have seen increasingly successful predictions. Note that as of this writing, the sixth blind test has recently been completed, but the results have not yet been released. There has also been a separate blind test of inorganic crystal structure prediction.[347]

A few techniques have proved particularly effective in the blind tests. The first group to achieve a perfect success rate in a single blind test was Neumann and co-workers, who correctly predicted all four crystal structures in the fourth blind test using their GRACE methodology.[20,343] They performed the initial crystal packing search using force fields parametrized from DFT-D,[348] followed by subsequent refinement of promising structures using periodic DFT-D.[50,328,343,345] Most published work using GRACE has relied on a custom DFT-D dispersion correction,[50] though Grimme's D3 correction has been used in some more recent work (e.g., ref 349).

The GRACE methodology also proved the most effective in the fifth blind test, correctly predicting three structures as their lowest energy.[21,345] If one includes studies that used these techniques to revisit the older blind tests,[350−352] this approach has now correctly predicted the experimental structure as the lowest-energy one in 15 out of 20 crystals. In the other five cases, the experimental structures were ranked 2, 3, 4, 7, and 81.

The rank 81 case was for a gallic acid hydrate from the fifth blind test. This hydrate exhibits large numbers of potential hydrogen bonding networks with very similar energies. Even a given set of positions for the non-hydrogen atoms often allows multiple proton arrangements. Accurately modeling those subtle energetic differences can be very challenging, as discussed for ices in section 3.5.2. Subsequent joint experimental/CSP studies on gallic acid have since revealed a very complex crystal energy landscape, with 5 monohydrates, three anhydrates, and over 20 solvates currently identified (see sections 3.4.7 and 3.4.8).[6]

Another class of techniques, which was developed by several groups over many years, typically utilize a hierarchy of screening procedures.[344,353] The first step uses low-discrepancy Sobol sequences to generate $\sim 10^5-10^6$ structures spanning different space groups and involving chosen numbers of molecules in the asymmetric unit.[354] Care must be taken when the molecules are flexible,[240] and various strategies[344,355−361] have been invoked to achieve QM-quality intramolecular potentials with lower computational cost.

The energy of each putative structure is initially minimized with respect to the lattice parameters and atomic coordinates (often with monomer geometries held rigid) using a simple point-charge force field. Subsequent rounds of refinement and winnowing of candidate structure are performed using ever-improving energy models, including distributed multipolar force fields,[362] high-quality treatment of the intramolecular conformation energetics, and perhaps final DFT refinement of the most promising structure candidates. This technique has resulted in a number of successful predictions in the more recent blind tests.[20,21,344] The challenge lies in deciding how many structures to advance to the next level of refinement at each stage. Advancing too few structures may cause one to miss the correct structures due to poor energy rankings from the simpler lattice energy models. On the other hand, advancing too many structures increases the computational costs.

A third technique for CSP uses evolutionary optimization algorithms such as those found in USPEX.[363−365] In the first blind test of inorganic crystal structure prediction,[347] which focused on the search problem rather than the energy problem (all methods were run using the same potential), USPEX found lower-energy structures with substantially fewer structure relaxations than random searching. In two of the cases, USPEX found lower energy structures after a few hundred structure relaxations than random search found in nearly 15 000 random search relaxations. The Oganov group has also performed studies demonstrating the performance of evolutionary algorithms for molecular crystals,[366] hydrates,[367] and polymers.[368] Two groups in the fifth (organic) blind test also used genetic algorithms, with a few successes.[21] Success in that test, however, requires both effective searching and energy ranking, and it is unclear whether the search algorithms or lattice energy models were problematic in the cases where the genetic algorithms were unsuccessful.

Other promising search algorithms have been developed in recent years. For example, simulated annealing was competitive in the inorganic blind test.[365] Particle swarm optimization[369] and ab initio random searching[370] have been used to explore the phase diagrams of many small molecule crystals, as described in section 3.5

Free energy simulations, which tackle the finite temperature and pressure issues directly, represent another interesting development in CSP. There have been a number of successful applications of molecular dynamics,[371,372] metadynamics,[373−376] adiabatic free energy dynamics,[377] and other enhanced sampling techniques[378−380] to crystal thermodynamics, polymorphism, and growth. Such methods are very promising, but currently they are typically limited by the

DOI: 10.1021/acs.chemrev.5b00648
Chem. Rev. 2016, 116, 5567−5613

quality of the force field used. Electronic structure methods are generally too computationally expensive given the extensive configurational sampling required.

Finally, while traditional crystal structure prediction does not rely on any experimental data, there is an increasingly important application of CSP which seeks to identify unknown structures in concert with limited experimental diffraction or spectroscopic data from experiment. Even in cases where the final energy ranking proves difficult for CSP, the combination of energy plus other experimental observables often enables structural determination. The combination of NMR and/or powder X-ray measurements with CSP has proved particularly effective (section 3.7).[381−388] Other examples, such as the combination of terahertz spectroscopy[389] (section 3.6.2) or transmission electron microscopy (TEM)[390] with CSP also exist.

The next section discusses specific examples of crystal structure prediction in the context of crystal polymorphism.

3.4. Polymorphism

Given the widespread occurrence of polymorphism and the potentially dramatic differences in their properties discussed in section 1, there is considerable interest in understanding the possible crystal packing motifs and the relative stabilities among polymorphs. On one hand, the prediction of relative stabilities in crystals can be slightly more forgiving than lattice energy prediction due to partial error cancellation arising from similarities in the crystal packing and/or intermolecular interactions. On the other hand, even small errors/biases in the prediction of the interactions can prove problematic when attempting to resolve kJ/mol energy differences. Below, a number of illustrative examples from the literature are discussed to provide insight into the successes and challenges in modeling crystal polymorphs. Several additional examples of polymorphism, including ice, nitrogen, and carbon dioxide, are discussed in the context of predicting phase diagrams in section 3.5.

3.4.1. Aspirin. Aspirin has two known polymorphs. The structure of form I has been known for decades. However, despite years of lingering suspicions that another form might exist, the structure of form II was predicted only in 2004[391] and solved experimentally a year later.[392] Several years of controversy followed due to the difficulty of obtaining pure form II crystals and the major similarities in the crystal packing.[393−397] The two forms differ primarily in their interlayer hydrogen bonding pattern and turn out to be nearly degenerate energetically. Whereas form I adopts a dimer pattern, form II rotates the acetyl group slightly to form catemeric chains of hydrogen bonds (Figure 3).[393,394]

Aspirin exemplifies the beneficial error cancellations that can occur when computing polymorphic energy differences. Converging the lattice energy for aspirin requires large basis sets, switching from aug-cc-pVDZ to aug-cc-pVTZ increases the MP2 lattice energy by almost 20 kJ/mol, or 16% (see Table 4).[235] On the other hand, the energy difference between the two forms varies by only 0.1 kJ/mol.

In fact, PBE-MBD,[82] SCS-MP2,[235] and MP2C[266] all predict the two crystal forms to be degenerate within a few tenths of a kJ/mol. This excellent error cancellation stems from strong similarities in the crystal packing of the two forms. Note that some other DFT calculations using more empirical dispersion corrections do predict a somewhat larger difference in stabilities,[398] so the error cancellation here still depends on a good underlying description of the inter- and intramolecular interactions.

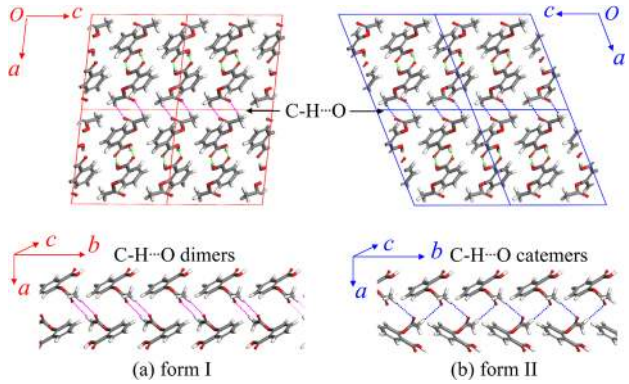

Figure 3. Comparison of the two polymorphs of aspirin. The primary difference arises in the interlayer hydrogen bonds: form I adopts dimers, while form II involves catemers. Reprinted with permission from ref 235. Copyright 2012 American Chemical Society.

Table 4. MP2 Lattice Energies of the Two Aspirin Polymorphs and the Relative Energy Difference $\Delta E_{I\rightarrow II}$ (kJ/mol)[235]

basis	form I	form II	$\Delta E_{I\rightarrow II}$
aug-cc-pVDZ	113.7	113.5	0.2
aug-cc-pVTZ	132.1	132.0	0.1

Of course, the near degeneracy of the electronic energies in aspirin raises the question of why form I dominates experimentally. Reilly and Tkatchenko[82] have argued that the preference for form I stems from the vibrational free energy contributions at room temperature. Interestingly, the strong stability preference in the vibrational free energy arises in the PBE-MBD model, but not in the PBE-TS model, which indicates that the many-body correlation effects captured by the MBD model are critical.

3.4.2. Oxalyl Dihydrazide. Oxalyl dihydrazide exhibits five known polymorphs: α, β, γ, δ, and ϵ. While detailed experimental energetics are not available, the β form is thought to be the least stable, and the α, δ, and ϵ forms all convert to γ upon heating.[400] However, the relative stabilities of α, β, and ϵ are unclear. Overall, this suggests the following relative energies: $\alpha, \delta, \epsilon < \gamma < \beta$.

Unlike aspirin, where a variety of different electronic structure methods predict essentially the same relative energies due to favorable error cancellation, in oxalyl dihydrazide, wide variations are observed as a function of basis set and electronic structure method used for both the structure optimization and the final single-point energies.

Figure 4 plots the relative MP2C energies (calculated with the HMBI fragment model) of the five polymorphs as a function of increasing basis set size. The qualitative polymorph ordering changes dramatically, from the α polymorph being the least stable in a small basis to being the most stable in the largest basis sets.

This marked basis set dependence stems from BSSE.[236] While the α form involves purely intermolecular hydrogen bonding, the other four forms involve a mixture of intra- and intermolecular hydrogen bonding. The standard counterpoise correction for BSSE was employed in the two-body (dimer) calculations. However, counterpoise corrections are ill-defined for intramolecular interactions. This means that while the

DOI: 10.1021/acs.chemrev.5b00648
Chem. Rev. 2016, 116, 5567−5613

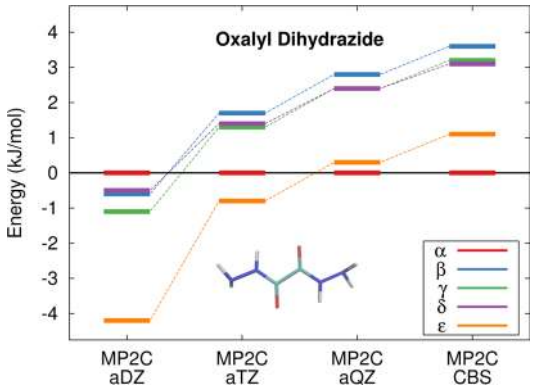

Figure 4. Relative polymorph energies in oxalyl dihydrazide are very sensitive to basis set. Predictions at the counterpoise-corrected HMBI MP2C level of theory.[236]

intermolecular hydrogen bond interactions computed are nominally BSSE-free, the intramolecular ones are artificially stabilized by BSSE. This causes the β, γ, δ, and ϵ polymorphs to be overstabilized in small basis sets. As the basis set is increased toward the CBS limit, the intramolecular BSSE decreases, and this artifactual bias toward intramolecular hydrogen bonds is eliminated. The MP2C/CBS limit polymorph ordering shown in Figure 4 is consistent with the experimental observations.

The variations in the relative stabilities predicted by different electronic structure methods prove even more perplexing. As shown in Figure 5, several plane wave DFT studies[127,399] using

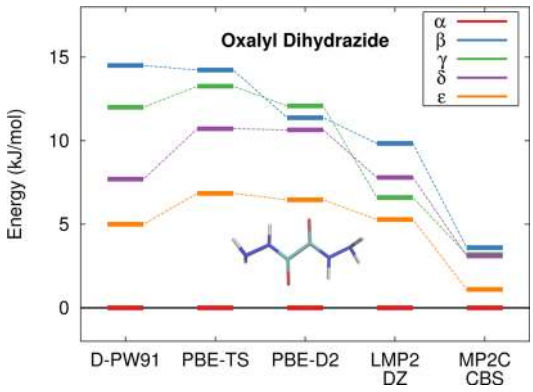

Figure 5. Relative polymorph energies in oxalyl dihydrazide are very sensitive to method. Comparison between several plane wave DFT calculations,[127,399] periodic local MP2/p-aug-6-31G(d,p),[127] and counterpoise-corrected HMBI MP2C/CBS limit.[236] Note that different optimized geometries were used in different studies, complicating the comparison.

different dispersion corrections predict that the polymorphs are distributed over a range of nearly 15 kJ/mol. The qualitative energy ordering is similar across all of them, though PBE-TS and PBE-D2 disagree on which polymorph is the least stable.

If B3LYP and Gaussian basis sets are used instead of plane waves (not shown here), one obtains qualitatively similar results without counterpoise correction.[127] However, efforts to counterpoise correct the periodic calculations drastically alter the energies, decreasing the energy spacing between the polymorphs.[127,236]

Similar variability in the polymorph energies is observed at the MP2 level, though other factors may also be involved. The periodic local MP2/p-aug-6-31G(d,p) energies, which do not include any counterpoise correction, predict a ~10 kJ/mol energy range and a partially correct ordering, though the γ polymorph incorrectly appears more stable than the δ one.[127] Note that these local MP2 results are completely different from the counterpoise-corrected double-ζ basis set fragment MP2 results,[236] which exhibit the same artificial stabilization of the β, γ, δ, and ϵ forms relative to the alpha one seen for MP2C in Figure 4. To whatever extent that BSSE is present in local MP2, it is affecting both the intra- and intermolecular hydrogen bonding nearly equally.

Fragment-based HMBI MP2/CBS (not shown) and MP2C/CBS calculations shrink the energy spacing substantially, and place the δ and γ forms at nearly the same energy.[236] Adding zero-point contributions to the HMBI results increases the separation among the δ, γ, and β forms, making the β and γ polymorphs somewhat less stable than the other three. The MP2C dispersion correction is significant: it shifts the energies of the β, γ, δ, and ϵ forms up by 1−2 kJ/mol relative to the α form.[236]

Geometry optimization also likely plays a significant factor in the variations seen in Figure 5. The stability of the α form (all-intermolecular hydrogen bonding motif) relative to the other forms (mix of inter- and intramolecular hydrogen bonding) is particularly sensitive to the structure optimization, for instance.[236] The lattice parameters obtained in three studies differ by relatively large amounts (see summary table in ref 127). Consider the α polymorph, for instance, where the predicted volumes range from 6.1% too small (PBE-D2 and norm-conserving pseudopotentials) to essentially perfect agreement with experiment (0.01% error with PBE-TS and norm-conserving pseudopotentials). However, the experimental structures were obtained at room temperature, while the predictions neglected temperature. Since some degree of thermal expansion is expected experimentally, the near perfect agreement obtained for PBE-TS is clearly fortuitous. Further analysis is needed to assess which structures are optimal.

In the end, it is unclear what the correct relative energies should be for this system. However, as noted earlier, a recent survey[14] found that half of all polymorph pairs were separated by less than 2 kJ/mol in lattice energy, and only 5% of cases exceeded 7.2 kJ/mol. This suggests (but does not prove!) that the smaller energy separations predicted by methods like the large-basis MP2C fragment calculations are more likely. Regardless, oxalyl dihydrazide continues to provide a challenging case of polymorphism for electronic structure predictions.

3.4.3. Diiodobenzene. Given the importance of getting polymorphic energy differences correct, there has been significant need for high-quality benchmark results. Hongo and co-workers[156−158] used DMC to predict the relative stability of the α and β polymorphs of diiodobenzene, an organic semiconductor material. This system represents the largest DMC calculations on a molecular crystal to date, and converging the results with respect to finite size effects, statistical sampling, and the fixed node approximation proved difficult.[157] Indeed, the DMC-predicted energy gap nearly doubled between the initial prediction of 4.4 ± 3.6 kJ/mol[156] and the recently refined value of 8.6 ± 5.3 kJ/mol.[157] The changes resulted from using a different supercell (1 × 3 × 3 instead of 1 × 1 × 1), a different trial nodal surface (PBE instead of LDA), and improved estimation of the finite cell effects (particularly for the kinetic energy).

DOI: 10.1021/acs.chemrev.5b00648
Chem. Rev. 2016, 116, 5567−5613

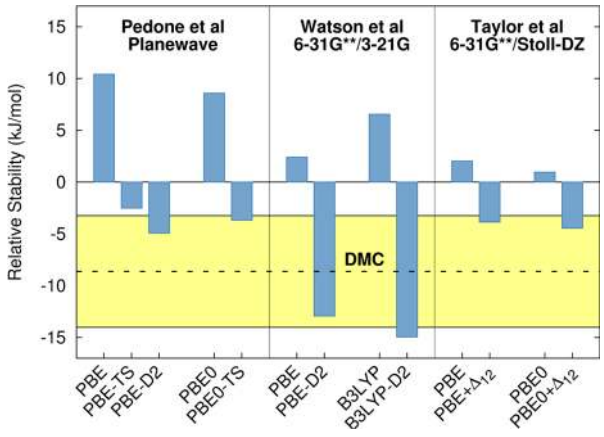

Figure 6. Comparison of the Diffusion Monte Carlo predicted energy difference between the α and β polymorphs of diiodobenzene[157] (yellow region) to values obtained using DFT,[158,159] dispersion-corrected DFT, and DFT corrected using 1- and 2-body SCS-MP2 increments.[160] Negative stability indicates an energetic preference for the α polymorph.

Given these DMC benchmarks, it is interesting to compare predictions from other methods. Figure 6 plots the stability difference between the two polymorphs as computed with a variety of methods (mostly DFT) across several studies[158−160] against the DMC predictions. First, note that dispersion is critical in this system. Without dispersion, PBE, B3LYP, and PBE0 all incorrectly predict the β polymorph as being more stable. Adding either the D2 or TS dispersion correction reverses the stability ordering. Alternatively, one can use an incremental approximation with SCS-MP2/aug-cc-pVTZ to correct the 1- and 2-body terms in the lattice energies (PBE $+\Delta_{12}$ and PBE0$+\Delta_{12}$), which also reverse the stability ordering.[160]

All of the dispersion-including results predict a stability ordering which lies within the DMC error bars, though none are particularly close to the central DMC value. It is interesting to note the sensitivity of the DFT results to the basis set approximations. For example, the plane wave/pseudopotential PBE and PBE0 results of Pedone et al.[159] favor β-diiodobenzene much more strongly than the double-ζ 6-31G** results of Watson et al.[158] and Taylor et al.[160]

Similarly, at the PBE-D2 level, the ∼13 kJ/mol energy preference for the α form found by Watson et al.[158] is 2.5 times larger than the ∼5 kJ/mol predicted by Pedone et al.[159] Both studies predict lattice parameters which underestimate the experimental cell volumes, which were measured at room temperature or higher, by 10−12%. However, crystals like this without strong intermolecular hydrogen bonding can undergo substantial thermal expansion (cf. carbon dioxide in Figure 2), so at least some of this underestimation simply arises from the neglect of any temperature affects in the geometry optimization.

Overall, these results do suggest that one can obtain good results with dispersion-corrected DFT models, but they also reiterate the importance of converging molecular crystal predictions as much as possible with respect to the model parameters. The small double-ζ basis sets used for the DFT calculations in refs 158 and 160 are probably inadequate. Civalleri and co-workers have demonstrated significant improvements in the unit cell volume predictions upon increasing from 6-31G** to a triple-ζ basis set, for instance.[53]

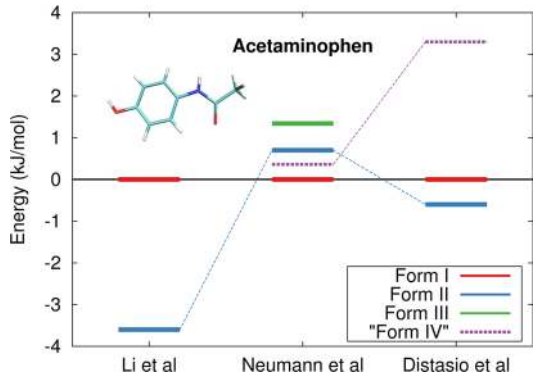

Figure 7. Relative energies of acetaminophen polymorphs, including the putative form IV,[405] from three dispersion-corrected DFT studies.[47,401,405]

3.4.4. Acetaminophen. Acetaminophen (paracetamol) represents another classically challenging case in polymorphism. It has two well-known polymorphs, forms I and II, and substantial controversy has surrounded which form is the most stable at 0 K, both experimentally and theoretically.

At the DFT level, three different studies have obtained somewhat different predictions (Figure 7). Using B3LYP and an empirical dispersion correction, Li et al.[401] predicted that form II is several kJ/mol more stable than form I. This difference seems larger than what has been suggested from analysis of thermochemical data.[402−404] In contrast, two other dispersion-corrected DFT studies predict a sub-kJ/mol energy separation between the two forms. However, while the empirical DFT-D model of Neumann and co-workers predicts form I to be more stable,[405] the PBE-MBD model of DiStasio and Tkatchenko favors form II.[47]

Two other notable features have arisen from electronic structure modeling of acetaminophen. First, while evidence of form III acetaminophen has existed for decades, its structure had long been a mystery. In 2009, Perrin and co-workers[406] obtained high-quality powder X-ray data, which they combined with crystal structure prediction to solve the structure. The sixth-most stable structure found in the CSP search had lattice parameters in good agreement with the experimental lattice parameters. Subsequently, improved powder X-ray data allowed the researchers to solve the structure independently and confirm the structure predicted with DFT. Nevertheless, limitations in the experimental data meant that having the CSP results was crucial for assigning the structure with confidence.

Interestingly, the same CSP study also predicted[405] forms I (rank 1) and II (rank 3). Several other low-energy crystal forms also arose in the CSP. Most of these exhibited very similar hydrogen bonding networks to forms II and III, and it was suggested that those predicted structures probably convert to form II readily. However, the rank 2 structure exhibited a completely different crystal packing motif than any of the other forms. This new structure consists of two interpenetrating 3-D networks of hydrogen bonds. The authors hypothesized that this might be a new, as yet unobserved polymorph, which they tentatively termed form IV.

As yet, there has been no experimental evidence to confirm this hypothesis. DiStasio and co-workers also computed the polymorph energetics of form IV with PBE-MBD,[47] and found that it lies a few kJ/mol above forms I and II. They argue that this reflects the importance of many-body dispersion effects. If

DOI: 10.1021/acs.chemrev.5b00648
Chem. Rev. 2016, 116, 5567−5613

these PBE-MBD energetics are correct, they substantially decrease the likelihood of observing form IV, since several other more stable forms exist. Nevertheless, there are examples of experimentally observed polymorphs in other systems whose energies differ by larger amounts,[14] so one cannot rule out form IV entirely.

3.4.5. Glycine. Glycine is another polymorphic crystal which proves challenging. It has three polymorphs lying extremely close in energy. Given the strong hydrogen bonds between glycine molecules and the zwitterionic nature of the glycine molecules, one might assume that van der Waals dispersion is relatively unimportant. However, Marom et al.[79] demonstrated that many-body van der Waals dispersion effects are critical to achieving the proper polymorph ordering.

Figure 8 compares the relative stability of the α, β, and γ polymorphs for PBE and PBE0 with different dispersion

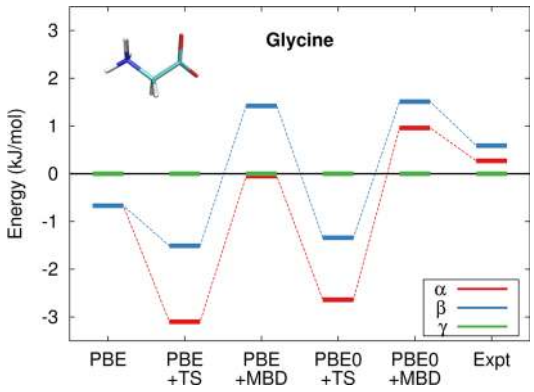

Figure 8. Relative energies of the glycine polymorphs from DFT and experiment.[79] PBE0-MBD is the only model which obtains the qualitatively correct ordering. Zero-point energy is included in all cases except the PBE case without dispersion correction.

corrections. Experimentally, the γ form is preferred, while the β form is the least stable: $\gamma < \alpha < \beta$. However, the energy separations are only a fraction of a kJ/mol in each case. Neither PBE, PBE-TS, nor PBE0-TS captures the correct ordering. All three incorrectly predict that the γ form is the least stable, instead of the most stable. The energy spacings between polymorphs are also much too large.

If one uses the many-body dispersion correction instead of the pairwise TS one, the γ polymorph becomes much more stable, and the β polymorph correctly becomes the least stable. However, whereas PBE-MBD slightly overstabilizes the α polymorph, PBE0-MBD gives a qualitatively correct stability ordering. PBE0 has been shown to describe hydrogen bonds and short-range van der Waals interactions more reliably than PBE.[101,149] Similar conclusions regarding the importance of many-body dispersion effects on the polymorphic ordering were drawn for oxalic acid and tetrolic acid in the same study.[79]

The glycine lattice parameters are also substantially improved by the inclusion of beyond-pairwise dispersion effects. The errors compared against low-temperature experimental structures drop from around 3% with PBE-TS to less than 1% with PBE-MBD.

Finally, glycine also represents a case where vibrational zero-point and thermal energy contributions are significant to the polymorphic ordering.[407] Indeed, a recent survey of 508 sets of polymorphic crystals found that vibrational contributions were sufficiently large to rerank polymorphs in 9% of cases.[14]

3.4.6. Chiral Crystals. While not technically polymorphism, the crystals of chiral molecules provide a closely related problem that is interesting and challenging to model. Crystallization from a racemic solution can result in a racemic compound (~90% of known cases), a conglomerate (~10%), or a pseudoracemate (rarely).[408] A racemic compound includes a heterochiral mixture of both enantiomers in a well-ordered lattice, while a conglomerate is a collection of enantiopure crystals. A pseudoracemate involves a heterochiral mixture of enantiomers which are randomly distributed through the lattice. Most chiral pharmaceuticals have traditionally been sold as racemic mixtures,[408] but enantiopure forms are increasingly preferred.[409] Accordingly, the nature of the crystal formed can be very important for the physiochemical properties of the drug. Alternatively, in some cases crystallization with a chiral coformer can be used for chiral separation.

From the electronic structure modeling perspective, the primary focus in this area has been on the prediction of whether crystals will preferentially form homochiral conglomerates or heterochiral racemates. Several studies have used CSP to predict potential homochiral and heterochiral structures and to compare their lattice energies. Two force field studies by Gourlay et al.[410,411] had mixed success. In several examples they correctly predicted whether a heterochiral or homochiral structure was preferred, though the specific structures predicted sometimes differed from the experimental ones. A subsequent reassessment[412] of these structures using the GRACE DFT-D methodology resulted in substantial improvements: they correctly predicted all structures that resolve spontaneously into homochiral crystals. The experimental structures also always appeared as rank 1 or 2 in the CSP prediction, lying no more than a couple tenths of a kJ/mol from the most stable structure found.

Another pair of studies examined a melatonin agonist, which exhibits both racemic and enatiopure crystallizations. Intriguingly, two enantiopure polymorphs of the biologically inactive *S* enantiomer have been produced, but only the less stable of the two has been achievable using the *R* enantiomer.[413] A recent DFT-D CSP study examined this system and suggested strategies for obtaining the "missing" *R* form.[414]

The aforementioned DFT-D study of several chiral crystals[412] highlighted the difficulty of predicting whether a racemate or a conglomerate of enantiopure crystals will form: the average predicted energy gap between racemic and enantiopure crystals they examined was less than 2 kJ/mol, and the smallest gap was only 0.4 kJ/mol. These small energy differences arise from the often very similar intermolecular packing motifs observed in homo- and heterochiral crystals, and they raise questions about the potential importance of entropic/finite-temperature effects and crystallization kinetics on the resulting crystals formed.[415,416] Indeed, the tartrate salts which Pasteur famously separated crystallize as a conglomerate only below 28 °C; at higher temperatures they form racemic crystals.[417]

Finally, with an eye toward separations/enrichment of a given enantiomer based on slight differences in solubility and enantiomeric excess (ee), Otero-dela-Roza et al.[90] predicted the ee for 10 different amino acids using DFT and the XDM dispersion correction. This represents a challenging test, since a range of 0−95% ee corresponds to an energy range of only 4.5 kJ/mol. They successfully predicted the ee with a mean error of only 10% relative to experiment.

DOI: 10.1021/acs.chemrev.5b00648
Chem. Rev. 2016, 116, 5567−5613

Finally, methods that combine QM intramolecular conformational energies with force field intermolecular modeling have also had successes.[415,418] In a notable example, CSP predicted that the therapeutically used homochiral naproxen should actually prefer to form a more stable racemic crystal.[418] The authors managed to characterize this racemic crystal experimentally and confirm that it is thermodynamically more stable. Unlike many such cases, homochiral and heterochiral structures of naproxen exhibit very different packing. It is worth noting, however, that the predicted thermodynamic preference for racemic naproxen was several times larger than the experimental one, and that more accurate energetics would be needed in many cases to make a useful prediction.

3.4.7. Multicomponent Crystals. The crystals discussed above have all consisted of a single chemical species. However, multicomponent crystals containing two or more distinct chemical species occur in many contexts. For instance, cocrystallization provides a powerful tool for tuning crystal properties, and there is considerable interest in predicting when cocrystals will form. There have been a number of studies using force-field based methodologies,[419,420] but one DFT-D study[421] scanned 102 known cocrystals and salts involving nicotinamide, isonicotinamide, and picolinamide. In 97% of the cases, DFT-D correctly predicted that the cocrystals were more stable than the independent coformers. The structures and/or stabilities of hydrates, solvates and salts have also been predicted successfully.[422,423] On the other hand, such species can be especially challenging. As noted in section 3.3, gallic acid proved particularly problematic in the fifth blind test, and it exhibits a particularly complicated crystal energy landscape (section 3.4.8).

3.4.8. Crystal Energy Landscapes. Another important advance has been the exploration of the crystal energy landscapes produced by CSP.[15,424,425] In drug development, for instance, extensive polymorph screening is often carried out to search for potential stable, low-energy polymorphs that might prove problematic, to avoid situations such as the one that happened to ritonavir.[9,10] Polymorph screening is usually done experimentally, but theoretical prediction has advanced to the point that CSP can prove helpful, particularly if it is involved early enough in the drug development process. Not only can CSP identify the most stable structures, but the crystal energy landscape provides insights into the types of packing motifs which are accessible and can drive the search for new crystal forms. A study on gallic acid, in which the experimental crystallization screening was motivated by CSP results, produced evidence for three anhydrate polymorphs, 5 monohydrates, and over 20 solvates![6]

A very recent GRACE DFT-D CSP study[349] on the drug dalcetrapib while it was still under development predicted two as yet unknown polymorphs which might be more thermodynamically stable than the experimentally known ones. Further calculations indicated that these dense polymorphs might be crystallized at high pressure. Subsequent high-pressure screening did in fact produce one of the two forms experimentally, though it turned out to be only metastable at atmospheric pressure.

Braun et al.[426] similarly demonstrated the relevance of crystal energy landscapes for two different small-molecule drugs, DB7 and B5. Both drug molecules have similar molecular structures, but they exhibit completely different crystallization behavior. DB7 in particular is known to form several polymorphs. Despite the relative complexity of these species from the perspective of CSP (flexible molecules with diverse intermolecular interaction possibilities), analysis of the predicted crystal energy landscape helped rationalize the experimentally observed crystallization behaviors and rule out the existence of unknown polymorphs with significantly greater stability and lower solubility.

However, obtaining reliable energy rankings of the different potential crystal structures proved difficult. In addition to various simpler models, the authors reoptimized a number of low-energy structures with PBE-TS and also performed single-point energy calculations on those structures with PBE-D2. For DB7, results from both dispersion corrections predict that form II is several kJ/mol more stable than form I, in reasonable agreement the energetics inferred from differential scanning calorimetry (DSC) experiments (Figure 9). However, they

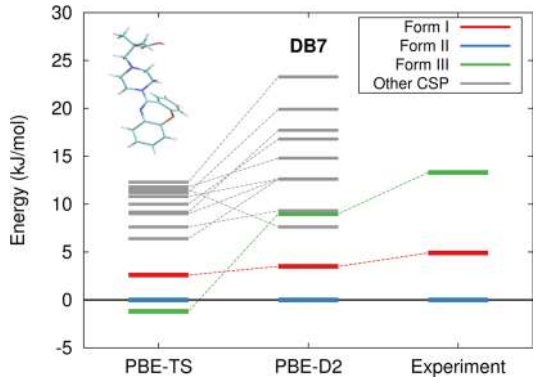

Figure 9. Energies of different DB7 structures generated via CSP using two different dispersion corrections on an identical set of crystal geometries.[426] The experimentally observed forms are highlighted, along with estimated energy differences from DSC. Other low-energy structures from the CSP search are in gray.

completely disagree on the relative stability of form III. PBE-TS predicts that it is the most stable form, while PBE-D2 says it is the least stable of the experimentally observed polymorphs. If one also considers other low-energy structures generated in the CSP search, the energy rankings between PBE-TS and PBE-D2 vary dramatically. Similar discrepancies in polymorph rankings between PBE-TS and PBE-D2 have been reported for B5[426] and methyl paraben.[427]

3.4.9. Summary. Substantial progress has been made in the effort to predict crystal polymorph energetics. The examples described above clearly demonstrate that dispersion-corrected DFT provides a powerful tool for modeling molecular crystal polymorphism. DFT will likely be the first (and in many cases only) electronic structure tool used to model polymorphs.

However, it is also clear that the subtle energy balances in polymorphic systems mean that it can be difficult to obtain unambiguous predictions for the relative stabilities of different packing motifs. This is particularly true when one compares very different crystal packings. The nature of error cancellation means that it tends to be easier to rank structures that share a common intermolecular packing motif than to resolve the energies between two very different motifs.

In particularly challenging polymorphic crystals, different density functionals or even different dispersion corrections applied to the same functional produce different relative polymorph orderings. Sometimes, this behavior can be rationalized. For example, in glycine, switching from a GGA to a hybrid density functional and including beyond-pairwise

DOI: 10.1021/acs.chemrev.5b00648
Chem. Rev. 2016, 116, 5567−5613

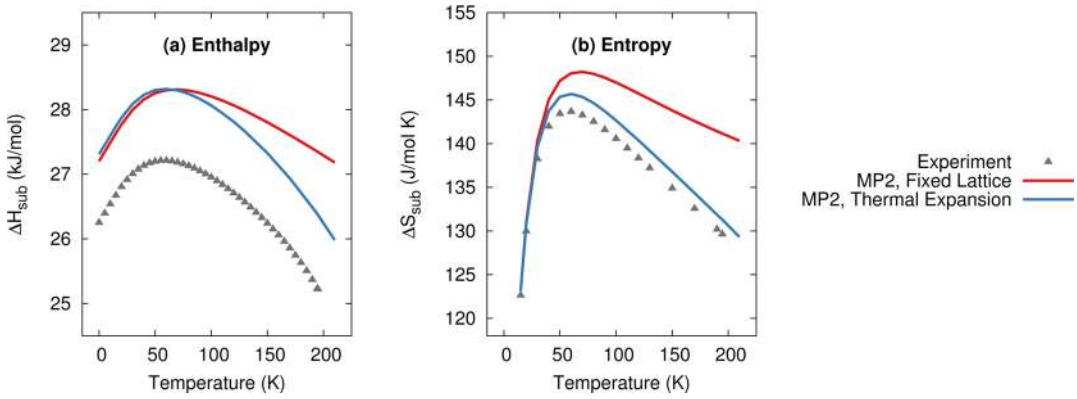

Figure 10. Enthalpy and entropy of sublimation in CO_2 exhibit considerable temperature dependence. MP2/CBS limit calculations including quasiharmonic thermal expansion capture the temperature dependence fairly well, while a simple fixed-lattice harmonic approximation overestimates the quantities at high temperatures.[233]

van der Waals interactions leads to improved agreement with experiment. In cases like the DB7, however, the reasons underlying the different energetics are less obvious.

In such scenarios, wave function methods (either fully periodic or fragment-based) offer an alternative that can help clarify the conflicting DFT predictions. In smaller molecules (up to a few dozen atoms), at least, one can explore how the polymorph energetics converge as a function of method (MP2, coupled cluster, etc.) and basis set in order to place plausible error bars on the relative energetics and to assess one's confidence in the predicted relative stabilities. Of course, one should not forget that the method used to optimize the structures can also have significant effects on the energetics (e.g., oxalyl dihydrazide).

3.5. Phase Diagrams

Predicting phase boundaries and phase diagrams is closely related to polymorph prediction. In this case, however, one typically seeks to find temperatures and pressures at which the most stable phase changes, as governed by the Gibbs free energy

$$G(T, P) = U_{el} + PV + F_{vib}(T, P) \quad (10)$$

which depends on the electronic energy U_{el}, a pressure−volume (PV) term which typically becomes significant in solids only at high pressures, and a Helmholtz vibrational free energy term F_{vib}.

The Nyman and Day survey[14] of 508 sets of polymorphic crystals found that harmonic Helmholtz vibrational free energy often contributes ∼1 kJ/mol or less to the relative stabilities between polymorphs at ambient conditions. While small, it was sufficiently large to alter stability orderings in about 10% of the cases. Interestingly, the vibrational free energy contribution often opposes the lattice energy difference, which will lead to temperature-dependent changes in polymorph phase stability at some temperature (unless the crystal melts first).

Most phase stability studies in the literature have focused on high-pressure phases, either ignoring temperature effects or employing a standard harmonic approximation to estimate the vibrational free energy contribution. As noted in section 3.2, however, crystal unit cell volumes can expand appreciably with temperature, which can result in a nontrivial temperature dependence for the enthalpy and entropy (see Figure 10). Perhaps surprisingly, thermal expansion can matter even at high pressures. At 5 or 10 GPa, thermal expansion increases the cell volume of phase I carbon dioxide by 4% and 1%, respectively.[233] A subsequent study[234] analyzed the importance of thermal expansion on enthalpies, entropies, and free energies of sublimation. At room temperature, neglecting thermal expansion introduces errors of up to a few kJ/mol in the enthalpy (ΔH) and entropy ($-T\Delta S$) contributions to the free energy. Notably, however, the signs of these errors frequently cancel to produce smaller errors in the final free energy. Nevertheless, the remaining 1−2 kJ/mol free energy errors at room temperature may be sufficient to affect relative stabilities for closely spaced polymorphs.

The quasiharmonic approximation provides a relatively simple means of incorporating thermal expansion effects, and it appears to work well, at least for small rigid molecules.[34,233,234,428] In carbon dioxide, for example, the quasiharmonic approximation captures the correct rate of thermal expansion (Figure 2) and reproduces the temperature dependence of the enthalpy and entropy of sublimation (Figure 10) over a broad temperature range.[233]

Alternatively, one might use molecular dynamics to estimate finite temperature and pressure effects and/or compute free energies. While the latter can be used very successfully with classical force fields,[373,374,377,379,429−431] such techniques are usually computationally prohibitive with electronic structure methods at present.

DFT studies of high-pressure molecular crystal phases under pressure have become routine. A variety of unusual phases for hydrogen, nitrogen, ice, carbon dioxide, and other small molecules have been detected experimentally in recent years, and theory can help determine the structures of these phases, identify their regions of phase stability, or even suggest potential new phases to look for experimentally. Monte Carlo searches,[432−436] global optimization,[369,437] and evolutionary crystal structure prediction algorithms[366−368] have proved particularly effective for these purposes.

High pressure phases do create some challenges for electronic structure methods. The errors observed for many widely used electronic structure models increase at short intermolecular separations, as shown for example in benchmarks on the S22 × 5[260] and other test sets. At ordinary pressures, the short-range behaviors are not too important because molecules do not inhabit those regions of the potential energy surface. However, extreme pressures push molecules closer together into these short-range repulsive regions of the PES.

DOI: 10.1021/acs.chemrev.5b00648
Chem. Rev. 2016, 116, 5567−5613

Many high-pressure DFT studies in the literature neglect dispersion corrections under the argument that dispersion effects become comparatively less important when crystals are compressed under several GPa of external pressure. Other studies have shown that inclusion of dispersion corrections can change the phase stability substantially and even alter the phase transition pressure among various high-pressure forms of ice by 1 GPa or more.[77,149] Many successful and inexpensive dispersion corrections are widely available, and it is probably better to include such corrections regardless of pressure.

At very high pressures, molecular phases sometimes give way to covalent or even metallic phases. Such transitions can provide problems for fragment-based methods, because fragmentation is either inappropriate (metallic phases) or because the definition of the individual fragments likely changes when a covalent solid is formed. Periodic DFT is generally more suitable in such cases, though it is not perfect. For example, DFT predicts a metallic hydrogen phase at pressures of 300−400 GPa, which contradicts both experimental and DMC results.[154,155]

The following sections provide example applications on some nominally simple compounds which exhibit rich solid-state phase behaviors. Of course, many of the same sorts of issues apply to more complicated organic compounds like benzene, for instance. Controversy has surrounded the possible existence of a $P4_32_12$ space group phase of benzene in the ∼2−4 GPa range.[438,439] The existence of this phase has been examined with both force field free energy models[373,377] and DFT calculations.[366,440] High-pressure phase transitions in tetracyanoethylene[441] and even the pharmaceutical dalcetrapib[349] have also been studied.

3.5.1. Nitrogen. Nitrogen exhibits an extraordinarily rich phase diagram, with at least a dozen reported solid phases, though many of these have not been fully characterized. A series of molecular phases exist at lower pressures. However, at pressures above 150 GPa, molecular nitrogen transforms to polymeric nitrogen. The transformation of nitrogen to a polymeric structure was first proposed in 1985,[442] and its cubic gauche polymeric structure was first predicted from DFT in 1992.[443] Not until a decade later was it actually produced and characterized experimentally.[444]

The success of these predictions have inspired many other studies trying to determine the structures of ill-characterized phases and seeking to predict new polymeric phases.[432,445−453] Advanced structure prediction algorithms which rely on random searching, particle swarm optimization, or evolutionary algorithms have proved particularly effective in identifying new polymeric bonding motifs.[432,451,452,454] Additionally, a recent study raised the possibility for a molecular N_8 crystal phase, which was predicted to be more stable than the polymeric phases for pressures below 20 GPa.[455] Some studies have also tried to unravel the transition mechanisms between phases.[8,446,456]

While most work on nitrogen has been carried out using DFT, a couple of studies were performed using periodic local MP2. Erba and co-workers[125] characterized the pressure-induced phase changes for three low-temperature molecular phases of solid nitrogen using periodic local MP2. They predicted a phase transition pressure of 0.42 GPa (vs 3.6 GPa experimentally) for the $\alpha \rightarrow \gamma$ transition, and a $\gamma \rightarrow \epsilon$ phase transition pressure of 2.25 GPa (vs 2 GPa experimentally). For comparison, a different study[432] using the PBE density functional without dispersion correction predicted the $\alpha \rightarrow \gamma$ transition at 0.47 GPa, in close agreement with MP2 and experiment. On the other hand, they found that PBE predicted that the ϵ phase never becomes more stable the γ phase.

Erba et al.[457] also investigated the transition to polymeric nitrogen with local MP2 and B3LYP-D*. In agreement with earlier DFT studies that did not include van der Waals dispersion, they found that both MP2 and B3LYP-D* predict the phase transition to polymeric nitrogen should occur at much lower temperatures and pressures than has been observed experimentally. This suggests an important role for kinetics in the experimental transition.

3.5.2. Ice. Ice provides ample opportunity for phase diagram studies. In addition to the aforementioned studies investigating the roles of dispersion in high-pressure phases,[77,149] there have been many other studies. Most ice phases come in pairs: a high-temperature one with disordered protons, and a lower-temperature proton-ordered one.[458] Much effort has gone into investigating these order−disorder phase transitions and determining the most stable proton arrangements in the ordered phases.[37,237,459−468]

Several new phases of ice have been proposed or discovered in recent years, and theory has played an important role in their characterization. For example, Tribello and co-workers[469] used blind crystal structure prediction to examine the potential proton orderings of ice XIV, and ended up proposing two potential metastable proton orderings that could help explain neutron diffraction data.

Another set of studies investigated the proton ordering in ice XV, which is the recently discovered proton-ordered analog of ice VI. Experiments (with the help of DFT to interpret the Raman spectrum[470]) suggest that the structure is an antiferroelectric one with $P\bar{1}$ symmetry, while multiple DFT studies have favored a ferroelectric Cc symmetry structure.[460,463] In contrast, fragment-based MP2 calculations suggested that the $P\bar{1}$ structure was actually more stable,[237] but subsequent fully periodic MP2 calculations have come to the opposite conclusion.[37]

Fragment-based MP2 has been used to argue against the existence of two types of hydrogen bonds in ice Ih[336] and against a previously predicted phase transition of ice VIII to a hypothetical ice VIII' form at 2−3 GPa.[184] In response to an earlier prediction of a metastable tetragonal ice 0 phase based on atomistic potentials, Quigley et al.[151] confirmed the mechanical stability of ice 0 and examined potential proton orderings using a mixture of DFT and DMC. Pickard et al.[436] went well beyond the standard gigapascal pressure range to examine the behavior of ice at terapascal pressures. They predicted that ice decomposes into hydrogen peroxide and a hydrogen-rich phase at pressures over 5 TPa. Finally, several potential new gas hydrate phases have been proposed on the basis of structures discovered using evolutionary algorithms.[367]

3.5.3. Carbon Dioxide. At least seven different solid carbon dioxide phases exist, and a few additional ones have been reported but not independently confirmed. At high pressure, it becomes a covalent solid thought to adopt a structure similar to that of SiO_2. Several phases at lower pressure are clearly molecular, but there has been significant controversy about whether phases II and IV form "intermediate" phases, perhaps with bent molecules and elongated C−O bond lengths. DFT studies[71,471] and more recent experimental studies[472,473] have challenged this intermediate bonding state hypothesis, however, arguing instead for a more traditional linear carbon dioxide molecule in both phases.

DOI: 10.1021/acs.chemrev.5b00648
Chem. Rev. 2016, 116, 5567−5613

Due to initial difficulties in characterizing the polymeric phase V experimentally, a number of DFT studies attempted to predict the structure of this high-pressure phase.[474−480] Most of these studies identified a structure which is isomorphic to the β-cristobalite phase of SiO_2. Recent X-ray diffraction results confirm the predicted β-cristobalite structure.[481]

Other studies have examined aspects of the phase diagram using fragment methods and correlated wave function methods. Li and co-workers[185] used fragment MP2 calculations to predict the phase transition between phases I (dry ice) and III (Figure 11). This transition occurs with much hysteresis, making the thermodynamic phase boundary difficult to determine experimentally. The MP2 calculations predict that the phase boundary occurs in the range of 12−13 GPa and exhibits weak temperature dependence, which agrees fairly well with the values of 10−12 GPa found in a number of experimental studies. For comparison, an earlier DFT study[471] using PBE predicted the phase transition to be somewhat higher at 16 GPa, and to have a much more pronounced temperature dependence. On the other hand, PBE-D3 predicts the transition pressure around 12 GPa,[71] in good agreement with the MP2 result.

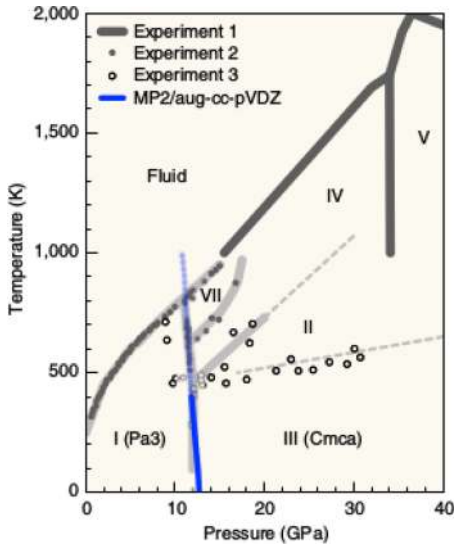

Figure 11. Phase diagram of carbon dioxide comparing predictions of the phase boundary between phases I and III at the MP2/aug-cc-pVDZ level (using binary interaction) with the experimental data.[185] Reprinted with permission from ref 185. Copyright 2013 Nature Publishing Group.

A separate study[233,234] predicted the sublimation temperature of phase I carbon dioxide at atmospheric pressure using fragment-based MP2 and CCSD(T) extrapolated to the CBS limit and quasiharmonic thermal expansion. CCSD(T) predicts a sublimation temperature of 198.0 K, in good agreement with the experimental value of 194.7 K.

3.5.4. Disordered Crystal Phases. Crystals can exhibit either static and/or dynamic disorder. Dynamic disorder can refer to, for instance, the thermal motions of an alkyl group or the dynamics of a hydrogen-bonded proton moving back and forth between the donor and acceptor. Modeling this sort of disorder can be very important when interpreting solid-state NMR experiments (section 3.7), for instance. Static disorder, also known as configurational disorder, occurs when a crystal exhibits a statistical mixture of configurations such that there exists local ordering in the crystal, but no long-range order.

Hexagonal ice (ice Ih) provides a classic example of static disorder. The oxygen atoms in ice Ih are arranged in a hexagonal wurtzite lattice, while the hydrogen atoms in each molecule are orientationally disordered. According to the Bernal−Fowler ice rules, the protons randomly occupy two of the four possible positions such that each water molecule donates two hydrogen bonds and accepts two others in a tetrahedral arrangement. The energy differences between these different proton orderings are small, and configurational entropy stabilizes the disordered form over the ordered one at higher temperatures. The ordered form eventually becomes more stable at sufficiently low temperatures. Similar behaviors are observed for most other phases of ice, as noted in section 3.5.2.

Predicting the temperatures at which these proton order/disorder transitions will occur thermodynamically has been an interesting problem, as discussed in section 3.5.2. The most straightforward approximation computes the energies of the different symmetry-unique arrangements of the protons in the primary unit cell or a small supercell.[463,465] Boltzmann averaging these configurations allows prediction of the phase transition temperature, though the accuracy is limited by the use of a small periodic cell.

A more elaborate model[459] combines small-cell DFT calculations and uses graph invariant representations to construct a model for how the energy depends on the hydrogen bond topology based on fitting to DFT results in small unit cells. This model can then be used to bootstrap the small-cell DFT results to much larger unit cells from which free energies can be computed using Monte Carlo thermodynamic integration techniques. Singer and co-workers have used this strategy to predict the order−disorder transitions in many different ice phases.[459−462,464]

Fragment methods provide another means of handling this sort of problem. Like many ices, nitrous oxide (N_2O) occurs as a disordered structure. N_2O adopts the same crystal packing and $Pa\bar{3}$ space group as carbon dioxide, albeit with with a statistical arrangement of the molecules (i.e., oriented as either N−O−O or O−O−N along the molecular axis). To model this system, Müller and Spångberg[482] computed the ensemble average over the ordered configuration and a set of 10^5 randomly selected disordered configurations cut out from the crystal. While there are large numbers of potential disordered crystal structures, the number of potential local environments surrounding a given molecule in the crystal is much smaller. Using the incremental approach, the authors were able to compute energies these 10^5 configurations in the ensemble using only $\sim 10^2$ fragment energies. Their estimated local CCSD(T) results predict that the disordered structure becomes more stable above 60 K.

3.6. Vibrational Spectroscopy

Crystal phonons contribute to the free energies used to assess phase stability (section 3.5), but they also provide a useful tool for characterizing crystal structures via infrared (IR), Raman, terahertz, and inelastic neutron scattering spectroscopy (INS) experiments. Theory complements such experiments nicely by predicting and assigning the vibrational spectra, as discussed in the following sections.

3.6.1. IR, Raman, and INS Spectra. Obtaining high-quality X-ray diffraction data for high-pressure crystal phases can be

DOI: 10.1021/acs.chemrev.5b00648
Chem. Rev. 2016, 116, 5567−5613

challenging, and vibrational spectroscopy can provide structural information even when full crystal structures cannot be readily obtained. For instance, phase VII carbon dioxide appears to adopt the same space group and similar lattice parameters as phase III, but its structure has not been solved. However, the distinction between the two structures has been argued in part based on differences in their respective Raman spectra.[483] In another example, the antiferroelectric proton-ordering in ice XV inferred from powder X-ray diffraction was confirmed via Raman spectroscopy and density functional predictions of the phonon modes in the different potential structures.[470]

Numerous other examples can be found in the literature. Many of the studies that have attempted to predict high-pressure phase diagrams of nitrogen[444,448,450−452,484] or carbon dioxide,[471,475,480] for instance, also predict phonon modes for comparison with existing or future spectroscopic experiments. Reilly et al.[485] studied the phonon spectrum of phase I ammonia using both molecular dynamics and lattice dynamics techniques. While both were in generally good agreement, the harmonic approximation in the lattice dynamics moderately overestimates the frequencies. More interestingly, the calculations allowed the reassignment of a number of the low-frequency phonon modes in the experimental spectrum. Examples in polymorphic crystals[486] and energetic materials[487,488] can also be found.

The Hirata group has performed a number of studies examining phonon modes in crystals under pressure using fragment-based MP2, as summarized in a recent account.[193] Fragment-based methods offer the advantage that they make the calculation of phonon dispersion away from the zone-center (k = 0) particularly facile. By exploiting the symmetry of the dimers and the distance cutoffs which truncate long-range dimer interactions, the additional computational cost associated with performing supercell calculations for lattice dynamics becomes marginal.[178] They have also implemented the ability to compute infrared and Raman band intensities in their binary interaction fragment approach.[336]

For example, Hirata[178] resolved a controversy regarding the interpretation of the vibrational spectra for formic acid by demonstrating that the experimental spectrum corresponded to the β_1 polymorph, rather than a mixture of multiple forms. In carbon dioxide, Li et al.[185] predicted the MP2-level Raman spectra as a function of pressure to confirm experimental spectra which had previously been assigned to phase I and III. Sode et al.[186−188] used a combination of an intramolecular force field fitted to CCSD(T) and intermolecular fragment MP2 to explain the Fermi resonance (a strong anharmonic mode−mode coupling between the symmetric stretch and first overtone of the bending vibration) in phase I. Interestingly, one can tune this resonance based on the distinct responses exhibited by the two modes under external pressure. The authors were able to reproduce the observed pressure dependence of the frequencies and intensity ratios with quantitative accuracy.

In ice Ih, it had been suggested (though not widely accepted) that the presence of two peaks in the hydrogen-bond stretching region of the INS spectrum might indicate two distinct types of hydrogen bonds: one weaker and one stronger. He et al.[336] refuted this hypothesis by showing that these peaks could be explained in terms of modulations of different Cartesian components of the dipole moment. Gilliard et al.[184] studied the pressure-dependent IR, Raman, and INS spectra and argued against a proposed phase transition from ice VIII to ice VIII' in the 2−3 GPa range. Figure 12 shows the high quality of the agreement between the predicted and experimental INS spectra.

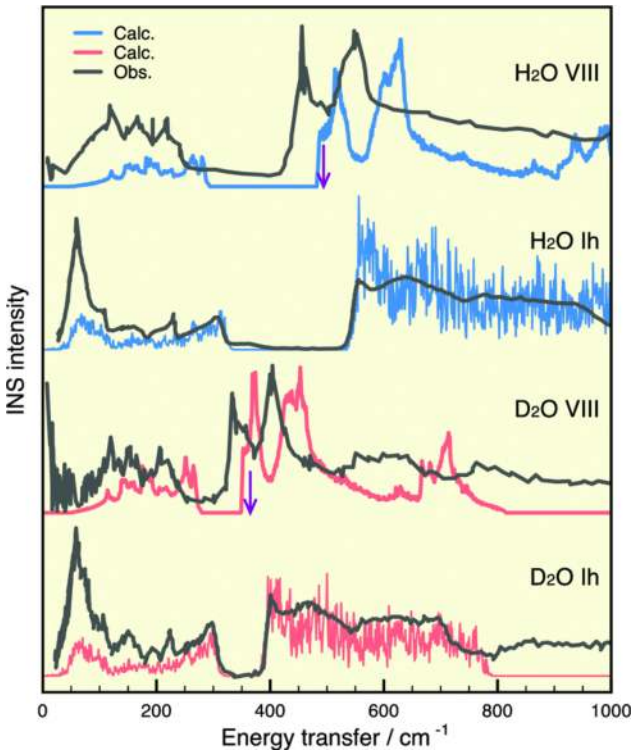

Figure 12. Comparison between experimental and predicted (binary interaction MP2/aug-cc-pVDZ) inelastic neutron scattering spectra for ices Ih and VIII.[184] Reprinted with permission from ref 184. Copyright 2014 American Institute of Physics.

Finally, Sode et al.[190] used MP2 and CCSD to predict the phonons in solid hydrogen fluoride. Both improve upon the phonon frequencies predicted using Hartree−Fock theory. Substantial further reduction in error between the predicted and experimental frequencies was obtained by including two-mode coupling anharmonic corrections. They also examined the high-pressure dependence of the phonons and predicted the phonon density of states to rationalize peaks observed in the INS spectra.[183,190]

3.6.2. Terahertz Spectroscopy. Terahertz spectroscopy[489] allows one to probe the low-frequency lattice vibrations below ~200 cm^{-1}, and it provides noninvasive and nondestructive "fingerprints" for the crystal packing. Even seemingly small changes in crystal packing can produce notable changes in the translations and librations observed in the terahertz region. Carbamazepine, for example, adopts the same hydrogen-bonded dimers across multiple polymorphs, but the structures differ in how these dimers pack relative to one another. These differences in crystal packing clearly manifest in the terahertz spectrum.[490] This makes terahertz spectroscopy particularly interesting for pharmaceutical applications, where it can distinguish among polymorphs, hydrates, and even racemates/enantiopure crystals.[491]

However, assignment of lattice vibration modes in this region is extremely difficult without theoretical solid-state phonon predictions. Periodic DFT calculations have proved helpful in interpreting terahertz spectra. Early examples include applications to β sheets of trialanine,[492] two different energetic materials,[493,494] lactose monohydrate,[495,496] and biotin.[496]

DOI: 10.1021/acs.chemrev.5b00648
Chem. Rev. 2016, 116, 5567−5613

More recently, DFT has been used to compare the terahertz spectrum in two dicyanobenzene isomers,[497] to distinguish between two different hyrdohalide salts of 5-(4-pyridul)-tetrazole[498] and to help assign the spectrum in a newly discovered polymorph of the same compound.[499]

The aforementioned studies did not employ dispersion corrections. By their very nature, terahertz-region frequencies are sensitive to the unit cell volume (see ref 490, for instance). Without a dispersion correction, DFT tends to overestimate the unit cell volume, which will lead to spurious phonon frequency predictions. Sometimes (as in many of the aforementioned studies) using known experimental lattice parameters to constrain the cell produces reasonable frequency predictions.

It is clear, however, that adding a dispersion correction improves the prediction of terahertz frequencies.[500,501] Unsurprisingly, even better agreement in the terahertz spectrum can be obtained by refitting the dispersion correction to reproduce the experimental lattice parameters,[502] albeit with the likely associated loss of generality in the model.

A number of more recent terahertz applications have employed dispersion-corrected DFT models. For instance, a CSP study predicted the previously unknown crystal structure of creatine using DFT-D, and they demonstrated that the predicted powder X-ray diffraction pattern and terahertz spectrum were in good agreement with the experimental ones.[503] Citric acid anhydrate and monohydrate provide an unusual example where the terahertz spectrum is similar in both forms, but again, DFT-D is able to reproduce the key features.[504] Other applications include salicylic acid,[505] amino acid crystals (Figure 13),[506] and anthracene.[501] A couple of recent studies have used similar techniques to explore potential organic nonlinear optical materials which could be used for terahertz generation or detection.[507,508]

Most of the existing literature has used pairwise dispersion corrections. However, Reilly and Tkatchenko[82] invoked couplings between electronic fluctuations and lattice vibrations to explain the free energy stability difference between aspirin forms I and II. Support for their predictions comes from the terahertz spectrum—a key band observed experimentally was predicted only by the MBD model, and not by the pairwise-only TS dispersion correction.

Note too that the low energies associated with these modes and their sensitivity to unit cell volume makes terahertz spectra also very temperature dependent (see ref 490, for instance). Most predictions have therefore focused on low-temperature spectra, which tend to be easier to predict.

Finally, force field methods have also been successfully used to model terahertz spectroscopy. For example, in 2006, Day et al.[490] used a rigid-body force field to model the lattice dynamics of several polymorphs of carbamazepine. These calculations were sufficiently accurate to assign groups of frequencies, though they were not accurate enough to identify individual peaks. A follow-up work on benzoic acid several years later compared force field and DFT calculations and found that both were capable of reproducing the low-temperature terahertz spectrum reasonably well.[509] Notably, this study also used the force field and supercell calculations to examine the effects of crystalline disorder on the spectrum. The combination of CSP and terahertz spectroscopy has also been studied.[389]

Most terahertz-region phonon predictions invoke the harmonic approximation when computing the phonon modes. Molecular dynamics allows one to avoid this approximation. Katz et al.[510] recently demonstrated this using the ReaxFF force field and a model that directly incorporates an oscillating electric field in the simulation (to avoid the linear-response approximation) on the triacetone triperoxide (TATP) and cyclotrimethylenetrinitramine (RDX) energetic materials.

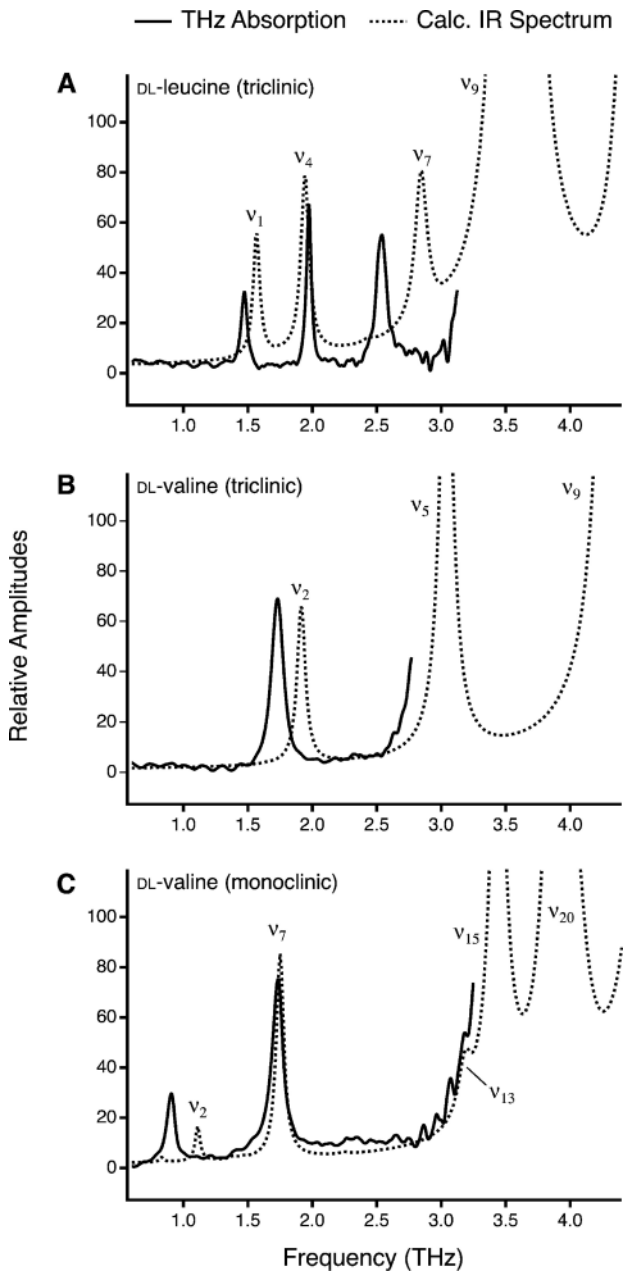

Figure 13. Comparison between experimental and vdW-DF predicted terahertz spectrum for several racemic amino acid crystals. Predicted frequencies were scaled by 0.9. Figure adapted from ref 506. Reprinted with permission. Copyright 2013 American Chemical Society.

3.7. NMR Spectroscopy

X-ray and neutron diffraction techniques have long provided the gold standard for crystal structure determination, but solid-state nuclear magnetic resonance plays an increasingly important role. Whereas diffraction techniques offer insight into the long-range order and symmetry of a crystal, nuclear chemical shielding is sensitive to the local structural details of the crystal packing. Solid-state NMR provides information about crystal packing, can reveal the location of hydrogen atoms (which can be hard to determine from X-ray diffraction),

DOI: 10.1021/acs.chemrev.5b00648
Chem. Rev. 2016, 116, 5567−5613

does not require large single crystals, can deal more readily with impurities, and can even be performed *in situ*. The increasingly popular NMR crystallography approach[511,512] typically combines powder X-ray diffraction, solid state NMR, and computational modeling to determine crystal structures. Computational chemical shift prediction enables mapping between the experimentally observed chemical shifts and three-dimensional crystal structures.

^{13}C chemical shifts are probably the most widely studied, though hydrogen, nitrogen, and oxygen chemical shifts are also increasingly used. Three major uses of chemical shift prediction are (1) crystal structure determination, (2) discrimination of different crystal polymorphs, and (3) the assignment of observed peaks in the NMR spectrum, especially when the unit cell contains multiple symmetrically inequivalent molecules. In all cases, the challenge stems from the fact that variations in chemical shifts between polymorphs or inequivalent monomers can be subtle.

Consider, for example, the first three polymorphs of the antibacterial agent sulfanilamide.[513] The polymorphs differ primarily in their intermolecular hydrogen bonding networks. As shown in Figure 14, the isotropic ^{13}C chemical shifts vary by

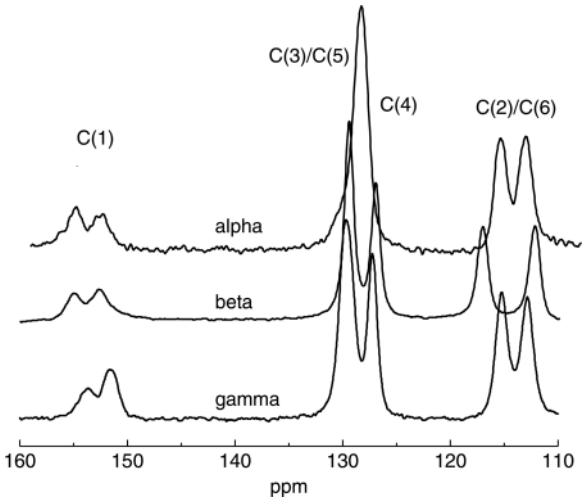

Figure 14. Three polymorphs of sulfanilamide differ primarily in the intermolecular hydrogen bonding networks, which introduces only subtle changes in the ^{13}C solid state NMR chemical shifts. Reproducing these differences can be challenging for theoretical predictions. Reprinted with permission from ref 513. Copyright 2004 John Wiley & Sons.

only 1−3 ppm across the different polymorphs. These differences are sufficient to provide a clear "fingerprint" for each polymorph, but resolving them correctly provides a stiff challenge for computational chemical shift prediction.

Ab initio chemical shift prediction in molecular crystals has advanced significantly over the past decade. The first uses of chemical shift prediction for molecular crystals focused on isolated molecules or very small clusters containing a handful of monomers. The earliest models attempted to capture the crystalline environment by embedding a single molecule in a field of point charges designed to reproduce the Madelung potential experienced by a molecule in the crystal due to the infinite lattice surrounding it. This includes models like the embedded ion method (EIM)[514] and the surface charge representation of the electrostatic embedding potential (SCREEP).[515]

However, chemical shift modeling in molecular crystals changed dramatically with the advent of the gauge-including projector augmented wave (GIPAW) plane wave DFT approach.[516,517] The vast majority of chemical shift predictions in molecular crystals are currently performed using GIPAW. Very recently, fragment-based chemical shift prediction methods have emerged as an alternative to GIPAW that can potentially offer higher accuracy and lower computational cost. Both method types are discussed below.

In the end, DFT calculations can provide ∼1−2 ppm accuracy for isotropic ^{13}C chemical shifts in the best cases.[197,198,518−524] Errors around ∼5 ppm for ^{15}N isotropic shifts[198,520,523,525,526] and ∼10 ppm for ^{17}O isotropic shifts[198,526,527] are achievable as well.

3.7.1. GIPAW Method. GIPAW explicitly includes the crystalline environment through periodic DFT, and it is computationally feasible for crystals containing hundreds of atoms in the unit cell. Applications of GIPAW extend beyond molecular crystals to inorganic materials, supramolecular assemblies, polymers, nanomaterials, etc. Details of the method and representative applications have been discussed in recent reviews.[517,528,529] Here, we highlight some representative studies in organic molecular crystal problems.

The 2006 study of testosterone crystals by Harris et al.[530] provides a nice example of how GIPAW DFT calculations can complement experiments in assigning a complicated NMR spectrum. The α polymorph of testosterone contains two inequivalent molecules, with 19 carbons each, for a total of 38 ^{13}C peaks in the NMR spectrum. Assignment of individual peaks is difficult, with many signals crowded together in the low-frequency region between 10−55 ppm (Figure 15). Two-

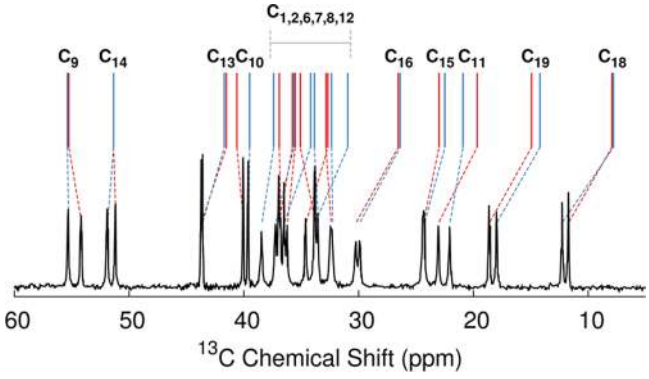

Figure 15. GIPAW-PBE assignment of the ^{13}C chemical shift low-frequency region for the α polymorph of testosterone.[530] The atom numbering is defined in the original work.

dimensional NMR experiments allowed the assignment of many of the observed shifts, but GIPAW chemical shift calculations were required to assign the remaining features and to determine which monomer they correspond to. Other examples of this type of assignment and polymorph discrimination problem include: cholesterol,[531] phenobarbital,[532] indomethacin,[533] the cholesterol drug Plavix,[534] various lactones,[535] and the colorful polymorphs of ROY.[536]

Another key application of these techniques involves refining crystal structures. Theoretical optimization of the atomic positions with constant unit cell parameters can often correct errors in bond lengths and other features, leading to increased agreement between the GIPAW predicted and experimental

DOI: 10.1021/acs.chemrev.5b00648
Chem. Rev. 2016, 116, 5567−5613

NMR spectrum.[324] In the case of the anticholinergic bronchodilator tiotropium bromide and its monohydrate, for example, GIPAW NMR ^{13}C chemical shift predictions based on the powder X-ray structures deposited in the Cambridge Structure Database (with hydrogen positions relaxed using DFT) produced disagreements with experiment of up to 40−50 ppm. Relaxing all atomic coordinates with DFT, however, improved the bond lengths and angles in the thiophenyl rings and reduced the errors in the predicted chemical shifts by an order of magnitude.[537] Tatton et al.[538] used GIPAW to help assign protonation states in pharmaceutical crystals. Other examples of using GIPAW chemical shift prediction to refine crystal structures include terbutaline sulfate,[539,540] phosphotyrosine,[541] and naproxen.[542]

GIPAW-DFT has also proved useful in concert with crystal structure prediction. CSP based on energy alone has long proved challenging, and chemical shifts provide an independent set of observables which can further discriminate among potential structures. A number of studies have combined GIPAW chemical shift calculations with powder X-ray diffraction and CSP to solve structures for a variety of pharmaceutical materials.[385−387,426,543,544] Harper et al.[382,383] have demonstrated improved discrimination by using full chemical shielding tensor information, instead of just the isotropic chemical shifts. Santos et al.[388] used genetic algorithms which incorporated NMR chemical shifts directly in the structure determination process to solve the structure of the antibiotic amoxicillin trihydrate. Other examples include ethoxzolamide,[545] quercetin,[546] and cocrystals of indomethacin and nicotinamide[547,548]

As discussed in section 3.5.4, molecular crystals sometimes exhibit disorder. NMR experiments typically average over molecular motions that occur on millisecond time scales or shorter. Accordingly, dynamical disorder can lead to observed chemical shifts that reflect a time-average over multiple conformations.

In such cases, one might vibrationally average the chemical shift predictions or average over configuration snapshots extracted from a molecular dynamics simulation. An early example of this can be found in the study of a solid state peptide by Gortari et al.[549] Dumez and Pickard[550] demonstrated that zero-point motion and anharmonicity can be very important in the solid state. They also note that care must be taken to average over a sufficiently long time scale to achieve convergence when using the MD snapshot approach. Often, one is faced with the choice between a long, classical MD simulation which may not provide the correct ensemble or an incompletely sampled ab initio MD ensemble.

To avoid this problem, Robinson and Haynes fitted a classical force field to QM forces in order to generate an good ensemble for averaging the chemical shifts in crystalline alanine.[551] Additional recent examples of treating dynamics include methyl α-L-rhamnofuranoside[552] and a study on various amino acid and nucleic acid crystals.[553] Note too that the similar techniques are used to handle dynamics in protein systems.[554,555]

Sometimes simpler models are sufficient. For example, a two-state model can be used to describe the variations in the oxygen chemical shifts due to dynamics associated with the hydrogen-bonded carboxylic acid dimers in aspirin or salicylic acid.[556]

3.7.2. Fragment Methods. GIPAW has proved very successful, with typical accuracy of ∼2−2.5 ppm for ^{13}C chemical shifts, for instance. However, given the often small differences between chemical shifts observed in polymorphic crystals, higher accuracy may sometimes be needed to help resolve structures. Fragment approaches provide an alternative to GIPAW which can enable higher accuracy in molecular crystals at a computational cost that is comparable to or lower than that of GIPAW.

The application of fragment methods to NMR chemical shift prediction has precedent in biological and other systems.[557−570] Electrostatically embedded monomer approaches[514,515] and cluster approaches[519,520,571] might also be considered examples of fragment methods. Recent work has demonstrated, however, that models which include explicit 1- and 2-body terms can be very effective in molecular crystals with low computational cost,[196−198] as discussed below.

The elements of the chemical shielding tensor $\boldsymbol{\sigma}$ are given by the second derivative of the energy with respect to the α-th component of the external magnetic field B_α and the βth component of the nuclear magnetic moment of interest μ_β^A

$$\boldsymbol{\sigma}^A \leftarrow \sigma_{\alpha\beta}^A = \frac{\partial^2 E}{\partial B_\alpha \partial \mu_\beta^A} \tag{11}$$

One can differentiate the many-body expansion for the energy (eq 1) accordingly to obtain a many-body expansion for the elements of the chemical shielding tensor of atom A on molecule i in the crystal, $\tilde{\boldsymbol{\sigma}}_i^A$

$$\tilde{\sigma}_i^A = \boldsymbol{\sigma}_i^A + \sum_{i,j} \Delta^2 \boldsymbol{\sigma}_{ij}^A + \sum_{ijk} \Delta^3 \boldsymbol{\sigma}_{ijk}^A + \cdots \tag{12}$$

where $\boldsymbol{\sigma}_i^A$ is the shielding tensor for atom A on the isolated monomer i, $\Delta^2\boldsymbol{\sigma}_{ij}^A$ and $\Delta^3\boldsymbol{\sigma}_{ijk}^A$ are the 2- and 3-body contributions to the shielding tensor elements on atom A due to nearby molecules. The summations run over all unique dimers, trimers, etc.

The many-body expansion for the chemical shielding tensor converges very rapidly, particularly when electrostatic embedding is employed. For ^{13}C or ^{1}H, it is already usually well-converged with the two-body term.[196−198] In fact, a two-body, charge-embedded model performs just as well as a much more expensive finite-cluster calculation.[197,198,519,520] Even for nuclei like ^{14}N and ^{17}O, which are much more sensitive to polarization effects, the three-body and higher contributions are modest as long as electrostatic embedding is employed.[196,198]

Benchmark studies indicate that for a given density functional (e.g., PBE), a two-body charge-embedded fragment based chemical shift models predicts ^{13}C chemical shifts on par with those from GIPAW. However, whereas hybrid density functionals are prohibitively expensive to use in existing plane wave GIPAW codes, they can be used routinely in a fragment-based code that uses Gaussian basis functions.

In a test of 25 molecular crystals and 169 ^{13}C chemical shifts,[197] using the hybrid PBE0 functional instead of PBE reduces the root-mean-square errors by a third, from 2.1 to 1.4 ppm. Similar improvements were observed for other hybrid functionals relative to several generalized gradient approximation (GGA) functionals. The increased accuracy offered by hybrid functionals provides enhanced discrimination power in challenging cases such as the polymorphs of sulfanilamide (see Figure 16).[196] Similarly good performance is found for chemical shifts of other nuclei, including ^{1}H, ^{15}N, ^{17}O, and ^{19}F, and ^{31}P.[198,520]

Fragment methods also offer distinct computational advantages for crystals with large numbers of molecules in

DOI: 10.1021/acs.chemrev.5b00648
Chem. Rev. 2016, 116, 5567−5613

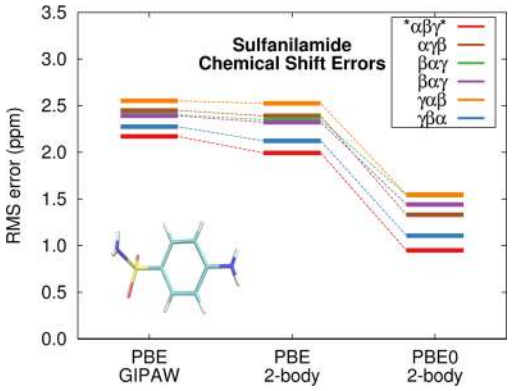

Figure 16. Root-mean-square errors in the predicted ^{13}C chemical shifts for different potential assignments of three polymorphs of sulfanilamide. All three methods predict the smallest errors for the correct $\alpha\beta\gamma$ polymorph assignment (red line). However, whereas fragment PBE and GIPAW-PBE give similar results, using the hybrid density functional in the fragment approach provides higher accuracy and increased discrimination among the potential assignments.[196]

the unit cell. They allow one to readily compute the chemical shifts only for the unique molecules that lie in the asymmetric unit cell. For a crystal like vitamin-D_3, which has 8 molecules and 576 atoms in the unit cell,[572] this is a major advantage. With a fragment approach, one would never need to compute chemical shifts on anything larger than a vitamin-D_3 dimer (144 atoms), and the computational cost scales linearly with the number of inequivalent monomers whose chemical shifts are desired. The embarrassingly parallel nature of fragment methods also means that, if enough processors are available, one can obtain the chemical shifts extremely rapidly, which is potentially important in high-throughput crystal structure prediction applications.

3.8. Chemical Insights into Crystal Packing

Chemical understanding of crystal packing can be very valuable for interpreting crystal behaviors, and quantum mechanical calculations provide useful insights into the nature of the intermolecular interactions. First, energy decomposition often proves useful. SAPT naturally decomposes the energies into electrostatics, induction, dispersion, and exchange terms, allowing one to characterize the nature of intermolecular interactions in detail.[287,288] Podeszwa et al.[279] provided nice insights into the 3-body interactions that contribute to the benzene lattice energy, for instance. These same decompositions can be used to parametrize accurate, physically motivated potentials[288,294] that can be used in crystal structure prediction.[295]

Analysis of the terms in the many-body expansion can also be useful when looking at the energy differences between polymorphs. In aspirin, for instance, such analysis revealed the physical nature underlying the conformational polymorphism.[235] In form II, the aspirin molecules adopt a slightly strained intramolecular conformation in order to form a catemeric chain of hydrogen bonds that allows for stronger long-range electrostatics and polarization. It turns out that the intramolecular conformational penalty and the more favorable intermolecular interactions cancel out almost perfectly, leading to nearly degenerate forms.

Second, it can also sometimes be difficult to understand the spatial relationships of molecules in a crystal and how they differ among various crystal structures. Spackman and coworkers have demonstrated the utility of Hirshfeld surfaces and two-dimensional fingerprints[573−575] derived from them for characterizing crystal packing. The Hirshfeld partitioning[576] provides a definition for extracting an atom in a molecule or a molecule in a crystal from an electron density. Hirshfeld surfaces correspond to isosurfaces of the weight function defining these partitionings. In practice, this Hirshfeld surface defines a region of space where the promolecule electron density exceeds that of all neighboring molecules. Accordingly, the Hirshfeld surface captures information about both the electron density of a molecule and the proximity of its neighboring molecules. Analysis of the curvature can indicate the presence and nature of close contacts (e.g stacking arrangements). Further information is gained by mapping properties such as the electrostatic potential onto these surfaces.

Fingerprints can be derived for a crystal by mapping the distances from the Hirshfeld surface to the nearest nucleus inside (d_i) the surfance versus the nearest nucleus outside (d_e)

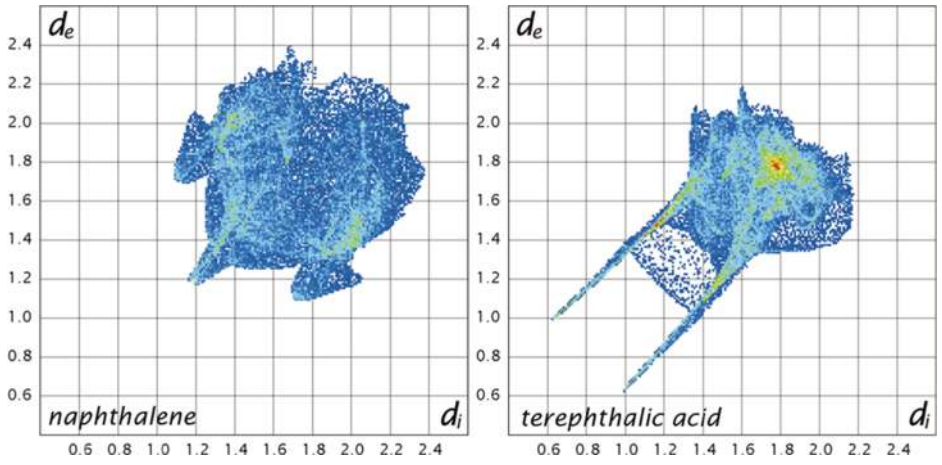

Figure 17. Hirshfeld fingerprint plots for naphthalene (left) and terephthalic acid (right).[574] The "wings" in the naphthalene plot are characteristic of C−H···π interactions, and the intensity near $d_i = d_e \sim 1.2$ Å reflects the H···H interactions. In contrast, the two long spikes in the terephthalic acid plot are indicative of strong hydrogen bonding, and the red area near $d_i = d_e = 1.8$ Å highlights $\pi-\pi$ stacking. Reproduced from ref 574 with permission of the International Union of Crystallography.

DOI: 10.1021/acs.chemrev.5b00648
Chem. Rev. 2016, 116, 5567−5613

the surface. These fingerprint plots are highly sensitive to the immediate environment of a molecular and are unique for a specific polymorphic form. They can be broken down into interactions between individual atom-type pairs to extract more detailed information about the intermolecular contacts. Figure 17 provides sample fingerprint plots for naphthalene and terephthalic acid.

The noncovalent interaction (NCI) analysis[577−579] plots the reduced density gradient, which maps the deviation from a homogeneous electron distribution, against the electron density. Density critical points and the corresponding troughs in the reduced density gradient indicate noncovalent interactions. The Laplacian of the density exhibits distinct features which indicate the type of interaction (hydrogen bonding, steric repulsion, or van der Waals), and the magnitude of the density itself indicates the strength of the interactions strength. Mapping these details onto isosurfaces provides three-dimensional plots that highlight the nature of the noncovalent interactions in a chemically intuitive way, as shown in Figure 18. Otero-dela-Roza et al. recently demonstrated how the NCI model could be used to compare differences in interactions upon substituting one atom type for another.[580]

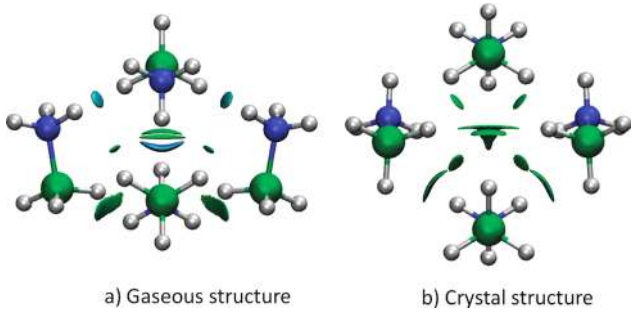

Figure 18. NCI analysis comparing a gaseous tetramer of BH_3NH_3 and a tetramer extracted from the crystal.[578] The mixture of blue and green NCI surfaces between molecules in the gas phase structure reflects a mixture of hydrogen bonding and dispersion interactions, while the presence of only green surfaces in the crystalline tetramer indicates it primarily involves dispersion interactions. Reprinted with permission from ref 578. Copyright 2011 American Chemical Society.

Finally, various other methods exist for characterizing crystal strutures. Valle and Oganov developed their own fingerprint approach which is based on atom pair radial distribution functions.[581] This fingerprint can be used to cluster and eliminate redundant structures generated during CSP.

The rmsd*n* metrics[335,582] compute the root-mean-square deviation of the atomic coordinates for an overlay of *n*-molecule clusters from two different crystal structures. These metrics can be used to quantify the agreement between predicted and experimental structures or to identify common packing motifs which may be conserved across structures (e.g., chains or layers). The rmsd*n* metrics are implemented in Mercury.[582] 15-molecule clusters are especially commonly used. By using a relatively large cluster, rmsd15 captures differences both within the central unit cell and how those errors grow in neighboring unit cells due to errors in the lattice parameters. The XPac software package provides another tool for identifying common supramolecular constructs across multiple crystal structures.[583]

4. CONCLUSIONS

Electronic structure techniques for modeling molecular crystals have advanced dramatically over the past decade, and reliable calculations on crystals containing hundreds of atoms in the unit cell are now feasible. As in many applications of quantum chemistry, dispersion-corrected density functional theory serves as the first tool of choice. However, advances in methods like periodic MP2, QMC, and fragment methods also allow further refinement or validation when doubts arise about the quality of the DFT predictions.

While much of the initial molecular crystal modeling work has focused on structures and energetics, research interests have now expanded to also include the prediction of a wide variety of crystal properties, ranging from phase diagrams to spectroscopic observables. Electronic structure theory is rapidly becoming a vital complement to experimental studies of molecular solids. With continuing algorithmic improvements and the exploitation of increasingly inexpensive and powerful computer hardware, modeling polymorphic molecular crystals with electronic structure theory should enjoy a bright future.

AUTHOR INFORMATION

Corresponding Author

*E-mail: gregory.beran@ucr.edu.

Notes

The authors declare no competing financial interest.

ACKNOWLEDGMENTS

Support from the National Science Foundation (CHE-1362465) is gratefully acknowledged.

REFERENCES

(1) Cruz-Cabeza, A. J.; Reutzel-Edens, S. M.; Bernstein, J. Facts and Fictions About Polymorphism. *Chem. Soc. Rev.* **2015**, *44*, 8619−8635.
(2) López-Mejías, V.; Kampf, J. W.; Matzger, A. J. Nonamorphism in Flufenamic Acid and a New Record for a Polymorphic Compound with Solved Structures. *J. Am. Chem. Soc.* **2012**, *134*, 9872−9875.
(3) Yu, L. Polymorphism in Molecular Solids: An Extraordinary System of Red, Orange, and Yellow Crystals. *Acc. Chem. Res.* **2010**, *43*, 1257−66.
(4) Reany, O.; Kapon, M.; Botoshansky, M.; Keinan, E. Rich Polymorphism in Triacetone-Triperoxide. *Cryst. Growth Des.* **2009**, *9*, 3661−3670.
(5) McCrone, W. C. In *Physics and Chemistry of the Organic Solid State*; Fox, D., Labes, M. M., Weissberger, A., Eds.; Wiley Interscience: New York, 1965; Vol. *2*, pp 725−767.
(6) Braun, D. E.; Bhardwaj, R. M.; Florence, A. J.; Tocher, D. A.; Price, S. L. Complex Polymorphic System of Gallic Acid-Five Monohydrates, Three Anhydrates, and over 20 Solvates. *Cryst. Growth Des.* **2013**, *13*, 19−23.
(7) Salzmann, C.; Radaelli, P.; Mayer, E.; Finney, J. Ice XV: A New Thermodynamically Stable Phase of Ice. *Phys. Rev. Lett.* **2009**, *103*, 105701.
(8) Katzke, H.; Toledano, P. Theoretical Description of Pressure- and Temperature-Induced Structural Phase Transition Mechanisms of Nitrogen. *Phys. Rev. B: Condens. Matter Mater. Phys.* **2008**, *78*, 064103.
(9) Chemburkar, S. R.; Bauer, J.; Deming, K.; Spiwek, H.; Patel, K.; Morris, J.; Henry, R.; Spanton, S.; Dziki, W.; Porter, W.; et al. Dealing with the Impact of Ritonavir Polymorphs on the Late Stages of Bulk Drug Process Development. *Org. Process Res. Dev.* **2000**, *4*, 413−417.
(10) Bauer, J.; Spanton, S.; Quick, R.; Quick, J.; Dziki, W.; Porter, W.; Morris, J. Ritonavir: An Extraordinary Example of Conformational Polymorphism. *Pharm. Res.* **2001**, *18*, 859−866.

DOI: 10.1021/acs.chemrev.5b00648
Chem. Rev. 2016, 116, 5567−5613

(11) Raw, A. S.; Furness, M. S.; Gill, D. S.; Adams, R. C.; Holcombe, F. O.; Yu, L. X. Regulatory Considerations of Pharmaceutical Solid Polymorphism in Abbreviated New Drug Applications (ANDAs). *Adv. Drug Delivery Rev.* **2004**, *56*, 397−414.
(12) Goldbeck, G., Pidcock, E., Groom, C. *Solid Form Informatics for Pharmaceuticals and Agrochemicals: Knowledge-Based Substance Development and Risk Assessment*. Cambridge Crystallographic Data Center, 2012 https://www.ccdc.cam.ac.uk/support-and-resources/ccdcresources/Solid_Form_Informatics.pdf Accessed March 14, 2016.
(13) Bernstein, J. *Polymorphism in Molecular Crystals*; Clarendon Press: Oxford, 2002.
(14) Nyman, J.; Day, G. M. Static and Lattice Vibrational Energy Differences Between Polymorphs. *CrystEngComm* **2015**, *17*, 5154−5165.
(15) Price, S. L. Predicting Crystal Structures of Organic Compounds. *Chem. Soc. Rev.* **2014**, *43*, 2098−111.
(16) Price, S. L. Computational Prediction of Organic Crystal Structures and Polymorphism. *Int. Rev. Phys. Chem.* **2008**, *27*, 541−568.
(17) Lommerse, J. P. M.; Motherwell, W. D. S.; Ammon, H. L.; Dunitz, J. D.; Gavezzotti, A.; Hofmann, D. W. M.; Leusen, F. J. J.; Mooij, W. T. M.; Price, S. L.; Schweizer, B.; et al. A Test of Crystal Structure Prediction of Small Organic Molecules. *Acta Crystallogr., Sect. B: Struct. Sci.* **2000**, *56*, 697−714.
(18) Motherwell, W. D. S.; Ammon, H. L.; Dunitz, J. D.; Dzyabchenko, A.; Erk, P.; Gavezzotti, A.; Hofmann, D. W. M.; Leusen, F. J. J.; Lommerse, J. P. M.; Mooij, W. T. M.; et al. Crystal Structure Prediction of Small Organic Molecules: A Second Blind Test. *Acta Crystallogr., Sect. B: Struct. Sci.* **2002**, *58*, 647−661.
(19) Day, G. M.; Motherwell, W. D. S.; Ammon, H. L.; Boerrigter, S. X. M.; Della Valle, R. G.; Venuti, E.; Dzyabchenko, A.; Dunitz, J. D.; Schweizer, B.; van Eijck, B. P.; et al. A Third Blind Test of Crystal Structure Prediction. *Acta Crystallogr., Sect. B: Struct. Sci.* **2005**, *61*, 511−27.
(20) Day, G. M.; Cooper, T. G.; Cruz-Cabeza, A. J.; Hejczyk, K. E.; Ammon, H. L.; Boerrigter, S. X. M.; Tan, J. S.; Della Valle, R. G.; Venuti, E.; Jose, J.; et al. Significant Progress in Predicting the Crystal Structures of Small Organic Molecules−A Report on the Fourth Blind Test. *Acta Crystallogr., Sect. B: Struct. Sci.* **2009**, *65*, 107−25.
(21) Bardwell, D. A.; Adjiman, C. S.; Arnautova, Y. A.; Bartashevich, E.; Boerrigter, S. X. M.; Braun, D. E.; Cruz-Cabeza, A. J.; Day, G. M.; Della Valle, R. G.; Desiraju, G. R.; et al. Towards Crystal Structure Prediction of Complex Organic Compounds−A Report on the Fifth Blind Test. *Acta Crystallogr., Sect. B: Struct. Sci.* **2011**, *67*, 535−51.
(22) Coropceanu, V.; Cornil, J.; da Silva Filho, D. A.; Olivier, Y.; Silbey, R.; Brédas, J.-L. Charge Transport in Organic Semiconductors. *Chem. Rev.* **2007**, *107*, 926−952.
(23) Kristyan, S.; Pulay, P. Can (Semi)Local Density Functional Theory Account for the London Dispersion Forces? *Chem. Phys. Lett.* **1994**, *229*, 175−180.
(24) Dion, M.; Rydberg, H.; Schröder, E.; Langreth, D. C.; Lundqvist, B. I. Van der Waals Density Functional for General Geometries. *Phys. Rev. Lett.* **2004**, *92*, 246401.
(25) Dion, M.; Rydberg, H.; Schröder, E.; Langreth, D. C.; Lundqvist, B. I. Erratum: Van der Waals Density Functional for General Geometries [Phys. Rev. Lett. 92, 246401 (2004)]. *Phys. Rev. Lett.* **2005**, *95*, 109902.
(26) Thonhauser, T.; Cooper, V. R.; Li, S.; Puzder, A.; Hyldgaard, P.; Langreth, D. C. Van der Waals Density Functional: Self-Consistent Potential and the Nature of the van der Waals Bond. *Phys. Rev. B: Condens. Matter Mater. Phys.* **2007**, *76*, 125112.
(27) Lee, K.; Murray, E. D.; Kong, L.; Langreth, B. I. L. D. C. Higher-Accuracy van der Waals Density Functional. *Phys. Rev. B: Condens. Matter Mater. Phys.* **2010**, *82*, 081101(R).
(28) Vydrov, O. A.; Van Voorhis, T. Nonlocal van der Waals Density Functional Made Simple. *Phys. Rev. Lett.* **2009**, *103*, 063004.
(29) Vydrov, O. A.; Van Voorhis, T. Nonlocal van der Waals Density Functional: The Simpler the Better. *J. Chem. Phys.* **2010**, *133*, 244103.
(30) Berland, K.; Cooper, V. R.; Lee, K.; Schröder, E.; Thonhauser, T.; Hyldgaard, P.; Lundqvist, B. I. van der Waals Forces in Density Functional Theory: A Review of the vdW-DF Method. *Rep. Prog. Phys.* **2015**, *78*, 066501.
(31) Hujo, W.; Grimme, S. Performance of the van der Waals Density Functional VV10 and (hybrid)GGA Variants for Thermochemistry and Noncovalent Interactions. *J. Chem. Theory Comput.* **2011**, *7*, 3866−3871.
(32) Vydrov, O. A.; Van Voorhis, T. Benchmark Assessment of the Accuracy of Several van der Waals Density Functionals. *J. Chem. Theory Comput.* **2012**, *8*, 1929−1934.
(33) Risthaus, T.; Grimme, S. Benchmarking of London Dispersion-Accounting Density Functional Theory Methods on Very Large Molecular Complexes. *J. Chem. Theory Comput.* **2013**, *9*, 1580−1591.
(34) Otero-de-la Roza, A.; Johnson, E. R. A Benchmark for Non-Covalent Interactions in Solids. *J. Chem. Phys.* **2012**, *137*, 054103.
(35) Carter, D. J.; Rohl, A. L. Benchmarking Calculated Lattice Parameters and Energies of Molecular Crystals Using van der Waals Density Functionals. *J. Chem. Theory Comput.* **2014**, *10*, 3423−3437.
(36) Hamada, I. A van der Waals Density Functional Study of Ice Ih. *J. Chem. Phys.* **2010**, *133*, 214503.
(37) Del Ben, M.; VandeVondele, J.; Slater, B. Periodic MP2, RPA, and Boundary Condition Assessment of Hydrogen Ordering in Ice XV. *J. Phys. Chem. Lett.* **2014**, *5*, 4122−4128.
(38) Wu, J.; Gygi, F. A Simplified Implementation of van der Waals Density Functionals for First-Principles Molecular Dynamics Applications. *J. Chem. Phys.* **2012**, *136*, 224107.
(39) Berland, K.; Borck, Ø; Hyldgaard, P. Van der Waals Density Functional Calculations of Binding in Molecular Crystals. *Comput. Phys. Commun.* **2011**, *182*, 1800−1804.
(40) Rezac, J.; Riley, K. E.; Hobza, P. S66: A Well-Balanced Database of Benchmark Interaction Energies Relevant to Biomolecular Structures. *J. Chem. Theory Comput.* **2011**, *7*, 2427−2438.
(41) Riley, K. E.; Hobza, P. Erratum to "S66: A Well-balanced Database of Benchmark Interaction Energies Relevant to Biomolecular Structures. *J. Chem. Theory Comput.* **2014**, *10*, 1359−1360.
(42) Grimme, S. Accurate Description of van der Waals Complexes by Density Functional Theory Including Empirical Corrections. *J. Comput. Chem.* **2004**, *25*, 1463−1473.
(43) Antony, J.; Grimme, S. Density Functional Theory Including Dispersion Corrections for Intermolecular Interactions in a Large Benchmark Set of Biologically Relevant Molecules. *Phys. Chem. Chem. Phys.* **2006**, *8*, 5287.
(44) Grimme, S.; Antony, J.; Ehrlich, S.; Krieg, H. A Consistent and Accurate ab Initio Parametrization of Density Functional Dispersion Correction (DFT-D) for the 94 Elements H-Pu. *J. Chem. Phys.* **2010**, *132*, 154104.
(45) Grimme, S.; Ehrlich, S.; Goerigk, L. Effect of the Damping Function in Dispersion Corrected Density Functional Theory. *J. Comput. Chem.* **2011**, *32*, 1456−1465.
(46) Tkatchenko, A.; Scheffler, M. Accurate Molecular van Der Waals Interactions from Ground-State Electron Density and Free-Atom Reference Data. *Phys. Rev. Lett.* **2009**, *102*, 073005.
(47) DiStasio, R. A.; von Lilienfeld, O. A.; Tkatchenko, A. Collective Many-Body van der Waals Interactions in Molecular Systems. *Proc. Natl. Acad. Sci. U. S. A.* **2012**, *109*, 14791−14795.
(48) Tkatchenko, A.; DiStasio, R. A.; Car, R.; Scheffler, M. Accurate and Efficient Method for Many-Body van der Waals Interactions. *Phys. Rev. Lett.* **2012**, *108*, 236402.
(49) Ambrosetti, A.; Reilly, A. M.; DiStasio, R. A.; Tkatchenko, A. Long-Range Correlation Energy Calculated from Coupled Atomic Response Functions. *J. Chem. Phys.* **2014**, *140*, 18A508.
(50) Neumann, M. A.; Perrin, M.-A. Energy Ranking of Molecular Crystals Using Density Functional Theory Calculations and an Empirical van der Waals Correction. *J. Phys. Chem. B* **2005**, *109*, 15531−41.
(51) Feng, S.; Li, T. Predicting Lattice Energy of Organic Crystals by Density Functional Theory with Empirically Corrected Dispersion Energy. *J. Chem. Theory Comput.* **2006**, *2*, 149−156.

DOI: 10.1021/acs.chemrev.5b00648
Chem. Rev. 2016, 116, 5567−5613

(52) Li, T.; Feng, S. Empirically Augmented Density Functional Theory for Predicting Lattice Energies of Aspirin, Acetaminophen Polymorphs, and Ibuprofen Homochiral and Racemic Crystals. *Pharm. Res.* **2006**, *23*, 2326−2332.
(53) Civalleri, B.; Zicovich-Wilson, C. M.; Valenzano, L.; Ugliengo, P. B3LYP Augmented with an Empirical Dispersion Term (B3LYP-D*) as Applied to Molecular Crystals. *CrystEngComm* **2008**, *10*, 405−410.
(54) Becke, A. D.; Johnson, E. R. Exchange-Hole Dipole Moment and the Dispersion Interaction: High-Order Dispersion Coefficients. *J. Chem. Phys.* **2006**, *124*, 014104.
(55) Becke, A. D.; Johnson, E. R. Exchange-Hole Dipole Moment and the Dispersion Interaction Revisited. *J. Chem. Phys.* **2007**, *127*, 154108.
(56) Johnson, E. R. Dependence of Dispersion Coefficients on Atomic Environment. *J. Chem. Phys.* **2011**, *135*, 234109.
(57) Otero-de-la Roza, A.; Johnson, E. R. Van der Waals Interactions in Solids Using the Exchange-Hole Dipole Moment Model. *J. Chem. Phys.* **2012**, *136*, 174109.
(58) Grimme, S. Density Functional Theory with London Dispersion Corrections. *WIRES: Comput. Mol. Sci.* **2011**, *1*, 211−228.
(59) Cohen, A. J.; Mori-Sanchez, P.; Yang, W. Challenges for Density Functional Theory. *Chem. Rev.* **2012**, *112*, 289−320.
(60) Klimeš, J.; Michaelides, A. Perspective: Advances and Challenges in Treating van der Waals Dispersion Forces in Density Functional Theory. *J. Chem. Phys.* **2012**, *137*.12090110.1063/1.4754130
(61) Reilly, A. M.; Tkatchenko, A. Van der Waals Dispersion Interactions in Molecular Materials: Beyond Pairwise Additivity. *Chem. Sci.* **2015**, *6*, 3289−3301.
(62) Kronik, L.; Tkatchenko, A. Understanding Molecular Crystals with Dispersion-Inclusive Density Functional Theory: Pairwise Corrections and Beyond. *Acc. Chem. Res.* **2014**, *47*, 3208−3216.
(63) Riley, K. E.; Pitonak, M.; Jurecka, P.; Hobza, P. Stabilization and Structure Calculations for Noncovalent Interactions in Extended Molecular Systems Based on Wave Function and Density Functional Theories. *Chem. Rev.* **2010**, *110*, 5023−63.
(64) Goerigk, L.; Kruse, H.; Grimme, S. Benchmarking Density Functional Methods Against the S66 and S66 × 8 Datasets for Non-Covalent Interactions. *ChemPhysChem* **2011**, *12*, 3421−33.
(65) Goerigk, L.; Grimme, S. A Thorough Benchmark of Density Functional Methods for General Main Group Thermochemistry, Kinetics, and Noncovalent Interactions. *Phys. Chem. Chem. Phys.* **2011**, *13*, 6670−88.
(66) Thanthiriwatte, K. S.; Hohenstein, E. G.; Burns, L. A.; Sherrill, C. D. Assessment of the Performance of DFT and DFT-D Methods for Describing Distance Dependence of Hydrogen-Bonded Interactions. *J. Chem. Theory Comput.* **2011**, *7*, 88−96.
(67) Burns, L. A.; Mayagoitia, A. V.; Sumpter, B. G.; Sherrill, C. D. Density-Functional Approaches to Noncovalent Interactions: A Comparison of Dispersion Corrections (DFT-D), Exchange-Hole Dipole Moment (XDM) Theory, and Specialized Functionals. *J. Chem. Phys.* **2011**, *134*, 084107.
(68) Řezáč, J.; Riley, K. E.; Hobza, P. Benchmark Calculations of Noncovalent Interactions of Halogenated Molecules. *J. Chem. Theory Comput.* **2012**, *8*, 4285−4292.
(69) Grimme, S. Supramolecular Binding Thermodynamics by Dispersion-Corrected Density Functional Theory. *Chem. - Eur. J.* **2012**, *18*, 9955−9964.
(70) Sedlak, R.; Janowski, T.; Pitonak, M.; Rezac, J.; Pulay, P.; Hobza, P. Accuracy of Quantum Chemical Methods for Large Noncovalent Complexes. *J. Chem. Theory Comput.* **2013**, *9*, 3364−3374.
(71) Gohr, S.; Grimme, S.; Söhnel, T.; Paulus, B.; Schwerdtfeger, P. Pressure Dependent Stability and Structure of Carbon Dioxide-A density functional study including long-range corrections. *J. Chem. Phys.* **2013**, *139*, 174501.
(72) Moellmann, J.; Grimme, S. DFT-D3 Study of Some Molecular Crystals. *J. Phys. Chem. C* **2014**, *118*, 7615−7621.
(73) Brandenburg, J. G.; Grimme, S. Dispersion Corrected Hartree-Fock and Density Functional Theory for Organic Crystal Structure Prediction. *Top. Curr. Chem.* **2014**, *345*, 1−23.
(74) Brandenburg, J. G.; Grimme, S. Accurate Modeling of Organic Molecular Crystals by Dispersion-Corrected Density Functional Tight Binding (DFTB). *J. Phys. Chem. Lett.* **2014**, *5*, 1785−1789.
(75) Tkatchenko, A.; Alfè, D.; Kim, K. S. First-Principles Modeling of Non-Covalent Interactions in Supramolecular Systems: The Role of Many-Body Effects. *J. Chem. Theory Comput.* **2012**, *8*, 4317−4322.
(76) Ambrosetti, A.; Alfè, D.; DiStasio, R. A.; Tkatchenko, A. Hard Numbers for Large Molecules: Toward Exact Energetics for Supramolecular Systems. *J. Phys. Chem. Lett.* **2014**, *5*, 849−855.
(77) Santra, B.; Klimeš, J.; Tkatchenko, A.; Alfè, D.; Slater, B.; Michaelides, A.; Car, R.; Scheffler, M. On the Accuracy of van der Waals Inclusive Density-Functional Theory Exchange-Correlation Functionals for Ice at Ambient and High Pressures. *J. Chem. Phys.* **2013**, *139*, 154702.
(78) Gobre, V. V.; Tkatchenko, A. Scaling Laws for van der Waals Interactions in Nanostructured Materials. *Nat. Commun.* **2013**, *4*, 2341.
(79) Marom, N.; DiStasio, R. A.; Atalla, V.; Levchenko, S.; Reilly, A. M.; Chelikowsky, J. R.; Leiserowitz, L.; Tkatchenko, A. Many-Body Dispersion Interactions in Molecular Crystal Polymorphism. *Angew. Chem., Int. Ed.* **2013**, *52*, 6629−6632.
(80) Reilly, A. M.; Tkatchenko, A. Understanding the Role of Vibrations, Exact Exchange, and Many-Body van der Waals Interactions in the Cohesive Properties of Molecular Crystals. *J. Chem. Phys.* **2013**, *139*, 024705.
(81) Reilly, A. M.; Tkatchenko, A. Seamless and Accurate Modeling of Organic Molecular Materials. *J. Phys. Chem. Lett.* **2013**, *4*, 1028−1033.
(82) Reilly, A. M.; Tkatchenko, A. Role of Dispersion Interactions in the Polymorphism and Entropic Stabilization of the Aspirin Crystal. *Phys. Rev. Lett.* **2014**, *113*, 055701.
(83) Liu, W.; Maaß, F.; Willenbockel, M.; Bronner, C.; Schulze, M.; Soubatch, S.; Tautz, F. S.; Tegeder, P.; Tkatchenko, A. Quantitative Prediction of Molecular Adsorption: Structure and Binding of Benzene on Coinage Metals. *Phys. Rev. Lett.* **2015**, *115*, 036104.
(84) Maurer, R. J.; Ruiz, V. G.; Tkatchenko, A. Many-Body Dispersion Effects in the Binding of Adsorbates on Metal Surfaces. *J. Chem. Phys.* **2015**, *143*, 102808.
(85) Wagner, C.; Fournier, N.; Ruiz, V. G.; Li, C.; Müllen, K.; Rohlfing, M.; Tkatchenko, A.; Temirov, R.; Tautz, F. S. Non-Additivity of Molecule-Surface van der Waals Potentials from Force Measurements. *Nat. Commun.* **2014**, *5*, 5568.
(86) DiLabio, G. A.; Johnson, E. R.; Otero-de-la Roza, A. Performance of Conventional and Dispersion-Corrected Density-Functional Theory Methods for Hydrogen Bonding Interaction Energies. *Phys. Chem. Chem. Phys.* **2013**, *15*, 12821.
(87) Otero-de-la Roza, A.; Johnson, E. R. Non-Covalent Interactions and Thermochemistry Using XDM-Corrected Hybrid and Range-Separated Hybrid Density Functionals. *J. Chem. Phys.* **2013**, *138*, 204109.
(88) Otero-de-la Roza, A.; Johnson, E. R.; DiLabio, G. A. Halogen Bonding from Dispersion-Corrected Density-Functional Theory: The Role of Delocalization Error. *J. Chem. Theory Comput.* **2014**, *10*, 5436−5447.
(89) Otero-de-la Roza, A.; Johnson, E. R. Predicting Energetics of Supramolecular Systems Using the XDM Dispersion Model. *J. Chem. Theory Comput.* **2015**, *11*, 4033−4040.
(90) Otero-De-La-Roza, A.; Cao, B. H.; Price, I. K.; Hein, J. E.; Johnson, E. R. Predicting the Relative Solubilities of Racemic and Enantiopure Crystals by Density-Functional Theory. *Angew. Chem., Int. Ed.* **2014**, *53*, 7879−7882.
(91) Chai, J.-D.; Head-Gordon, M. Long-Range Corrected Hybrid Density Functionals with Damped Atom-Atom Dispersion Corrections. *Phys. Chem. Chem. Phys.* **2008**, *10*, 6615−5520.

DOI: 10.1021/acs.chemrev.5b00648
Chem. Rev. 2016, 116, 5567−5613

(92) Sharkas, K.; Toulouse, J.; Maschio, L.; Civalleri, B. Double-Hybrid Density-Functional Theory Applied to Molecular Crystals. *J. Chem. Phys.* **2014**, *141*, 044105.
(93) Steinmann, S. N.; Corminboeuf, C. Comprehensive Benchmarking of a Density-Dependent Dispersion Correction. *J. Chem. Theory Comput.* **2011**, *7*, 3567−3577.
(94) von Lilienfeld, O. A.; Tavernelli, I.; Rothlisberger, U.; Sebastiani, D. Optimization of Effective Atom Centered Potentials for London Dispersion Forces in Density Functional Theory. *Phys. Rev. Lett.* **2004**, *93*, 153004.
(95) Lin, I. C.; Coutinho-Neto, M. D.; Felsenheimer, C.; Von Lilienfeld, O. A.; Tavernelli, I.; Rothlisberger, U. Library of Dispersion-Corrected Atom-Centered Potentials for Generalized Gradient Approximation Functionals: Elements H, C, N, O, He, Ne, Ar, and Kr. *Phys. Rev. B: Condens. Matter Mater. Phys.* **2007**, *75*, 1−5.
(96) Karalti, O.; Su, X.; Al-Saidi, W. A.; Jordan, K. D. Correcting Density Functionals For Dispersion Interactions using Pseudopotentials. *Chem. Phys. Lett.* **2014**, *591*, 133−136.
(97) Axilrod, P. M.; Teller, E. Interaction of the van der Waals Type Between Three Atoms. *J. Chem. Phys.* **1943**, *11*, 299−300.
(98) Muto, Y. Force Between Nonpolar Molecules. *Proc. Phys. Math. Soc. Japan* **1943**, *17*, 629−631.
(99) Otero-de-la Roza, A.; Johnson, E. R. Many-Body Dispersion Interactions from the Exchange-Hole Dipole Moment Model. *J. Chem. Phys.* **2013**, *138*, 054103.
(100) von Lilienfeld, O. A.; Tkatchenko, A. Two- and Three-Body Interatomic Dispersion Energy Contributions to Binding in Molecules and Solids. *J. Chem. Phys.* **2010**, *132*, 234109.
(101) Tkatchenko, A.; Von Lilienfeld, O. A. Popular Kohn-Sham Density Functionals Strongly Overestimate Many-Body Interactions in van der Waals Systems. *Phys. Rev. B: Condens. Matter Mater. Phys.* **2008**, *78*, 045116.
(102) Řezáč, J.; Huang, Y.; Hobza, P.; Beran, G. J. O. Benchmark Calculations of Three-Body Intermolecular Interactions and the Performance of Low-Cost Electronic Structure Methods. *J. Chem. Theory Comput.* **2015**, *11*, 3065−3079.
(103) Cohen, A. J.; Mori-Sánchez, P.; Yang, W. Insights into Current Limitations of Density Functional Theory. *Science* **2008**, *321*, 792−794.
(104) Gillan, M. J. Many-Body Exchange-Overlap Interactions in Rare Gases and Water. *J. Chem. Phys.* **2014**, *141*, 224106.
(105) Suhai, S. Quasiparticle Energy-Band Structures in Semiconducting Polymers: Correlation Effects on the Band Gap in Polyacetylene. *Phys. Rev. B: Condens. Matter Mater. Phys.* **1983**, *27*, 3506−3518.
(106) Sun, J.-Q.; Bartlett, R. J. Second-Order Many-Body Perturbation-Theory Calculations in Extended Systems. *J. Chem. Phys.* **1996**, *104*, 8553−8565.
(107) Hirata, S.; Iwata, S. Analytical Energy Gradients in Second-Order Møller-Plesset Perturbation Theory for Extended Systems. *J. Chem. Phys.* **1998**, *109*, 4147−4155.
(108) Ohnishi, Y.-Y.; Hirata, S. Logarithm Second-Order Many-Body Perturbation Method for Extended Systems. *J. Chem. Phys.* **2010**, *133*, 034106.
(109) Willow, S. Y.; Kim, K. S.; Hirata, S. Brueckner-Goldstone Quantum Monte Carlo for Correlation Energies and Quasiparticle Energy Bands of One-Dimensional Solids. *Phys. Rev. B: Condens. Matter Mater. Phys.* **2014**, *90*, 201110.
(110) Shiozaki, T.; Hirata, S. Communications: Explicitly Correlated Second-Order Møller-Plesset Perturbation Method for Extended Systems. *J. Chem. Phys.* **2010**, *132*, 151101.
(111) He, X.; Ryu, S.; Hirata, S. Finite-Temperature Second-Order Many-Body Perturbation and Hartree-Fock Theories for One-Dimensional Solids: An Application to Peierls and Charge-Density-Wave Transitions in Conjugated Polymers. *J. Chem. Phys.* **2014**, *140*, 024702.
(112) Del Ben, M.; Hutter, J.; Vandevondele, J. Second-order Møller-Plesset Perturbation Theory in the Condensed Phase: An Efficient and Massively Parallel Gaussian and Plane Waves Approach. *J. Chem. Theory Comput.* **2012**, *8*, 4177−4188.
(113) Ren, X.; Rinke, P.; Blum, V.; Wieferink, J.; Tkatchenko, A.; Sanfilippo, A.; Reuter, K.; Scheffler, M. Resolution-of-Identity Approach to Hartree-Fock, Hybrid Density Functionals, RPA, MP2 and GW with Numeric Atom-Centered Orbital Basis Functions. *New J. Phys.* **2012**, *14*, 053020.
(114) Del Ben, M.; Hutter, J.; Vandevondele, J. Electron Correlation in the Condensed Phase from a Resolution of Identity Approach Based on the Gaussian and Plane Waves Scheme. *J. Chem. Theory Comput.* **2013**, *9*, 2654−2671.
(115) Ayala, P. Y.; Kudin, K. N.; Scuseria, G. E. Atomic Orbital Laplace-Transformed Second-Order Møller-Plesset Perturbation Theory for Periodic Systems. *J. Chem. Phys.* **2001**, *115*, 9698−9707.
(116) Izmaylov, A. F.; Scuseria, G. E. Resolution of the Identity Atomic Orbital Laplace Transformed Second-Order Møller-Plesset Theory for Nonconducting Periodic Systems. *Phys. Chem. Chem. Phys.* **2008**, *10*, 3421−3429.
(117) Izmaylov, A. F; Scuseria, G. E. In *Accurate Quantum Chemistry in the Condensed Phase*; Manby, F., Ed.; CRC Press: Boca Raton, FL, 2010; pp 1−28.
(118) Casassa, S.; Halo, M.; Maschio, L.; Roetti, C.; Pisani, C. Beyond a Hartree-Fock Description of Crystalline Solids: The Case of Lithium Hydride. *Theor. Chem. Acc.* **2007**, *117*, 781−791.
(119) Maschio, L.; Usvyat, D.; Manby, F. R.; Casassa, S.; Pisani, C.; Schütz, M. Fast Local-MP2 Method with Density-Fitting for Crystals. I. Theory and Algorithms. *Phys. Rev. B: Condens. Matter Mater. Phys.* **2007**, *76*, 075101.
(120) Usvyat, D.; Maschio, L.; Manby, F. R.; Casassa, S.; Pisani, C.; Schütz, M. Fast Local-MP2 Method with Density-Fitting for Crystals. II. Test Calculations and Applications to the Carbon Dioxide Crystal. *Phys. Rev. B: Condens. Matter Mater. Phys.* **2007**, *76*, 075102.
(121) Pisani, C.; Maschio, L.; Casassa, S.; Halo, M.; Schütz, M.; Usvyat, D. Periodic Local MP2 Method for the Study of Electronic Correlation in Crystals: Theory and Preliminary Applications. *J. Comput. Chem.* **2008**, *29*, 2113−2124.
(122) Maschio, L. Local MP2 with Density Fitting for Periodic Systems: A Parallel Implementation. *J. Chem. Theory Comput.* **2011**, *7*, 2818−2830.
(123) Maschio, L.; Usvyat, D.; Schütz, M.; Civalleri, B. Periodic Local Møller-Plesset Second Order Perturbation Theory Method Applied to Molecular Crystals: Study of Solid NH_3 and CO_2 Using Extended Basis Sets. *J. Chem. Phys.* **2010**, *132*, 134706.
(124) Maschio, L.; Usvyat, D.; Civalleri, B. Ab Initio Study of van der Waals and Hydrogen-Bonded Molecular Crystals with a Periodic Local-MP2 Method. *CrystEngComm* **2010**, *12*, 2429−2435.
(125) Erba, A.; Maschio, L.; Salustro, S.; Casassa, S. A Post-Hartree-Fock Study of Pressure-Induced Phase Transitions in Solid Nitrogen: The Case of the α, γ, and ϵ Low-Pressure Phases. *J. Chem. Phys.* **2011**, *134*, 074502.
(126) Erba, A.; Pisani, C.; Casassa, S.; Maschio, L.; Schütz, M.; Usvyat, D. MP2 Versus Density-Functional Theory Study of the Compton Profiles of Crystalline Urea. *Phys. Rev. B: Condens. Matter Mater. Phys.* **2010**, *81*, 165108.
(127) Presti, D.; Pedone, A.; Menziani, M. C.; Civalleri, B.; Maschio, L. Oxalyl Dihydrazide Polymorphism: A Periodic Dispersion-Corrected DFT and MP2 Investigation. *CrystEngComm* **2014**, *16*, 102−109.
(128) Usvyat, D.; Civalleri, B.; Maschio, L.; Dovesi, R.; Pisani, C.; Schutz, M. Approaching the Theoretical Limit in Periodic Local MP2 Calculations with Atomic-Orbital Basis Sets: The Case of LiH. *J. Chem. Phys.* **2011**, *134*, 214105.
(129) Usvyat, D. Linear-Scaling Explicitly Correlated Treatment of Solids: Periodic Local MP2-F12 Method. *J. Chem. Phys.* **2013**, *139*, 194101.
(130) Maschio, L.; Civalleri, B.; Ugliengo, P.; Gavezzotti, A. Intermolecular Interaction Energies in Molecular Crystals: Comparison and Agreement of Localized Møller-Plesset 2, Dispersion-

DOI: 10.1021/acs.chemrev.5b00648
Chem. Rev. 2016, 116, 5567−5613

Corrected Density Functional, and Classical Empirical Two-Body Calculations. *J. Phys. Chem. A* **2011**, *115*, 11179−86.
(131) Müller, C.; Usvyat, D.; Stoll, H. Local Correlation Methods for Solids: Comparison of Incremental and Periodic Correlation Calculations for the Argon fcc Crystal. *Phys. Rev. B: Condens. Matter Mater. Phys.* **2011**, *83*, 245136.
(132) Müller, C.; Usvyat, D. Incrementally Corrected Periodic Local MP2 Calculations: I. The Cohesive Energy of Molecular Crystals. *J. Chem. Theory Comput.* **2013**, *9*, 5590−5598.
(133) Usvyat, D.; Maschio, L.; Schütz, M. Periodic Local MP2 Method Employing Orbital Specific Virtuals. *J. Chem. Phys.* **2015**, *143*, 102805.
(134) Marsman, M.; Grüneis, A.; Paier, J.; Kresse, G. Second-Order Møller-Plesset Perturbation Theory Applied to Extended Systems. I. Within the Projector-Augmented-Wave Formalism using a Plane Wave Basis Set. *J. Chem. Phys.* **2009**, *130*, 184103.
(135) Grüneis, A.; Marsman, M.; Kresse, G. Second-order Møller-Plesset Perturbation Theory Applied to Extended Systems. II. Structural and Energetic Properties. *J. Chem. Phys.* **2010**, *133*, 074107.
(136) Grüneis, A.; Booth, G. H.; Marsman, M.; Spencer, J.; Alavi, A.; Kresse, G. Natural Orbitals for Wave Function Based Correlated Calculations using a Plane Wave Basis Set. *J. Chem. Theory Comput.* **2011**, *7*, 2780−2785.
(137) Grüneis, A. A Coupled Cluster and Møller-Plesset Perturbation Theory Study of the Pressure Induced Phase Transition in the LiH Crystal. *J. Chem. Phys.* **2015**, *143*, 102817.
(138) Katouda, M.; Nagase, S. Application of Second-Order Møller-Plesset Perturbation Theory with Resolution-of-Identity Approximation to Periodic Systems. *J. Chem. Phys.* **2010**, *133*, 184103.
(139) Ihrig, A. C.; Weiferink, J.; Zhang, I. Y.; Ropo, M.; Ren, X.; Rinke, P.; Scheffler, M.; Blum, V. Accurate Localized Resolution of Identity Approach for Linear-Scaling Hybrid Density Functionals and for Many-Body Perturbation Theory. *New. J. Phys.* **2014**, *093020*, 1−15.
(140) Del Ben, M.; Hutter, J.; VandeVondele, J. Forces and Stress in Second Order Møller-Plesset Perturbation Theory for Condensed Phase Systems within the Resolution-of-Identity Gaussian and Plane Waves Approach. *J. Chem. Phys.* **2015**, *143*, 102803.
(141) Macher, M.; Klimeš, J.; Franchini, C.; Kresse, G. The Random Phase Approximation Applied to Ice. *J. Chem. Phys.* **2014**, *140*, 084502.
(142) Paier, J.; Diaconu, C. V.; Scuseria, G. E.; Guidon, M.; VandeVondele, J.; Hutter, J. Accurate Hartree-Fock Energy of Extended Systems using Large Gaussian Basis Sets. *Phys. Rev. B: Condens. Matter Mater. Phys.* **2009**, *80*, 174114.
(143) Civalleri, B.; Orlando, R.; Zicovich-Wilson, C. M.; Roetti, C.; Saunders, V. R.; Pisani, C.; Dovesi, R. Comment on "Accurate Hartree-Fock Energy of Extended Systems using Large Gaussian Basis Sets. *Phys. Rev. B: Condens. Matter Mater. Phys.* **2010**, *81*, 106101.
(144) Gruüneis, A.; Shepherd, J. J.; Alavi, A.; Tew, D. P.; Booth, G. H. Explicitly Correlated Plane Waves: Accelerating Convergence in Periodic Wavefunction Expansions. *J. Chem. Phys.* **2013**, *139*, 084112.
(145) Alfè, D.; Bartók, A. P.; Csányi, G.; Gillan, M. J. Communication: Energy Benchmarking with Quantum Monte Carlo for Water Nano-Droplets and Bulk Liquid Water. *J. Chem. Phys.* **2013**, *138*, 221102.
(146) Gillan, M. J.; Alfe, D.; Bartok, A. P.; Csányi, G. First-Principles Energetics of Water Clusters and Ice: A Many-Body Analysis. *J. Chem. Phys.* **2013**, *139*, 244504.
(147) Karalti, O.; Alfe, D.; Gillan, M. J.; Jordan, K. D. Adsorption of a Water Molecule on the MgO(100) Surface as Described by Cluster and Slab Models. *Phys. Chem. Chem. Phys.* **2012**, *14*, 7846−7853.
(148) Deible, M. J.; Tuguldur, O.; Jordan, K. D. Theoretical Study of the Binding Energy of a Methane Molecule in a $(H_2O)_{20}$ Dodecahedral Cage. *J. Phys. Chem. B* **2014**, *118*, 8257.
(149) Santra, B.; Klimes, J.; Alfe, D.; Tkatchenko, A.; Slater, B.; Michaelides, A.; Car, R.; Scheffler, M. Hydrogen Bonds and van der Waals Forces in Ice at Ambient and High Pressures. *Phys. Rev. Lett.* **2011**, *107*, 185701.
(150) Gillan, M. J.; Alfè, D.; Bygrave, P. J.; Taylor, C. R.; Manby, F. R. Energy Benchmarks for Water Clusters and Ice Structures from an Embedded Many-Body Expansion. *J. Chem. Phys.* **2013**, *139*, 114101.
(151) Quigley, D.; Alfe, D.; Slater, B. Communication: On the Stability of Ice 0, Ice i, and Ih. *J. Chem. Phys.* **2014**, *141*, 161102.
(152) Cox, S. J.; Towler, M. D.; Alfe, D.; Michaelides, A. Benchmarking the Performance of Density Functional Theory and Point Charge Force Fields in Their Description of sI Methane Hydrate Against Diffusion Monte Carlo. *J. Chem. Phys.* **2014**, *140*, 174703.
(153) Gillan, M. J.; Alfe, D.; Manby, F. R. Energy Benchmarks for Methane-Water Systems from Quantum Monte Carlo and Second-Order Møller-Plesset Calculations. *J. Chem. Phys.* **2015**, *143*, 102812.
(154) Chen, J.; Ren, X.; Li, X.-Z.; Alfè, D.; Wang, E. On the Room-Temperature Phase Diagram of High Pressure Hydrogen: An ab Initio Molecular Dynamics Perspective and a Diffusion Monte Carlo Study. *J. Chem. Phys.* **2014**, *141*, 024501.
(155) Drummond, N. D.; Monserrat, B.; Lloyd-Williams, J. H.; Rios, P. L.; Pickard, C. J.; Needs, R. J. Quantum Monte Carlo Study of the Phase Diagram of Solid Molecular Hydrogen at Extreme Pressures. *Nat. Commun.* **2015**, *6*, 7794.
(156) Hongo, K.; Watson, M. A.; Sanchez-Carrera, R. S.; Iitaka, T.; Aspuru-Guzik, A. Failure of Conventional Density Functionals for the Prediction of Molecular Crystal Polymorphism: A Quantum Monte Carlo Study. *J. Phys. Chem. Lett.* **2010**, *1*, 1789−1794.
(157) Hongo, K.; Watson, M. a.; Iitaka, T.; Aspuru-Guzik, A.; Maezono, R. Diffusion Monte Carlo Study of Para-Diiodobenzene Polymorphism Revisited. *J. Chem. Theory Comput.* **2015**, *11*, 907−917.
(158) Watson, M. A.; Hongo, K.; Iitaka, T.; Aspuru-Guzik, A. *Advances in Quantum Monte Carlo*; American Chemical Society: Washington, DC, 2012; Vol. *1094*, Chapter 9, pp 101−117.
(159) Pedone, A.; Presti, D.; Menziani, M. C. On the Ability of Periodic Dispersion-Corrected DFT Calculations to Predict Molecular Crystal Polymorphism in para-Diiodobenzene. *Chem. Phys. Lett.* **2012**, *541*, 12−15.
(160) Taylor, C. R.; Bygrave, P. J.; Hart, J. N.; Allan, N. L.; Manby, F. R. Improving Density Functional Theory for Crystal Polymorph Energetics. *Phys. Chem. Chem. Phys.* **2012**, *14*, 7739−7743.
(161) Booth, G. H.; Grüneis, A.; Kresse, G.; Alavi, A. Towards an Exact Description of Electronic Wavefunctions in Real Solids. *Nature* **2013**, *493*, 365−370.
(162) Richard, R. M.; Herbert, J. M. A generalized many-body expansion and a unified view of fragment-based methods in electronic structure theory. *J. Chem. Phys.* **2012**, *137*, 064113.
(163) Mayhall, N. J.; Raghavachari, K. Many-Overlapping-Body (MOB) Expansion: A Generalized Many Body Expansion for Nondisjoint Monomers in Molecular Fragmentation Calculations of Covalent Molecules. *J. Chem. Theory Comput.* **2012**, *8*, 2669−2675.
(164) Gordon, M. S.; Fedorov, D. G.; Pruitt, S. R.; Slipchenko, L. Fragmentation Methods: A Route to Accurate Calculations on Large Systems. *Chem. Rev.* **2012**, *112*, 632−672.
(165) Raghavachari, K.; Saha, A. Accurate Composite and Fragment-Based Quantum Chemical Models for Large Molecules. *Chem. Rev.* **2015**, *115*, 5643−5677.
(166) Collins, M. A.; Bettens, R. P. A. Energy-Based Molecular Fragmentation Methods. *Chem. Rev.* **2015**, *115*, 5607−5642.
(167) Wen, S.; Nanda, K.; Huang, Y.; Beran, G. J. O. Practical Quantum Mechanics-Based Fragment Methods for Predicting Molecular Crystal Properties. *Phys. Chem. Chem. Phys.* **2012**, *14*, 7578−7590.
(168) Wen, S.; Beran, G. J. O. Accurate Molecular Crystal Lattice Energies from a Fragment QM/MM Approach with on-the-fly *ab Initio* Force-Field Parameterization. *J. Chem. Theory Comput.* **2011**, *7*, 3733−3742.
(169) Yang, J.; Hu, W.; Usvyat, D.; Matthews, D.; Schutz, M.; Chan, G. K.-L. Ab Initio Determination of the Crystalline Benzene Lattice Energy to Sub-Kilojoule/Mole Accuracy. *Science* **2014**, *345*, 640−643.
(170) Richard, R. M.; Lao, K. U.; Herbert, J. M. Understanding the Many-Body Expansion for Large Systems. I. Precision Considerations. *J. Chem. Phys.* **2014**, *141*, 014108.

DOI: 10.1021/acs.chemrev.5b00648
Chem. Rev. 2016, 116, 5567−5613

(171) Richard, R. M.; Lao, K. U.; Herbert, J. M. Achieving the CCSD(T) Basis-Set Limit in Sizable Molecular Clusters: Counterpoise Corrections for the Many-Body Expansion. *J. Phys. Chem. Lett.* **2013**, *4*, 2674−2680.
(172) Ouyang, J. F.; Cvitkovic, M. W.; Bettens, R. P. A. Trouble with the Many-Body Expansion. *J. Chem. Theory Comput.* **2014**, *10*, 3699−3707.
(173) Manby, F. R.; Alfè, D.; Gillan, M. J. Extension of Molecular Electronic Structure Methods to the Solid State: Computation of the Cohesive Energy of Lithium Hydride. *Phys. Chem. Chem. Phys.* **2006**, *8*, 5178−80.
(174) Nolan, S. J.; Bygrave, P. J.; Allan, N. L.; Manby, F. R. Comparison of the Incremental and Hierarchical Methods for Crystalline Neon. *J. Phys.: Condens. Matter* **2010**, *22*, 074201.
(175) Nolan, S. J.; Bygrave, P. J.; Allan, N. L.; Gillan, J.; Binnie, S.; Manby, F. R. In *Accurate Quantum Chemistry in the Condensed Phase*; Manby, F., Ed.; CRC Press: Boca Raton, FL, 2010; pp 85−103.
(176) Hirata, S.; Valiev, M.; Dupuis, M.; Xantheas, S. S.; Sugiki, S.; Sekino, H. Fast Electron Correlation Methods for Molecular Clusters in the Ground and Excited States. *Mol. Phys.* **2005**, *103*, 2255−2265.
(177) Kamiya, M.; Hirata, S.; Valiev, M. Fast electron Correlation Methods for Molecular Clusters without Basis Set Superposition Errors. *J. Chem. Phys.* **2008**, *128*, 074103.
(178) Hirata, S. Fast Electron-Correlation Methods for Molecular Crystals: An Application to the α, β_1, and β_2 Modifications of Solid Formic Acid. *J. Chem. Phys.* **2008**, *129*, 204104.
(179) Kitaura, K.; Ikeo, E.; Asada, T.; Nakano, T.; Uebayasi, M. Fragment Molecular Orbital Method: An Approximate Computational Method for Large Molecules. *Chem. Phys. Lett.* **1999**, *313*, 701−706.
(180) Fedorov, D. G.; Kitaura, K. Extending the Power of Quantum Chemsitry to Large Systems with the Fragment Molecular Orbital Method. *J. Phys. Chem. A* **2007**, *111*, 6904−6914.
(181) Nagayoshi, K.; Ikeda, T.; Kitaura, K.; Nagase, S. Computational Procedure of Lattice Energy using the ab Initio MO method. *J. Theor. Comput. Chem.* **2003**, *2*, 233−244.
(182) Momany, F. A. Determination of Partial Atomic Charges from ab Initio Molecular Electrostatic Potentials. Application to Formamide, Methanol, and Formic Acid. *J. Phys. Chem.* **1978**, *82*, 592−601.
(183) Sode, O.; Hirata, S. Second-Order Many-Body Perturbation Study of Solid Hydrogen Fluoride under Pressure. *Phys. Chem. Chem. Phys.* **2012**, *14*, 7765−7779.
(184) Gilliard, K.; Sode, O.; Hirata, S. Second-Order Many-Body Perturbation and Coupled-Cluster Singles and Doubles Study of Ice VIII. *J. Chem. Phys.* **2014**, *140*, 174507.
(185) Li, J.; Sode, O.; Voth, G. A.; Hirata, S. A Solid-Solid Phase Transition in Carbon Dioxide at High Pressures and Intermediate Temperatures. *Nat. Commun.* **2013**, *4*, 2647.
(186) Sode, O.; Keceli, M.; Yagi, K.; Hirata, S. Fermi Resonance in Solid CO_2 Under Pressure. *J. Chem. Phys.* **2013**, *138*, 074501.
(187) Cardini, G.; Schettino, V. Comment on "Fermi Resonance In Solid CO_2 Under Pressure" [J. Chem. Phys.138, 074501 (2013)]. *J. Chem. Phys.* **2014**, *074501*, 2013−2014.
(188) Hirata, S.; Sode, O.; Keçeli, M.; Yagi, K.; Li, J. Response to "Comment on 'Fermi Resonance in Solid CO_2 Under Pressure'" [J. Chem. Phys. 140, 177101 (2014)]. *J. Chem. Phys.* **2014**, *140*, 177102.
(189) Li, J.; Sode, O.; Hirata, S. Second-Order Many-Body Perturbation Study on Thermal Expansion of Solid Carbon Dioxide. *J. Chem. Theory Comput.* **2015**, *11*, 224−229.
(190) Sode, O.; Keceli, M.; Hirata, S.; Yagi, K. Coupled-Cluster and Many-Body Perturbation Study of Energies, Structures, and Phonon Dispersions of Solid Hydrogen Fluoride. *Int. J. Quantum Chem.* **2009**, *109*, 1928−1939.
(191) Sode, O.; Hirata, S. Second-Order Many-Body Perturbation Study of Solid Hydrogen Fluoride. *J. Phys. Chem. A* **2010**, *114*, 8873−7.
(192) Willow, S. Y.; Salim, M. a.; Kim, K. S.; Hirata, S. Ab Initio Molecular Dynamics of Liquid Water using Second-Order Many-Body Perturbation Theory. *Sci. Rep.* **2015**, *5*, 14358.
(193) Hirata, S.; Gilliard, K.; He, X.; Li, J.; Sode, O. Ab Initio Molecular Crystal Structures, Spectra, and Phase Diagrams. *Acc. Chem. Res.* **2014**, *47*, 2721−30.
(194) Bygrave, P. J.; Allan, N. L.; Manby, F. R. The Embedded Many-Body Expansion for Energetics of Molecular Crystals. *J. Chem. Phys.* **2012**, *137*, 164102.
(195) Gillan, M. J.; Alfè, D.; Bygrave, P. J.; Taylor, C. R.; Manby, F. R. Energy Benchmarks for Water Clusters and Ice Structures from an Embedded Many-Body Expansion. *J. Chem. Phys.* **2013**, *139*, 114101.
(196) Hartman, J. D.; Beran, G. J. O. Fragment-Based Electronic Structure Approach for Computing Nuclear Magnetic Resonance Chemical Shifts in Molecular Crystals. *J. Chem. Theory Comput.* **2014**, *10*, 4862−4872.
(197) Hartman, J. D.; Monaco, S.; Schatschneider, B.; Beran, G. J. O. Fragment-Based ^{13}C Nuclear Magnetic Resonance Chemical Shift Predictions in Molecular Crystals: An Alternative to Plane-Wave Methods. *J. Chem. Phys.* **2015**, *143*, 102809.
(198) Hartman, J. D.; Kudla, R. A.; Mueller, L. J.; Beran, G. J. O. Reliable Fragment-Based ^{1}H, ^{15}N and ^{17}O Chemical Shift Predictions in Molecular Crystals. 2016, submitted.
(199) Fang, T.; Li, W.; Gu, F.; Li, S. Accurate Prediction of Lattice Energies and Structures of Molecular Crystals with Molecular Quantum Chemistry Methods. *J. Chem. Theory Comput.* **2015**, *11*, 91−98.
(200) Manby, F. R.; Stella, M.; Goodpaster, J. D.; Miller, T. F. A Simple, Exact Density-Functional-Theory Embedding Scheme. *J. Chem. Theory Comput.* **2012**, *8*, 2564−2568.
(201) Goodpaster, J. D.; Barnes, T. A.; Manby, F. R.; Miller, T. F. Accurate and Systematically Improvable Density Functional Theory Embedding for Correlated Wavefunctions. *J. Chem. Phys.* **2014**, *140*, 18A507.
(202) Knizia, G.; Chan, G. K. L. Density Matrix Embedding: A Strong-Coupling Quantum Embedding Theory. *J. Chem. Theory Comput.* **2013**, *9*, 1428−1432.
(203) Bulik, I. W.; Chen, W.; Scuseria, G. E. Electron Correlation in Solids via Density Embedding Theory. *J. Chem. Phys.* **2014**, *141*, 0−10.
(204) Fornace, M. E.; Lee, J.; Miyamoto, K.; Manby, F. R.; Miller, T. F. Embedded Mean-Field Theory. *J. Chem. Theory Comput.* **2015**, *11*, 568−580.
(205) Dresselhaus, T.; Neugebauer, J. Part and Whole in Wave-function/DFT Embedding. *Theor. Chem. Acc.* **2015**, *134*, 97.
(206) Stoll, H. Correlation Energy of Diamond. *Phys. Rev. B: Condens. Matter Mater. Phys.* **1992**, *46*, 6700−6704.
(207) Stoll, H. On the Correlation Energy of Graphite. *J. Chem. Phys.* **1992**, *97*, 8449.
(208) Stoll, H. The Correlation Energy of Crystalline Silicon. *Chem. Phys. Lett.* **1992**, *191*, 548−552.
(209) Paulus, B. The Method of Increments−A Wavefunction-Based ab Initio Correlation Method for Solids. *Phys. Rep.* **2006**, *428*, 1−52.
(210) Svensson, M.; Humbel, S.; Froese, R. D.; Matasubara, T.; Sieber, S.; Morokuma, K. ONIOM: A Multilayer Integrated MO+MM Method for Geometry Optimizations and Single Point Energy Predictions. A Test for Diels-Alder Reactions and Pt(P(t-Bu)(3))(2)+H-2 Oxidative Addition. *J. Phys. Chem.* **1996**, *100*, 19357−19363.
(211) Chung, L. W.; Sameera, W. M. C.; Ramozzi, R.; Page, A. J.; Hatanaka, M.; Petrova, G. P.; Harris, T. V.; Li, X.; Ke, Z.; Liu, F.; et al. The ONIOM Method and Its Applications. *Chem. Rev.* **2015**, *115*, 5678−5796.
(212) Hopkins, B. W.; Tschumper, G. S. Multicentered QM/QM Methods for Overlapping Model Systems. *Mol. Phys.* **2005**, *103*, 309−315.
(213) Tschumper, G. S. Multicentered Integrated QM:QM Methods for Weakly Bound Clusters: An Efficient and Accurate 2-Body:Many-Body Treatment of Hydrogen Bonding and van der Waals Interactions. *Chem. Phys. Lett.* **2006**, *427*, 185−191.
(214) Dahlke, E. E.; Truhlar, D. G. Electrostatically Embedded Many-Body Correlation Energy, with Applications to the Calculation of Accurate Second-Order Møller-Plesset Perturbation Theory

DOI: 10.1021/acs.chemrev.5b00648
Chem. Rev. 2016, 116, 5567−5613

Energies for Large Water Clusters. *J. Chem. Theory Comput.* **2007**, *3*, 1342−1348.
(215) Müller, C.; Paulus, B. Wavefunction-Based Electron Correlation Methods For Solids. *Phys. Chem. Chem. Phys.* **2012**, *14*, 7605−7614.
(216) Rosciszewski, K.; Paulus, B.; Fulde, P.; Stoll, H. Ab Initio Calculation of Ground-State Properties of Rare-Gas Crystals. *Phys. Rev. B: Condens. Matter Mater. Phys.* **1999**, *60*, 7905−7910.
(217) Schwerdtfeger, P.; Assadollahzadeh, B.; Hermann, A. Convergence of the Møller-Plesset Perturbation Series for the fcc Lattices of Neon and Argon. *Phys. Rev. B: Condens. Matter Mater. Phys.* **2010**, *82*, 205111.
(218) Hermann, A.; Schwerdtfeger, P. Ground-State Properties of Crystalline Ice from Periodic Hartree-Fock Calculations and a Coupled-Cluster-Based Many-Body Decomposition of the Correlation Energy. *Phys. Rev. Lett.* **2008**, *101*, 183005.
(219) Bludsky, O.; Rubes, M.; Soldan, P. *Ab Initio* Investigation of Intermolecular Interactions in Solid Benzene. *Phys. Rev. B: Condens. Matter Mater. Phys.* **2008**, *77*, 092103.
(220) Tsuzuki, S.; Orita, H.; Honda, K.; Mikami, M. First-Principles Lattice Energy Calculation of Urea and Hexamine Crystals by a Combination of Periodic DFT and MP2 Two-Body Interaction Energy Calculations. *J. Phys. Chem. B* **2010**, *114*, 6799−6805.
(221) Bartok, A. P.; Gillan, M. J.; Manby, F. R.; Csanyi, G. Machine-Learning Approach for One- and Two-Body Corrections to Density Functional Theory: Applications to Molecular and Condensed Water. *Phys. Rev. B: Condens. Matter Mater. Phys.* **2013**, *88*, 054104.
(222) Huang, Y.; Beran, G. J. O. Reliable Prediction of Three-Body Intermolecular Interactions using Dispersion-Corrected Second-Order Møller-Plesset Perturbation Theory. *J. Chem. Phys.* **2015**, *143*, 044113.
(223) Beran, G. J. O. Approximating Quantum Many-Body Intermolecular Interactions in Molecular Clusters using Classical Polarizable Force Fields. *J. Chem. Phys.* **2009**, *130*, 164115.
(224) Beran, G. J. O.; Nanda, K. Predicting Organic Crystal Lattice Energies with Chemical Accuracy. *J. Phys. Chem. Lett.* **2010**, *1*, 3480−3487.
(225) Beran, G. J. O.; Wen, S.; Nanda, K.; Huang, Y.; Heit, Y. Accurate Molecular Crystal Modeling with Fragment-Based Electronic Structure Methods. *Top. Curr. Chem.* **2014**, *345*, 59−93.
(226) Neill, D. P. O.; Allan, N. L.; Manby, F. R. In *Accurate Quantum Chemistry in the Condensed Phase*; Manby, F., Ed.; CRC Press: Boca Raton, FL, 2010; pp 163−193.
(227) Ren, P.; Ponder, J. W. Polarizable Atomic Multipole Water Model for Molecular Mechanics Simulation. *J. Phys. Chem. B* **2003**, *107*, 5933−5947.
(228) Ren, P.; Wu, C.; Ponder, J. W. Polarizable Atomic Multipole-based Molecular Mechanics for Organic Molecules. *J. Chem. Theory Comput.* **2011**, *7*, 3143−3161.
(229) Wu, J. C.; Chattree, G.; Ren, P. Automation of AMOEBA Polarizable Force Field Parameterization for Small Molecules. *Theor. Chem. Acc.* **2012**, *131*, 1138.
(230) Sebetci, A.; Beran, G. J. O. Spatially Homogeneous QM/MM for Systems of Interacting Molecules with on-the-fly ab Initio Force-Field Parameterization. *J. Chem. Theory Comput.* **2010**, *6*, 155−167.
(231) Nanda, K.; Beran, G. J. O. Prediction of Organic Molecular Crystal Geometries from MP2-Level Fragment Quantum Mechanical/Molecular Mechanical Calculations. *J. Chem. Phys.* **2012**, *137*, 174106.
(232) Heit, Y.; Beran, G. J. O. Exploting Space Group Symmetry in Fragment-Based Molecular Crystal Calculations. *J. Comput. Chem.* **2014**, *35*, 2205−2214.
(233) Heit, Y. N.; Nanda, K. D.; Beran, G. J. O. Predicting Finite-Temperature Properties of Crystalline Carbon Dioxide from First Principles with Quantitative Accuracy. *Chem. Sci.* **2016**, *7*, 246−255.
(234) Heit, Y. N.; Beran, G. J. O. How Important Is Thermal Expansion for Predicting Molecular Crystal Structures and Thermochemistry at Finite Temperatures? 2016, submitted.
(235) Wen, S.; Beran, G. J. O. Accidental Degeneracy in Crystalline Aspirin: New Insights from High-Level ab Initio Calculations. *Cryst. Growth Des.* **2012**, *12*, 2169−2172.
(236) Wen, S.; Beran, G. J. O. Crystal Polymorphism in Oxalyl Dihydrazide: Is Empirical DFT-D Accurate Enough? *J. Chem. Theory Comput.* **2012**, *8*, 2698−2705.
(237) Nanda, K.; Beran, G. J. O. What Governs the Proton-Ordering in Ice XV? *J. Phys. Chem. Lett.* **2013**, *4*, 3165−3169.
(238) Pruitt, S. R.; Addicoat, M. A.; Collins, M. A.; Gordon, M. S. The Fragment Molecular Orbital and Systematic Molecular Fragmentation Methods Applied to Water Clusters. *Phys. Chem. Chem. Phys.* **2012**, *14*, 7752.
(239) Boese, A. D.; Oren, M.; Atasoylu, O.; Martin, J. M. L.; Kallay, M.; Gauss, J. W3 Theory: Robust Computational Thermochemistry in the kJ/mol Accuracy Range. *J. Chem. Phys.* **2004**, *120*, 4129−4141.
(240) Thompson, H. P. G.; Day, G. M. Which Conformations Make Stable Crystal Structures? Mapping Crystalline Molecular Geometries to the Conformational Energy Landscape. *Chem. Sci.* **2014**, *5*, 3173−3182.
(241) Dunlap, B. I. Fitting the Coulomb Potential Variationally in *Xα* Molecular Calculations. *J. Chem. Phys.* **1983**, *78*, 3140−3142.
(242) Weigend, F.; Häser, M.; Patzelt, H.; Ahlrichs, R. RI-MP2: Optimized Auxiliary Basis Sets and Demonstration of Efficiency. *Chem. Phys. Lett.* **1998**, *294*, 143−152.
(243) Feyereisen, M. W.; Fitzgerald, G.; Komornicki, A. Use of Approximate Integrals in ab Initio Theory. An Application in MP2 Energy Calculations. *Chem. Phys. Lett.* **1993**, *208*, 359−363.
(244) Weigend, F. A Fully Direct RI-HF Algorithm: Implementation, Optimised Auxiliary Basis Sets, Demonstration of Accuracy and Efficiency. *Phys. Chem. Chem. Phys.* **2002**, *4*, 4285−4291.
(245) Sinnokrot, M. O.; Sherrill, C. D. High-Accuracy Quantum Mechanical Studies of *π*-*π* Interactions in Benzene Dimers. *J. Phys. Chem. A* **2006**, *110*, 10656−10668.
(246) Hesselmann, A. Improved Supermolecular Second Order Møller-Plesset Intermolecular Interaction Energies using Time-Dependent Density Functional Response Theory. *J. Chem. Phys.* **2008**, *128*, 144112.
(247) Tsuzuki, S.; Uchimaru, T.; Mikami, M.; Tanabe, K. Intermolecular Interaction Potential of the Carbon Dioxide Dimer. *J. Chem. Phys.* **1998**, *109*, 2169−2175.
(248) Chalasinski, G.; Szczesniak, M. M. On the Connection Between the Supermolecular Møller-Plesset Treatment of the Interaction Energy and the Perturbation Theory of Intermolecular Forces. *Mol. Phys.* **1988**, *63*, 205−224.
(249) Cybulski, S. M.; Chalasinski, G.; Moszynski, R. On Decomposition of Second-Order Møller-Plesset Supermolecular Interaction Energy and Basis Set Effects. *J. Chem. Phys.* **1990**, *92*, 4357−4363.
(250) Gerenkamp, M.; Grimme, S. Spin-Component Scaled Second-Order Møller-Plesset Perturbation Theory for the Calculation of Molecular Geometries and Harmonic Vibrational Frequencies. *Chem. Phys. Lett.* **2004**, *392*, 229−235.
(251) Hill, J. G.; Platts, J. A. Spin-Component Scaling Methods for Weak and Stacking Interactions. *J. Chem. Theory Comput.* **2007**, *3*, 80.
(252) Distasio, R. A.; Head-Gordon, M. Optimized Spin-Component-Scaled Second-Order Møller-Plesset Perturbation Theory for Intermolecular Interaction Energies. *Mol. Phys.* **2007**, *105*, 1073−1083.
(253) Burns, L. A.; Marshall, M. S.; Sherrill, C. D. Appointing Silver and Bronze Standards for Noncovalent Interactions: A Comparison of Spin-Component-Scaled (SCS), Explicitly Correlated (F12), and Specialized Wavefunction Approaches. *J. Chem. Phys.* **2014**, *141*, 234111.
(254) Jurečka, P.; Šponer, J.; Černý, J.; Hobza, P. Benchmark Database of Accurate (MP2 and CCSD(T) Complete Basis Set Limit) Interaction Energies of Small Model Complexes, DNA Base Pairs, and Amino Acid Pairs. *Phys. Chem. Chem. Phys.* **2006**, *8*, 1985−1993.
(255) Goldey, M.; Head-Gordon, M. Separate Electronic Attenuation Allowing a Spin-Component-Scaled Second-Order Møller-Plesset Theory to Be Effective for Both Thermochemistry and Noncovalent Interactions. *J. Phys. Chem. B* **2014**, *118*, 6519−6525.

DOI: 10.1021/acs.chemrev.5b00648
Chem. Rev. 2016, 116, 5567−5613

(256) Marchetti, O.; Werner, H.-J. Accurate Calculations of Intermolecular Interaction Energies Using Explicitly Correlated Coupled Cluster Wave Functions and a Dispersion-Weighted MP2 Method. *J. Phys. Chem. A* **2009**, *113*, 11580−11585.
(257) Tkatchenko, A.; Distasio, R. A.; Head-Gordon, M.; Scheffler, M. Dispersion-Corrected Møller-Plesset Second-Order Perturbation Theory. *J. Chem. Phys.* **2009**, *131*, 094106.
(258) Cybulski, S. M.; Lytle, M. L. The Origin of Deficiency of the Supermolecule Second-Order Møller-Plesset Approach for Evaluating Interaction Energies. *J. Chem. Phys.* **2007**, *127*, 141102.
(259) Pitonak, M.; Hesselmann, A. Accurate Intermolecular Interaction Energies from a Combination of MP2 and TDDFT Response Theory. *J. Chem. Theory Comput.* **2010**, *6*, 168−178.
(260) Grafova, L.; Pitonak, M.; Rezac, J.; Hobza, P. Comparative Study of Selected Wave Function and Density Functional Methods for Noncovalent Interaction Energy Calculations Using the Extended S22 Data Set. *J. Chem. Theory Comput.* **2010**, *6*, 2365−2376.
(261) Hesselmann, A.; Korona, T. On the Accuracy of DFT-SAPT, MP2, SCS-MP2, MP2C, and DFT+Disp Methods for the Interaction Energies of Endohedral Complexes of the C_{60} Fullerene with a Rare Gas Atom. *Phys. Chem. Chem. Phys.* **2011**, *13*, 732−43.
(262) Jenness, G. R.; Karalti, O.; Al-Saidi, W. A.; Jordan, K. D. Evaluation of Theoretical Approaches for Describing the Interaction of Water with Linear Acenes. *J. Phys. Chem. A* **2011**, *115*, 5955−5964.
(263) Hohenstein, E. G.; Jaeger, H. M.; Carrell, E. J.; Tschumper, G. S.; Sherrill, C. D. Accurate Interaction Energies for Problematic Dispersion-Bound Complexes: Homogeneous Dimers of NCCN, P_2, and PCCP. *J. Chem. Theory Comput.* **2011**, *7*, 2842−2851.
(264) Granatier, J.; Pitonak, M.; Hobza, P. Accuracy of Several Wave Function and Density Functional Theory Methods for Description of Noncovalent Interaction of Saturated and Unsaturated Hydrocarbon Dimers. *J. Chem. Theory Comput.* **2012**, *8*, 2282−2292.
(265) Heßelmann, A.; Korona, T. Intermolecular Symmetry-Adapted Perturbation Theory Study of Large Organic Complexes. *J. Chem. Phys.* **2014**, *141*, 094107.
(266) Huang, Y.; Shao, Y.; Beran, G. J. O. Accelerating MP2C Dispersion Corrections for Dimers and Molecular Crystals. *J. Chem. Phys.* **2013**, *138*, 224112.
(267) Huang, Y.; Goldey, M.; Head-Gordon, M.; Beran, G. J. O. Achieving High-Accuracy Intermolecular Interactions by Combining Coulomb-Attenuated Second-Order Møller-Plesset Perturbation Theory with Coupled Kohn-Sham Dispersion. *J. Chem. Theory Comput.* **2014**, *10*, 2054−2063.
(268) Goldey, M.; Head-Gordon, M. Attenuating Away the Errors in Inter- and Intramolecular Interactions from Second-Order Møller-Plesset Calculations in the Small Aug-cc-pVDZ Basis Set. *J. Phys. Chem. Lett.* **2012**, *3*, 3592−3598.
(269) Goldey, M.; Dutoi, A.; Head-Gordon, M. Attenuated Second-Order Møller-Plesset Perturbation Theory: Performance within the aug-cc-pVTZ Basis. *Phys. Chem. Chem. Phys.* **2013**, *15*, 15869−15875.
(270) Dutoi, A. D.; Head-Gordon, M. A Study of the Effect of Attenuation Curvature on Molecular Correlation Energies by Introducing an Explicit Cutoff Radius into Two-Electron Integrals. *J. Phys. Chem. A* **2008**, *112*, 2110−2119.
(271) Masur, O.; Usvyat, D.; Schütz, M. Efficient and Accurate Treatment of Weak Pairs in Local CCSD(T) Calculations. *J. Chem. Phys.* **2013**, *139*, 164116.
(272) Schütz, M.; Masur, O.; Usvyat, D. Efficient and Accurate Treatment of Weak Pairs in Local CCSD(T) Calculations. II. Beyond the Ring Approximation. *J. Chem. Phys.* **2014**, *140*, 244107.
(273) Goldey, M. B.; Belzunces, B.; Head-Gordon, M. Attenuated MP2 with a Long-Range Dispersion Correction for Treating Nonbonded Interactions. *J. Chem. Theory Comput.* **2015**, *11*, 4159.
(274) Gonthier, J. F.; Corminboeuf, C. Exploration of Zeroth-Order Wavefunctions and Energies as a First Step toward Intramolecular Symmetry-Adapted Perturbation Theory. *J. Chem. Phys.* **2014**, *140*, 154107.
(275) Parrish, R. M.; Gonthier, J. F.; Corminbœuf, C.; Sherrill, C. D. Communication: Practical intramolecular symmetry adapted perturbation theory via Hartree-Fock embedding. *J. Chem. Phys.* **2015**, *143*, 051103.
(276) Pastorczak, E.; Prlj, A.; Gonthier, J. F.; Corminboeuf, C. Intramolecular Symmetry-Adapted Perturbation Theory with a Single-Determinant Wavefunction. *J. Chem. Phys.* **2015**, *143*, 224107.
(277) Pitonak, M.; Neogrady, P.; Cerny, J.; Grimme, S.; Hobza, P. Scaled MP3 Non-Covalent Interaction Energies Agree Closely with Accurate CCSD(T) Benchmark Data. *ChemPhysChem* **2009**, *10*, 282−289.
(278) Sedlak, R.; Riley, K. E.; Řezáč, J.; Pitoňák, M.; Hobza, P. MP2.5 and MP2.X: Approaching CCSD(T) Quality Description of Noncovalent Interaction at the Cost of a Single CCSD Iteration. *ChemPhysChem* **2013**, *14*, 698−707.
(279) Podeszwa, R.; Rice, B. M.; Szalewicz, K. Predicting Structure of Molecular Crystals from First Principles. *Phys. Rev. Lett.* **2008**, *101*, 115503.
(280) Podeszwa, R.; Szalewicz, K. Three-Body Symmetry-Adapted Perturbation Theory Based on Kohn-Sham Description of the Monomers. *J. Chem. Phys.* **2007**, *126*, 194101.
(281) Neese, F.; Wennmohs, F.; Hansen, A. Efficient and Accurate Local Approximations to Coupled-Electron Pair Approaches: An Attempt to Revive the Pair Natural Orbital Method. *J. Chem. Phys.* **2009**, *130*, 114108.
(282) Riplinger, C.; Sandhoefer, B.; Hansen, A.; Neese, F. Natural Triple Excitations in Local Coupled Cluster Calculations with Pair Natural Orbitals *J. Chem. Phys.* **2013**, *139*.13410110.1063/1.4821834
(283) Taube, A. G.; Bartlett, R. J. Frozen Natural Orbital Coupled-Cluster Theory: Forces and Application to Decomposition of Nitroethane. *J. Chem. Phys.* **2008**, *128*, 164101.
(284) DePrince, A. E.; Sherrill, C. D. Accuracy and Efficiency of Coupled-Cluster Theory Using Density Fitting/Cholesky Decomposition, Frozen Natural Orbitals, and a t_1 Transformed Hamiltonian. *J. Chem. Theory Comput.* **2013**, *9*, 2687−2696.
(285) Yang, J.; Chan, G. K. L.; Manby, F. R.; Schütz, M.; Werner, H. J. The Orbital-Specific-Virtual Local Coupled Cluster Singles and Doubles Method. *J. Chem. Phys.* **2012**, *136*, 144105.
(286) Kennedy, M. R.; McDonald, A. R.; DePrince, A. E.; Marshall, M. S.; Podeszwa, R.; Sherrill, C. D. Communication: Resolving the Three-Body Contribution to the Lattice Energy of Crystalline Benzene: Benchmark Results from Coupled-Cluster Theory. *J. Chem. Phys.* **2014**, *140*, 121104.
(287) Jeziorski, B.; Moszynski, R.; Szalewicz, K. Perturbation Theory Approach to Intermolecular Potential Energy Surfaces of van der Waals Complexes. *Chem. Rev.* **1994**, *94*, 1887−1930.
(288) Szalewicz, K. Symmetry-Adapted Perturbation Theory of Intermolecular Forces. *WIRES: Comput. Mol. Sci.* **2012**, *2*, 254−272.
(289) Lotrich, V. F.; Szalewicz, K. Symmetry-Adapted Perturbation Theory of Three-Body Nonadditivity of Intermolecular Interaction Energy. *J. Chem. Phys.* **1997**, *106*, 9668−9687.
(290) Hesselmann, A.; Jansen, G.; Schütz, M. Density-Functional Theory-Symmetry-Adapted Intermolecular Perturbation Theory with Density Fitting: A New Efficient Method to Study Intermolecular Interaction Energies. *J. Chem. Phys.* **2005**, *122*, 14103.
(291) Misquitta, A. J.; Szalewicz, K. Symmetry-Adapted Perturbation-Theory Calculations of Intermolecular Forces Employing Density-Functional Description of Monomers. *J. Chem. Phys.* **2005**, *122*, 214109.
(292) Parker, T. M.; Burns, L. A.; Parrish, R. M.; Ryno, A. G.; Sherrill, C. D. Levels of Symmetry Adapted Perturbation Theory (SAPT). I. Efficiency and Performance for Interaction Energies. *J. Chem. Phys.* **2014**, *140*, 094106.
(293) Podeszwa, R.; Cencek, W.; Szalewicz, K. Efficient Calculations of Dispersion Energies for Nanoscale Systems from Coupled Density Response Functions. *J. Chem. Theory Comput.* **2012**, *8*, 1963−1969.
(294) Podeszwa, R.; Bukowski, R.; Rice, B. M.; Szalewicz, K. Potential Energy Surface for Cyclotrimethylene Trinitramine Dimer from Symmetry-Adapted Perturbation Theory. *Phys. Chem. Chem. Phys.* **2007**, *9*, 5561−9.

DOI: 10.1021/acs.chemrev.5b00648
Chem. Rev. 2016, 116, 5567−5613

(295) Podeszwa, R.; Rice, B. M.; Szalewicz, K. Crystal Structure Prediction for Cyclotrimethylene Trinitramine (RDX) from First Principles. *Phys. Chem. Chem. Phys.* **2009**, *11*, 5512−8.
(296) Jacobson, L. D.; Herbert, J. M. An Efficient, Fragment-Based Electronic Structure Method for Molecular Systems: Self-Consistent Polarization with Perturbative Two-Body Exchange and Dispersion. *J. Chem. Phys.* **2011**, *134*, 094118.
(297) Lao, K. U.; Herbert, J. M. Accurate Intermolecular Interactions at Dramatically Reduced Cost: XPol+SAPT with Empirical Dispersion. *J. Phys. Chem. Lett.* **2012**, *3*, 3241−3248.
(298) Lao, K. U.; Herbert, J. M. An improved treatment of empirical dispersion and a many-body energy decomposition scheme for the explicit polarization plus symmetry-adapted perturbation theory (XSAPT) method. *J. Chem. Phys.* **2013**, *139*, 034107.
(299) Klopper, W.; Manby, F. R.; Ten-No, S.; Valeev, E. F. R12 methods in explicitly correlated molecular electronic structure theory. *Int. Rev. Phys. Chem.* **2006**, *25*, 427−468.
(300) Hättig, C.; Klopper, W.; Köhn, A.; Tew, D. P. Explicitly Correlated Electrons in Molecules. *Chem. Rev.* **2012**, *112*, 4−74.
(301) Kong, L.; Bischoff, F. A.; Valeev, E. F. Explicitly Correlated R12/F12 Methods for Electronic Structure. *Chem. Rev.* **2012**, *112*, 75−107.
(302) Marchetti, O.; Werner, H.-J. Accurate Calculations of Intermolecular Interaction Energies using Explicitly Correlated Wave Functions. *Phys. Chem. Chem. Phys.* **2008**, *10*, 3400−3409.
(303) Riley, K. E.; Platts, J. A.; Řezáč, J.; Hobza, P.; Hill, J. G. Assessment of the Performance of MP2 and MP2 Variants for the Treatment of Noncovalent Interactions. *J. Phys. Chem. A* **2012**, *116*, 4159−69.
(304) Platts, J. A.; Hill, J. G.; Riley, K. E.; Řezáč, J.; Hobza, P. Basis Set Dependence of Interaction Energies Computed Using Composite Post-MP2 Methods. *J. Chem. Theory Comput.* **2013**, *9*, 330−337.
(305) de Lange, K. M.; Lane, J. R. Explicit Correlation and Intermolecular Interactions: Investigating Carbon Dioxide Complexes with the CCSD(T)-F12 Method. *J. Chem. Phys.* **2011**, *134*, 034301.
(306) Valeev, E. F. Improving on the Resolution of the Identity in Linear R12 ab Initio Theories. *Chem. Phys. Lett.* **2004**, *395*, 190−195.
(307) Knizia, G.; Adler, T. B.; Werner, H.-J. Simplified CCSD(T)-F12 Methods: Theory and Benchmarks. *J. Chem. Phys.* **2009**, *130*, 054104.
(308) Boys, S. F.; Bernardi, F. The Calculation of Small Molecular Interactions by the Differences of Separate Total Energies. Some Procedures with Reduced Errors. *Mol. Phys.* **1970**, *19*, 553−566.
(309) Wells, B. H.; Wilson, S. Van der Waals Interaction Potentials: Many-Body Basis Set Superposition Effects. *Chem. Phys. Lett.* **1983**, *101*, 429−434.
(310) Turi, L.; Dannenberg, J. J. Correcting for Basis Set Superposition Error. *J. Phys. Chem.* **1993**, *97*, 2488−2490.
(311) Valiron, P.; Mayer, I. Hierarchy of Counterpoise Corrections for N-Body Clusters: Generalization of the Boys-Bernardi Scheme. *Chem. Phys. Lett.* **1997**, *275*, 46−55.
(312) Góra, U.; Podeszwa, R.; Cencek, W.; Szalewicz, K. Interaction Energies of Large Clusters from Many-Body Expansion. *J. Chem. Phys.* **2011**, *135*, 224102.
(313) Beran, G. J. O. A New Era for ab Initio Molecular Crystal Lattice Energy Prediction. *Angew. Chem., Int. Ed.* **2015**, *54*, 396−398.
(314) Price, S. L. Lattice Energy, Nailed? *Science* **2014**, *345*, 619−620.
(315) Ringer, A. L.; Sherrill, C. D. First-Principles Computation of Lattice Energies of Organic Solids: The Benzene Crystal. *Chem. - Eur. J.* **2008**, *14*, 2542−2547.
(316) Huang, Y. Fast and Accurate Electronic Structure Methods for Predicting Two- and Three-Body Noncovalent Interactions. Ph.D. thesis, University of California, Riverside, 2015.
(317) Lu, D.; Li, Y.; Rocca, D.; Galli, G. *Ab Initio* Calculation of van der Waals Bonded Molecular Crystals. *Phys. Rev. Lett.* **2009**, *102*, 206411.
(318) Ikabata, Y.; Tsukamoto, Y.; Imamura, Y.; Nakai, H. Local Response Dispersion Method in Periodic Systems: Implementation and Assessment. *J. Comput. Chem.* **2015**, *36*, 303−311.
(319) Acree, W.; Chickos, J. S. Phase Transition Enthalpy Measurements of Organic and Organometallic Compounds. Sublimation, Vaporization and Fusion Enthalpies From 1880 to 2010. *J. Phys. Chem. Ref. Data* **2010**, *39*, 043101.
(320) Brandenburg, J. G.; Maas, T.; Grimme, S. Benchmarking DFT and Semiempirical Methods on Structures and Lattice Energies for Ten Ice Polymorphs. *J. Chem. Phys.* **2015**, *142*, 124104.
(321) Červinka, C.; Fulem, M.; Růžička, K. CCSD(T)/CBS Fragment-Based Calculations of Lattice Energy of Molecular Crystals. *J. Chem. Phys.* **2016**, *144*, 064505.
(322) Krupskii, I. N.; Prokhvatilov, A. I.; Erenburg, A. I.; Barylnik, A. S. Thermal Expansion X-Ray Studies of Solid CO_2. *Fiz. Nizk. Temp.* **1982**, *8*, 533.
(323) Röttger, K.; Endriss, A.; Ihringer, J.; Doyle, S.; Kuhs, W. F. Lattice Constants and Thermal Expansion of H_2O and D_2O Ice Ih between 10 and 265 K. *Acta Crystallogr., Sect. B: Struct. Sci.* **1994**, *50*, 644−648.
(324) Harper, J. K.; Iuliucci, R.; Gruber, M.; Kalakewich, K. Refining Crystal Structures with Experimental ^{13}C NMR Shift Tensors and Lattice-Including Electronic Structure Methods. *CrystEngComm* **2013**, *15*, 8693.
(325) Byrd, E. F. C.; Scuseria, G. E.; Chabalowski, C. F. An ab Initio Study of Solid Nitromethane, HMX, RDX, and CL20: Successes and Failures of DFT. *J. Phys. Chem. B* **2004**, *108*, 13100−13106.
(326) Byrd, E.; Rice, B. Ab Initio Study of Compressed 1,3,5,7-Tetranitro-1,3,5,7-tetraazacyclooctane (HMX), Cyclotrimethylenetrinitramine (RDX), 2,4,6,8,10,12-Hexanitrohexaazaisowurzitane (CL-20), 2,4,6-Trinitro-1,3,5-benzenetriamine (TATB), and Pentaerythritol Tetranitrate (PETN). *J. Phys. Chem. C* **2007**, *111*, 2787−2796.
(327) van de Streek, J.; Neumann, M. A. Validation of Experimental Molecular Crystal Structures with Dispersion-Corrected Density Functional Theory Calculations. *Acta Crystallogr., Sect. B: Struct. Sci.* **2010**, *66*, 544−58.
(328) Neumann, M. A.; Perrin, M. A. Energy Ranking of Molecular Crystals using Density Functional Theory Calculations and an Empirical van der Waals Correction. *J. Phys. Chem. B* **2005**, *109*, 15531−15541.
(329) Bond, A. D.; Solanko, K. A.; van de Streek, J.; Neumann, M. A. Experimental Verification of a Subtle Low-Temperature Phase Transition Suggested by DFT-D Energy Minimisation. *CrystEngComm* **2011**, *13*, 1768.
(330) van de Streek, J.; Neumann, M. A. Validation of Molecular Crystal Structures from Powder Diffraction Data with Dispersion-Corrected Density Functional Theory (DFT-D). *Acta Crystallogr., Sect. B: Struct. Sci., Cryst. Eng. Mater.* **2014**, *70*, 1020−1032.
(331) Sorescu, D. C.; Rice, B. M. Theoretical Predictions of Energetic Molecular Crystals at Ambient and Hydrostatic Compression Conditions Using Dispersion Corrections to Conventional Density Functionals (DFT-D). *J. Phys. Chem. C* **2010**, *114*, 6734−6748.
(332) Balu, R.; Byrd, E. F. C.; Rice, B. M. Assessment of Dispersion Corrected Atom Centered Pseudopotentials: Application to Energetic Molecular Crystals. *J. Phys. Chem. B* **2011**, *115*, 803−10.
(333) Sorescu, D. C.; Byrd, E. F. C.; Rice, B. M.; Jordan, K. D. Assessing the Performances of Dispersion-Corrected Density Functional Methods for Predicting the Crystallographic Properties of High Nitrogen Energetic Salts. *J. Chem. Theory Comput.* **2014**, *10*, 4982−4994.
(334) Blood-Forsythe, M. A.; Markovich, T.; DiStasio, R. A., Jr.; Roberto, C.; Aspuru-Guzik, A. Analytical nUclear Gradients for the Range-Separated Many-Body Dispersion Model of Noncovalent Interactions. *Chem. Sci.* **2016**, *7*, 1712.
(335) Chisholm, J. A.; Motherwell, W. D. S. COMPACK: A Program for Identifying Crystal Structure Similarity using Distances. *J. Appl. Crystallogr.* **2005**, *38*, 228−231.

DOI: 10.1021/acs.chemrev.5b00648
Chem. Rev. 2016, 116, 5567−5613

(336) He, X.; Sode, O.; Xantheas, S. S.; Hirata, S. Second-Order Many-Body Perturbation Study of Ice Ih. *J. Chem. Phys.* **2012**, *137*, 204505.
(337) Manzhelii, V. G.; Tolkachev, A. M.; Bagatskii, M. I.; Voitovich, E. I. Thermal Expansion, Heat Capacity, and Compressibility of Solid CO. *Phys. Status Solidi B* **1971**, *44*, 39−49.
(338) Keesom, W. H.; Kohler, J. W. L. The Lattice Constant and Expansion Coeffcient of Solid Carbon Dioxide. *Physica* **1934**, *1*, 655−658.
(339) Curzon, A. A Comment on the Lattice Parameter of Solid Carbon Dioxide At −190 C. *Physica* **1972**, *59*, 733.
(340) Brock, C. P.; Dunitz, J. D. Towards a Grammar of Crystal Packing. *Chem. Mater.* **1994**, *6*, 1118−1127.
(341) van de Streek, J.; Neumann, M. A. Crystal-Structure Prediction of Pyridine with Four Independent Molecules. *CrystEngComm* **2011**, *13*, 7135.
(342) Gavezzotti, A.; Filippini, G. Polymorphic Forms of Organic Crystals at Room Conditions: Thermodynamic and Structural Implications. *J. Am. Chem. Soc.* **1995**, *117*, 12299−12305.
(343) Neumann, M. A.; Leusen, F. J. J.; Kendrick, J. A Major Advance in Crystal Structure Prediction. *Angew. Chem., Int. Ed.* **2008**, *47*, 2427−2430.
(344) Kazantsev, A. V.; Karamertzanis, P. G.; Adjiman, C. S.; Pantelides, C. C.; Price, S. L.; Galek, P. T. A.; Day, G. M.; Cruz-Cabeza, A. J. Successful Prediction of a Model Pharmaceutical in the Fifth Blind Test of Crystal Structure Prediction. *Int. J. Pharm.* **2011**, *418*, 168−178.
(345) Kendrick, J.; Leusen, F. J. J.; Neumann, M. A.; van de Streek, J. Progress in Crystal Structure Prediction. *Chem. - Eur. J.* **2011**, *17*, 10736−10744.
(346) Price, S. L.; Price, L. S. In *Solid State Characterization of Pharmaceuticals*, 1st ed.; Storey, R., Ymen, I., Eds.; Blackwell: London, 2011; pp 427−450.
(347) Oganov, A. R.; Schön, J. C.; Jansen, M.; Woodley, S. M.; Tipton, W. W.; Hennig, R. G. In *Modern Methods of Crystal Structure Prediction*; Oganov, A. R., Ed.; Wiley: Weinheim, Germany, 2011; pp 223−231.
(348) Neumann, M. A. Tailor-Made Force Fields for Crystal-Structure Prediction. *J. Phys. Chem. B* **2008**, *112*, 9810−29.
(349) Neumann, M. A.; van de Streek, J.; Fabbiani, F. P. A.; Hidber, P.; Grassmann, O. Combined Crystal Structure Prediction and High-Pressure Crystallization in Rational Pharmaceutical Polymorph Screening. *Nat. Commun.* **2015**, *6*, 7793.
(350) Asmadi, A.; Neumann, M. A.; Kendrick, J.; Girard, P.; Perrin, M. A.; Leusen, F. J. J. Revisiting the Blind Tests in Crystal Structure Prediction: Accurate Energy Ranking of Molecular Crystals. *J. Phys. Chem. B* **2009**, *113*, 16303−16313.
(351) Chan, H. C. S.; Kendrick, J.; Leusen, F. J. J. Molecule VI, a Benchmark Crystal-Structure-Prediction Sulfonimide: Are Its Polymorphs Predictable? *Angew. Chem., Int. Ed.* **2011**, *50*, 2979−2981.
(352) Chan, H. C. S.; Kendrick, J.; Leusen, F. J. J. Predictability of the Polymorphs of Small Organic Compounds: Crystal Structure Predictions of Four Benchmark Blind Test Molecules. *Phys. Chem. Chem. Phys.* **2011**, *13*, 20361−70.
(353) Karamertzanis, P. G.; Kazantsev, A. V.; Issa, N.; Welch, G. W. A.; Adjiman, C. S.; Pantelides, C. C.; Price, S. L. Can the Formation of Pharmaceutical Cocrystals Be Computationally Predicted? 2. Crystal Structure Prediction. *J. Chem. Theory Comput.* **2009**, *5*, 1432−1448.
(354) Karamertzanis, P. G.; Pantelides, C. C. Ab Initio Crystal Structure Prediction−I. Rigid molecules. *J. Comput. Chem.* **2005**, *26*, 304−324.
(355) van Eijck, B. P.; Mooij, W. T. M.; Kroon, J. Attempted Prediction of the Crystal Structures of Six Monosaccharides. *Acta Crystallogr., Sect. B: Struct. Sci.* **1995**, *51*, 99−103.
(356) Mooij, W. T. M.; van Eijck, B. P.; Kroon, J. *Ab Initio* Crystal Structure Predictions for Flexible Hydrogen-Bonded Molecules. *J. Am. Chem. Soc.* **2000**, *122*, 3500−3505.
(357) van Eijck, B. P.; Mooij, W. T. M.; Kroon, J. *Ab Initio* Crystal Structure Predictions for Flexible Hydrogen-Bonded Molecules. Part II. Accurate Energy Minimization. *J. Comput. Chem.* **2001**, *22*, 805−815.
(358) van Eijck, B. P. Ab Initio Crystal Structure Predictions for Flexible Hydrogen-Bonded Molecules. Part III. Effect of Lattice Vibrations. *J. Comput. Chem.* **2001**, *22*, 816−826.
(359) Karamertzanis, P. G.; Price, S. L. Energy Minimisation Of crystal Structures Containing Flexible Molecules. *J. Chem. Theory Comput.* **2006**, *2*, 1184−1199.
(360) Karamertzanis, P. G.; Pantelides, C. C. Crystal Structure Prediction. II. Flexible Molecules. *Mol. Phys.* **2007**, *105*, 273−291.
(361) Kazantsev, A. V.; Karamertzanis, P. G.; Adjiman, C. S.; Pantelides, C. C. Efficient Handling of Molecular Flexibility in Lattice Energy Minimization of Organic Crystals. *J. Chem. Theory Comput.* **2011**, *7*, 1998−2016.
(362) Price, S. L.; Leslie, M.; Welch, G. W. A.; Habgood, M.; Price, L. S.; Karamertzanis, P. G.; Day, G. M. Modelling Organic Crystal Structures using Distributed Multipole and Polarizability-Based Model Intermolecular Potentials. *Phys. Chem. Chem. Phys.* **2010**, *12*, 8478−90.
(363) Oganov, A. R.; Glass, C. W. Crystal Structure Prediction using ab Initio Evolutionary Techniques: Principles and Applications. *J. Chem. Phys.* **2006**, *124*, 244704.
(364) Glass, C. W.; Oganov, A. R.; Hansen, N. USPEX−Evolutionary Crystal Structure Prediction. *Comput. Phys. Commun.* **2006**, *175*, 713−720.
(365) Oganov, A. R.; Lyakhov, A. O.; Valle, M. How Evolutionary Crystal Structure Prediction Works−and Why. *Acc. Chem. Res.* **2011**, *44*, 227−237.
(366) Zhu, Q.; Oganov, A. R.; Glass, C. W.; Stokes, H. T. Constrained Evolutionary Algorithm for Structure Prediction of Molecular Crystals: Methodology and Applications. *Acta Crystallogr., Sect. B: Struct. Sci.* **2012**, *68*, 215−226.
(367) Qian, G.-R.; Lyakhov, A. O.; Zhu, Q.; Oganov, A. R.; Dong, X. Novel Hydrogen Hydrate Structures under Pressure. *Sci. Rep.* **2014**, *4*, 5606.
(368) Zhu, Q.; Sharma, V.; Oganov, A. R.; Ramprasad, R. Predicting Polymeric Crystal Structures by Evolutionary Algorithms. *J. Chem. Phys.* **2014**, *141*, 154102.
(369) Wang, Y.; Ma, Y. Perspective: Crystal Structure Prediction at High Pressures. *J. Chem. Phys.* **2014**, *140*, 040901.
(370) Pickard, C. J.; Needs, R. J. Ab Initio Random Structure Searching. *J. Phys.: Condens. Matter* **2011**, *23*, 053201.
(371) Buch, V.; Martonák, R.; Parrinello, M. A New Molecular-Dynamics Based Approach for Molecular Crystal Structure Search. *J. Chem. Phys.* **2005**, *123*, 051108.
(372) Buch, V.; Martonák, R.; Parrinello, M. Exploration of NVE Classical Trajectories as a Tool for Molecular Crystal Structure Prediction, with Tests on Ice Polymorphs. *J. Chem. Phys.* **2006**, *124*, 204705.
(373) Raiteri, P.; Martonák, R.; Parrinello, M. Exploring Polymorphism: The Case of Benzene. *Angew. Chem., Int. Ed.* **2005**, *44*, 3769−73.
(374) Zykova-Timan, T.; Raiteri, P.; Parrinello, M. Investigating the Polymorphism in PR179: a Combined Crystal Structure Prediction and Metadynamics Study. *J. Phys. Chem. B* **2008**, *112*, 13231−7.
(375) Salvalaglio, M.; Vetter, T.; Giberti, F.; Mazzotti, M.; Parrinello, M. Uncovering Molecular Details of Urea Crystal Growth in The Presence of Additives. *J. Am. Chem. Soc.* **2012**, *134*, 17221−17233.
(376) Salvalaglio, M.; Vetter, T.; Mazzotti, M.; Parrinello, M. Controlling and Predicting Crystal Shapes: The Case of Urea. *Angew. Chem., Int. Ed.* **2013**, *52*, 13369−72.
(377) Yu, T.-Q.; Tuckerman, M. Temperature-Accelerated Method for Exploring Polymorphism in Molecular Crystals Based on Free Energy. *Phys. Rev. Lett.* **2011**, *107*, 015701.
(378) Schnieders, M. J.; Baltrusaitis, J.; Shi, Y.; Chattree, G.; Zheng, L.; Yang, W.; Ren, P. The Structure, Thermodynamics and Solubility of Organic Crystals from Simulation with a Polarizable Force Field. *J. Chem. Theory Comput.* **2012**, *8*, 1721−1736.
(379) Park, J.; Nessler, I.; Mcclain, B.; Macikenas, D.; Baltrusaitis, J.; Schnieders, M. J. Absolute Organic Crystal Thermodynamics: Growth

DOI: 10.1021/acs.chemrev.5b00648
Chem. Rev. 2016, 116, 5567−5613

of the Asymmetric Unit into a Crystal via Alchemy. *J. Chem. Theory Comput.* **2014**, *10*, 2781−2791.
(380) Duff, N.; Peters, B. Polymorph Specific RMSD Local Order Parameters for Molecular Crystals And Nuclei: α-, β-, and γ-Glycine. *J. Chem. Phys.* **2011**, *135*, 134101.
(381) Tremayne, M.; Grice, L.; Pyatt, J. C.; Seaton, C. C.; Kariuki, B. M.; Tsui, H. H. Y.; Price, S. L.; Cherryman, J. C. Characterization of Complicated New Polymorphs of Chlorothalonil by X-Ray Diffraction and Computer Crystal Structure Prediction. *J. Am. Chem. Soc.* **2004**, *126*, 7071−81.
(382) Harper, J. K.; Grant, D. M. Enhancing Crystal-Structure Prediction with NMR Tensor Data. *Cryst. Growth Des.* **2006**, *6*, 2315−2321.
(383) Kalakewich, K.; Iuliucci, R.; Harper, J. K. Establishing Accurate High-Resolution Crystal Structures in the Absence of Diffraction Data and Single Crystals−An NMR Approach. *Cryst. Growth Des.* **2013**, *13*, 5391−5396.
(384) Cruz-Cabeza, A. J.; Karki, S.; Fábián, L.; Friščić, T.; Day, G. M.; Jones, W. Predicting Stoichiometry and Structure of Solvates. *Chem. Commun.* **2010**, *46*, 2224−2226.
(385) Salager, E.; Day, G. M.; Stein, R. S.; Pickard, C. J.; Elena, B.; Emsley, L. Powder Crystallography by Combined Crystal Structure Prediction and High-Resolution ^{1}H Solid-State NMR Spectroscopy. *J. Am. Chem. Soc.* **2010**, *132*, 2564−2566.
(386) Baias, M.; Widdifield, C. M.; Dumez, J.-N.; Thompson, H. P. G.; Cooper, T. G.; Salager, E.; Bassil, S.; Stein, R. S.; Lesage, A.; Day, G. M.; et al. Powder Crystallography of Pharmaceutical Materials by Combined Crystal Structure Prediction and Solid-State ^{1}H NMR Spectroscopy. *Phys. Chem. Chem. Phys.* **2013**, *15*, 8069−8080.
(387) Baias, M.; Dumez, J.-N.; Svensson, P. H.; Schantz, S.; Day, G. M.; Emsley, L. De Novo Determination of the Crystal Structure of a Large Drug Molecule by Crystal Structure Prediction-Based Powder NMR Crystallography. *J. Am. Chem. Soc.* **2013**, *135*, 17501−7.
(388) Santos, S. M.; Rocha, J.; Mafra, L. NMR Crystallography: Toward Chemical Shift-Driven Crystal Structure Determination of the β-Lactam Antibiotic Amoxicillin Trihydrate. *Cryst. Growth Des.* **2013**, *13*, 2390−2395.
(389) Parrott, E. P. J.; Zeitler, J. A.; Friscic, T.; Pepper, M.; Jones, W.; Day, G. M.; Gladden, L. F. Testing the Sensitivity of Terahertz Spectroscopy to Changes in Molecular and Supramolecular Structure: A Study of Structurally Similar Cocrystals. *Cryst. Growth Des.* **2009**, *9*, 1452−1460.
(390) Eddleston, M. D.; Hejczyk, K. E.; Bithell, E. G.; Day, G. M.; Jones, W. Polymorph Identification and Crystal Structure Determination by a Combined Crystal Structure Prediction and Transmission Electron Microscopy Approach. *Chem. - Eur. J.* **2013**, *19*, 7874−82.
(391) Ouvrard, C.; Price, S. L. Toward Crystal Structure Prediction for Conformationally Flexible Molecules: The Headaches Illustrated by Aspirin. *Cryst. Growth Des.* **2004**, *4*, 1119−1127.
(392) Vishweshwar, P.; McMahon, J. A.; Oliveira, M.; Peterson, M. L.; Zaworotko, M. J. The Predictably Elusive Form II of Aspirin. *J. Am. Chem. Soc.* **2005**, *127*, 16802−3.
(393) Bond, A. D.; Boese, R.; Desiraju, G. R. On the Polymorphism of Aspirin. *Angew. Chem., Int. Ed.* **2007**, *46*, 615−7.
(394) Bond, A. D.; Boese, R.; Desiraju, G. R. On the Polymorphism of Aspirin: Crystalline Aspirin as Intergrowths of Two "Polymorphic" Domains. *Angew. Chem., Int. Ed.* **2007**, *46*, 618−22.
(395) Chan, E. J.; Welberry, T. R.; Heerdege, A. P.; Goossens, D. J. Diffuse Scattering Study of Aspirin Forms (I) and (II). *Acta Crystallogr., Sect. B: Struct. Sci.* **2010**, *66*, 696−707.
(396) Bauer, J. D.; Haussuhl, E.; Winkler, B.; Arbeck, D.; Milman, V.; Robertson, S. Elastic Properties, Thermal Expansion, and Polymorphism of Acetylsalicylic Acid. *Cryst. Growth Des.* **2010**, *10*, 100527101541018.
(397) Bond, A. D.; Solanko, K. A.; Parsons, S.; Redder, S.; Boese, R. Single Crystals of Aspirin Form II: Crystallisation and Stability. *CrystEngComm* **2011**, *13*, 399.
(398) Li, T. Understanding the Polymorphism of Aspirin with Electronic Calculations. *J. Pharm. Sci.* **2007**, *96*, 755−760.
(399) Karamertzanis, P. G.; Day, G. M.; Welch, G. W. A.; Kendrick, J.; Leusen, F. J. J.; Neumann, M. A.; Price, S. L. Modeling the Interplay of Inter- and Intramolecular Hydrogen Bonding in Conformational Polymorphs. *J. Chem. Phys.* **2008**, *128*, 244708.
(400) Ahn, S.; Guo, F.; Kariuki, B. M.; Harris, K. D. M. Abundant Polymorphism in a System with Multiple Hydrogen-Bonding Opportunities: Oxalyl Dihydrazide. *J. Am. Chem. Soc.* **2006**, *128*, 8441−52.
(401) Li, T.; Feng, S. Empirically Augmented Density Functional Theory for Predicting Lattice Energies of Aspirin, Acetaminophen Polymorphs, and Ibuprofen Homochiral and Racemic Crystals. *Pharm. Res.* **2006**, *23*, 2326−2332.
(402) Sacchetti, M. Thermodynamic Analysis of DSC Data for Acetaminophen Polymorphs. *J. Therm. Anal. Cal.* **2001**, *63*, 345−350.
(403) Espeau, P.; Céolin, R.; Tamarit, J.-L.; Perrin, M.-A.; Gauchi, J.-P.; Leveiller, F. Polymorphism of Paracetamol: Relative Stabilities of the Monoclinic and Orthorhombic Phases Inferred from Topological Pressure-Temperature and Temperature-Volume Phase Diagrams. *J. Pharm. Sci.* **2005**, *94*, 524−39.
(404) Picciochi, R.; Diogo, H. P.; Minas da Piedade, M. E. Thermochemistry of paracetamol. *J. Therm. Anal. Calorim.* **2010**, *100*, 391−401.
(405) Neumann, M. A.; Perrin, M.-A. Can Crystal Structure Prediction Guide Experimentalists to a New Polymorph of Paracetamol? *CrystEngComm* **2009**, *11*, 2475.
(406) Perrin, M.-A.; Neumann, M. A.; Elmaleh, H.; Zaske, L. Crystal Structure Determination of the Elusive Paracetamol Form III. *Chem. Commun.* **2009**, 3181−3.
(407) Rivera, S. A.; Allis, D. G.; Hudson, B. S. Importance of Vibrational Zero-Point Energy Contribution to the Relative Polymorph Energies of Hydrogen-Bonded Species. *Cryst. Growth Des.* **2008**, *8*, 3905−3907.
(408) Datta, S.; Grant, D. J. W. Crystal Structures of Drugs: Advances in Determination, Prediction and Engineering. *Nat. Rev. Drug Discovery* **2004**, *3*, 42−57.
(409) Thayer, A. M. Centering On Chirality. *Chem. Eng. News* **2007**, *85*, 11−19.
(410) Gourlay, M. D.; Kendrick, J.; Leusen, F. J. J. Rationalization of Racemate Resolution: Predicting Spontaneous Resolution through Crystal Structure Prediction. *Cryst. Growth Des.* **2007**, *7*, 56−63.
(411) Gourlay, M. D.; Kendrick, J.; Leusen, F. J. J. Predicting the Spontaneous Chiral Resolution by Crystallization of a Pair of Flexible Nitroxide Radicals. *Cryst. Growth Des.* **2008**, *8*, 2899−2905.
(412) Kendrick, J.; Gourlay, M. D.; Neumann, M. A.; Leusen, F. J. J. Predicting Spontaneous Racemate Resolution using Recent Developments in Crystal Structure Prediction. *CrystEngComm* **2009**, *11*, 2391.
(413) Stephenson, G. a.; Kendrick, J.; Wolfangel, C.; Leusen, F. J. J. Symmetry Breaking: Polymorphic Form Selection by Enantiomers of the Melatonin Agonist and Its Missing Polymorph. *Cryst. Growth Des.* **2012**, *12*, 3964−3976.
(414) Kendrick, J.; Stephenson, G. A.; Neumann, M. A.; Leusen, F. J. J. Crystal Structure Prediction of a Flexible Molecule of Pharmaceutical Interest with Unusual Polymorphic Behavior. *Cryst. Growth Des.* **2013**, *13*, 581−589.
(415) D'Oria, E.; Karamertzanis, P. G.; Price, S. L. Spontaneous Resolution of Enantiomers by Crystallization: Insights from Computed Crystal Energy Landscapes. *Cryst. Growth Des.* **2010**, *10*, 1749−1756.
(416) Hylton, R. K.; Tizzard, G. J.; Threlfall, T. L.; Ellis, A. L.; Coles, S. J.; Seaton, C. C.; Schulze, E.; Lorenz, H.; Seidel-Morgenstern, A.; Stein, M.; et al. Are the Crystal Structures of Enantiopure and Racemic Mandelic Acids Determined by Kinetics or Thermodynamics? *J. Am. Chem. Soc.* **2015**, *137*, 11095−11104.
(417) Jacques, J.; Collet, A.; Wilen, S. H. *Enantiomers, Racemates, and Resolutions*; Krieger: Malabar, FL, 1994.
(418) Braun, D. E.; Ardid-Candel, M.; Oria, E. D.; Karamertzanis, P. G.; Arlin, J.-b.; Florence, A. J.; Jones, A. G.; Price, S. L. Racemic Naproxen: A Multidisciplinary Structural and Thermodynamic

DOI: 10.1021/acs.chemrev.5b00648
Chem. Rev. 2016, 116, 5567−5613

Comparison with the Enantiopure Form. *Cryst. Growth Des.* **2011**, *11*, 5659−5669.
(419) Issa, N.; Karamertzanis, P. G.; Welch, G. W. A.; Price, S. L. Can the Formation of Pharmaceutical Cocrystals Be Computationally Predicted? 1. Comparison of Lattice Energies. *Cryst. Growth Des.* **2009**, *9*, 442−453.
(420) Karamertzanis, P. G.; Kazantsev, A. V.; Issa, N.; Welch, G. W. A.; Adjiman, C. S.; Pantelides, C. C.; Price, S. L. Can the Formation of Pharmaceutical Cocrystals Be Computationally Predicted? 2. Crystal Structure Prediction. *J. Chem. Theory Comput.* **2009**, *5*, 1432−1448.
(421) Chan, H. C. S.; Kendrick, J.; Neumann, M. A.; Leusen, F. J. J. Towards ab Initio Screening of Co-Crystal Formation through Lattice Energy Calculations and Crystal Structure Prediction of Nicotinamide, Isonicotinamide, Picolinamide and Paracetamol Multi-Component Crystals. *CrystEngComm* **2013**, *15*, 3799.
(422) van de Streek, J.; Neumann, M. A.; Perrin, M.-A. Validation of Dispersion-Corrected Density Functional Theory Calculations for the Crystal Structure Prediction of Molecular Salts: A Crystal Structure Prediction Study of Pyridinium Chloride. *CrystEngComm* **2010**, *12*, 3827.
(423) Braun, D. E.; Karamertzanis, P. G.; Price, S. L. Which, If Any, Hydrates Will Crystallise? Predicting Hydrate Formation of Two Dihydroxybenzoic Acids. *Chem. Commun.* **2011**, *47*, 5443−5.
(424) Price, S. L. Why Don't We Find More Polymorphs? *Acta Crystallogr., Sect. B: Struct. Sci., Cryst. Eng. Mater.* **2013**, *69*, 313−28.
(425) Price, S. L. Computed Crystal Energy Landscapes for Understanding and Predicting Organic Crystal Structures and Polymorphism. *Acc. Chem. Res.* **2009**, *42*, 117−26.
(426) Braun, D. E.; McMahon, J. A.; Koztecki, L. H.; Price, S. L.; Reutzel-Edens, S. M. Contrasting Polymorphism of Related Small Molecule Drugs Correlated and Guided by the Computed Crystal Energy Landscape. *Cryst. Growth Des.* **2014**, *14*, 2056−2072.
(427) Gelbrich, T.; Braun, D. E.; Ellern, A.; Griesser, U. J. Four Polymorphs of Methyl Paraben: Structural Relationships and Relative Energy Differences. *Cryst. Growth Des.* **2013**, *13*, 1206−1217.
(428) Pamuk, B.; Soler, J. M.; Ramírez, R.; Herrero, C. P.; Stephens, P. W.; Allen, P. B.; Fernández-Serra, M.-V. Anomalous Nuclear Quantum Effects in Ice. *Phys. Rev. Lett.* **2012**, *108*, 193003.
(429) Gray, A. E.; Day, G. M.; Leslie, M.; Price, S. L. Dynamics in Crystals of Rigid Organic Molecules: Contrasting the Phonon Frequencies Calculated by Molecular Dynamics with Harmonic Lattice Dynamics for Imidazole and 5-Azauracil. *Mol. Phys.* **2004**, *102*, 1067−1083.
(430) Karamertzanis, P. G.; Raiteri, P.; Parrinello, M.; Leslie, M.; Price, S. L. The Thermal Stability of Lattice-Energy Minima of 5-Fluorouracil: Metadynamics as an Aid to Polymorph Prediction. *J. Phys. Chem. B* **2008**, *112*, 4298−308.
(431) Aragones, J. L.; Noya, E. G.; Valeriani, C.; Vega, C. Free Energy Calculations for Molecular Solids using GROMACS. *J. Chem. Phys.* **2013**, *139*, 034104.
(432) Pickard, C. J.; Needs, R. J. High-Pressure Phases of Nitrogen. *Phys. Rev. Lett.* **2009**, *102*, 125702.
(433) Sun, J.; Martinez-Canales, M.; Klug, D. D.; Pickard, C. J.; Needs, R. J. Persistence and Eventual Demise of Oxygen Molecules at Terapascal Pressures. *Phys. Rev. Lett.* **2012**, *108*, 045503.
(434) Griffiths, G. I. G.; Needs, R. J.; Pickard, C. J. High-Pressure Ionic and Molecular Phases of Ammonia within Density Functional Theory. *Phys. Rev. B: Condens. Matter Mater. Phys.* **2012**, *86*, 144102.
(435) Griffiths, G. I.; Misquitta, A. J.; Fortes, A. D.; Pickard, C. J.; Needs, R. J. High Pressure Ionic and Molecular Crystals of Ammonia Monohydrate Within Density Functional Theory. *J. Chem. Phys.* **2012**, *137*, 064506.
(436) Pickard, C. J.; Martinez-Canales, M.; Needs, R. J. Decomposition and Terapascal Phases of Water Ice. *Phys. Rev. Lett.* **2013**, *110*, 245701.
(437) Errea, I.; Calandra, M.; Pickard, C. J.; Nelson, J.; Needs, R. J.; Li, Y.; Liu, H.; Zhang, Y.; Ma, Y.; Mauri, F. High-Pressure Hydrogen Sulfide from First Principles: A Strongly Anharmonic Phonon-Mediated Superconductor. *Phys. Rev. Lett.* **2015**, *114*, 157004.
(438) Theiry, M. M.; Leger, J. M. High Pressure Solid Phases of Benzene. I. Raman and X-Ray Studies of C_6H_6 at 294 K up to 25 GPa. *J. Chem. Phys.* **1988**, *89*, 4255−4271.
(439) Ciabini, L.; Gorelli, F.; Santoro, M.; Bini, R.; Schettino, V.; Mezouar, M. High-Pressure and High-Temperature Equation of State and Phase Diagram of Solid Benzene. *Phys. Rev. B: Condens. Matter Mater. Phys.* **2005**, *72*, 094108.
(440) Wen, X.-D.; Hoffmann, R.; Ashcroft, N. W. Benzene under High Pressure: a Story of Molecular Crystals Transforming to Saturated Networks, with a Possible Intermediate Metallic Phase. *J. Am. Chem. Soc.* **2011**, *133*, 9023−9035.
(441) Schatschneider, B.; Liang, J.-J.; Jezowski, S.; Tkatchenko, A. Phase Transition between Cubic and Monoclinic Polymorphs of the Tetracyanoethylene Crystal: The Role of Temperature and Kinetics. *CrystEngComm* **2012**, *14*, 4656−4663.
(442) McMahan, A. K.; Lesar, R. Pressure Dissociation of Solid Nitrogen under 1 Mbar. *Phys. Rev. Lett.* **1985**, *54*, 1929−1932.
(443) Mailhiot, C.; Yang, L. H.; McMahan, A. K. Polymeric Nitrogen. *Phys. Rev. B: Condens. Matter Mater. Phys.* **1992**, *46*, 14419−14435.
(444) Eremets, M. I.; Gavriliuk, A. G.; Trojan, I. A.; Dzivenko, D. A.; Boehler, R. Single-Bonded Cubic Form of Nitrogen. *Nat. Mater.* **2004**, *3*, 558−563.
(445) Alemany, M.; Martins, J. Density-Functional Study of Nonmolecular Phases of Nitrogen: Metastable Phase at Low Pressure. *Phys. Rev. B: Condens. Matter Mater. Phys.* **2003**, *68*, 024110.
(446) Mattson, W. D.; Sanchez-Portal, D.; Chiesa, S.; Martin, R. M. Prediction of New Phases of Nitrogen at High Pressure from First-Principles Simulations. *Phys. Rev. Lett.* **2004**, *93*, 1−4.
(447) Zahariev, F.; Dudiy, S. V.; Hooper, J.; Zhang, F.; Woo, T. K. Systematic Method to New Phases of Polymeric Nitrogen under High Pressure. *Phys. Rev. Lett.* **2006**, *97*, 11−14.
(448) Zahariev, F.; Hooper, J.; Alavi, S.; Zhang, F.; Woo, T. K. Low-Pressure Metastable Phase of Single-Bonded Polymeric Nitrogen from a Helical Structure Motif and First-Principles Calculations. *Phys. Rev. B: Condens. Matter Mater. Phys.* **2007**, *75*, 1−4.
(449) Wang, X. L.; He, Z.; Ma, Y. M.; Cui, T.; Liu, Z. M.; Liu, B. B.; Li, J. F.; Zou, G. T. Prediction of a New Layered Phase of Nitrogen from First-Principles Simulations. *J. Phys.: Condens. Matter* **2007**, *19*, 425226.
(450) Caracas, R.; Hemley, R. J. New Structures of Dense Nitrogen: Pathways to the Polymeric Phase. *Chem. Phys. Lett.* **2007**, *442*, 65−70.
(451) Ma, Y.; Oganov, A. R.; Li, Z.; Xie, Y.; Kotakoski, J. Novel High Pressure Structures of Polymeric Nitrogen. *Phys. Rev. Lett.* **2009**, *102*, 100−103.
(452) Wang, X.; Wang, Y.; Miao, M.; Zhong, X.; Lv, J.; Cui, T.; Li, J.; Chen, L.; Pickard, C. J.; Ma, Y. Cagelike Diamondoid Nitrogen at High Pressures. *Phys. Rev. Lett.* **2012**, *109*, 175502.
(453) Beaudet, T. D.; Mattson, W. D.; Rice, B. M. New Form of Polymeric Nitrogen from Dynamic Shock Simulation. *J. Chem. Phys.* **2013**, *138*, 054503.
(454) Yao, Y.; Tse, J. S.; Tanaka, K. Metastable High-Pressure Single-Bonded Phases of Nitrogen Predicted via Genetic Algorithm. *Phys. Rev. B: Condens. Matter Mater. Phys.* **2008**, *77*, 1−4.
(455) Hirshberg, B.; Gerber, R. B.; Krylov, A. I. Calculations Predict a Stable Molecular Crystal of N_8. *Nat. Chem.* **2014**, *6*, 52−6.
(456) Plasienka, D.; Martonak, R. Transformation Pathways in High-Pressure Solid Nitrogen: From Molecular N_2 to Polymeric cg-N. *J. Chem. Phys.* **2015**, *142*, 094505.
(457) Erba, A.; Maschio, L.; Pisani, C.; Casassa, S. Pressure-Induced Transitions in Solid Nitrogen: Role of Dispersive Interactions. *Phys. Rev. B: Condens. Matter Mater. Phys.* **2011**, *84*, 012101.
(458) Salzmann, C. G.; Radaelli, P. G.; Slater, B.; Finney, J. L. The Polymorphism of Ice: Five Unresolved Questions. *Phys. Chem. Chem. Phys.* **2011**, *13*, 18468−80.
(459) Singer, S. J.; Kuo, J.-L.; Hirsch, T. K.; Knight, C.; Ojamäe, L.; Klein, M. L. Hydrogen-Bond Topology and the Ice VII/VIII and Ice Ih/XI Proton-Ordering Phase Transitions. *Phys. Rev. Lett.* **2005**, *94*, 135701.

DOI: 10.1021/acs.chemrev.5b00648
Chem. Rev. 2016, 116, 5567−5613

(460) Knight, C.; Singer, S. J. Prediction of a Phase Transition to a Hydrogen Bond Ordered Form of Ice VI. *J. Phys. Chem. B* **2005**, *109*, 21040−6.
(461) Knight, C.; Singer, S. J. A Reexamination of The Ice III/IX Hydrogen Bond Ordering Phase Transition. *J. Chem. Phys.* **2006**, *125*, 64506.
(462) Knight, C.; Singer, S.; Kuo, J.-L.; Hirsch, T.; Ojamäe, L.; Klein, M. Hydrogen Bond Topology and the Ice VII/VIII and Ih/XI Proton Ordering Phase Transitions. *Phys. Rev. E* **2006**, *73*, 056113.
(463) Kuo, J.-L.; Kuhs, W. F. A First Principles Study on the Structure of Ice-VI: Static Distortion, Molecular Geometry, and Proton Ordering. *J. Phys. Chem. B* **2006**, *110*, 3697−703.
(464) Knight, C.; Singer, S. J. Hydrogen Bond Ordering in Ice V and the Transition to Ice XIII. *J. Chem. Phys.* **2008**, *129*, 164513.
(465) Umemoto, K.; Wentzcovitch, R. M.; de Gironcoli, S.; Baroni, S. Order-Disorder Phase Boundary between Ice VII and VIII Obtained by First Principles. *Chem. Phys. Lett.* **2010**, *499*, 236−240.
(466) Hirsch, T. K.; Ojamae, L. Quantum-Chemical and Force-Field Investigations of Ice Ih: Computation of Proton-Ordered Structures and Prediction of Their Lattice Energies. *J. Phys. Chem. B* **2004**, *108*, 15856−15864.
(467) Tribello, G. A.; Slater, B. Proton Ordering Energetics in Ice Phases. *Chem. Phys. Lett.* **2006**, *425*, 246−250.
(468) Fan, X.; Bing, D.; Zhang, J.; Shen, Z.; Kuo, J.-L. Predicting the Hydrogen Bond Ordered Structures Of Ice Ih, II, III, VI and Ice VII: DFT Methods with Localized Based Set. *Comput. Mater. Sci.* **2010**, *49*, S170−S175.
(469) Tribello, G. A.; Slater, B.; Salzmann, C. G. A Blind Structure Prediction of Ice XIV. *J. Am. Chem. Soc.* **2006**, *128*, 12594−5.
(470) Whale, T. F.; Clark, S. J.; Finney, J. L.; Salzmann, C. G. DFT-Assisted Interpretation of the Raman Spectra of Hydrogen-Ordered Ice XV. *J. Raman Spectrosc.* **2013**, *44*, 290−298.
(471) Bonev, S. A.; Gygi, F.; Ogitsu, T.; Galli, G. High-Pressure Molecular Phases of Solid Carbon Dioxide. *Phys. Rev. Lett.* **2003**, *91*, 065501.
(472) Datchi, F.; Giordano, V. M.; Munsch, P.; Saitta, a. M. Structure of Carbon Dioxide Phase IV: Breakdown of the Intermediate Bonding State Scenario. *Phys. Rev. Lett.* **2009**, *103*, 185701.
(473) Datchi, F.; Mallick, B.; Salamat, A.; Rousse, G.; Ninet, S.; Garbarino, G.; Bouvier, P.; Mezouar, M. Structure and Compressibility of the High-Pressure Molecular Phase II of Carbon Dioxide. *Phys. Rev. B: Condens. Matter Mater. Phys.* **2014**, *89*, 144101.
(474) Serra, S. Pressure-Induced Solid Carbonates from Molecular CO_2 by Computer Simulation. *Science* **1999**, *284*, 788−790.
(475) Dong, J.; Tomfohr, J.; Sankey, O. Rigid Intertetrahedron Angular Interaction of Nonmolecular Carbon Dioxide Solids. *Phys. Rev. B: Condens. Matter Mater. Phys.* **2000**, *61*, 5967−5971.
(476) Dong, J.; Tomfohr, J. K.; Sankey, O. F.; Leinenweber, K.; Somayazulu, M.; McMillan, P. F. Investigation of Hardness in Tetrahedrally Bonded Nonmolecular CO_2 Solids by Density-Functional Theory. *Phys. Rev. B: Condens. Matter Mater. Phys.* **2000**, *62*, 14685−14689.
(477) Holm, B.; Ahuja, R.; Belonoshko, A.; Johansson, B. Theoretical Investigation of High Pressure Phases of Carbon Dioxide. *Phys. Rev. Lett.* **2000**, *85*, 1258−1261.
(478) Oganov, A. R.; Ono, S.; Ma, Y.; Glass, C. W.; Garcia, A. Novel High-Pressure Structures of $MgCO_3$, $CaCO_3$ and CO_2 and Their Role in Earth's Lower Mantle. *Earth Planet. Sci. Lett.* **2008**, *273*, 38−47.
(479) Togo, A.; Oba, F.; Tanaka, I. Transition Pathway of CO_2 Crystals under High Pressures. *Phys. Rev. B: Condens. Matter Mater. Phys.* **2008**, *77*, 184101.
(480) Sun, J.; Klug, D. D.; Martonák, R.; Montoya, J. A.; Lee, M.-S.; Scandolo, S.; Tosatti, E. High-Pressure Polymeric Phases of Carbon Dioxide. *Proc. Natl. Acad. Sci. U. S. A.* **2009**, *106*, 6077−6081.
(481) Datchi, F.; Mallick, B.; Salamat, A.; Ninet, S. Structure of Polymeric Carbon Dioxide CO_2-V. *Phys. Rev. Lett.* **2012**, *108*, 125701.
(482) Muller, C.; Spangberg, D. Calculation of the Stability of Nonperiodic Solids using Classical Force Fields and the Method of Increments: N_2O as an Example. *J. Comput. Chem.* **2015**, *36*, 1420−1427.
(483) Giordano, V. M.; Datchi, F. Molecular Carbon Dioxide at High Pressure and High Temperature. *Europhys. Lett.* **2007**, *77*, 46002.
(484) Zhao, J. First-Principles Study of Atomic Nitrogen Solid with Cubic Gauche Structure. *Phys. Lett. A* **2007**, *360*, 645−648.
(485) Reilly, A. M.; Middlemiss, D. S.; Siddick, M. M.; Wann, D. A.; Ackland, G. J.; Wilson, C. C.; Rankin, D. W. H.; Morrison, C. A. The Phonon Spectrum of Phase-I Ammonia: Reassignment of Lattice Mode Symmetries from Combined Molecular and Lattice Dynamics Calculations. *J. Phys. Chem. A* **2008**, *112*, 1322−9.
(486) Dračínský, M.; Procházková, E.; Kessler, J.; Šebestík, J.; Matějka, P.; Bouř, P. Resolution of Organic Polymorphic Crystals by Raman Spectroscopy. *J. Phys. Chem. B* **2013**, *117*, 7297−7307.
(487) Peiris, S. M.; Wong, C. P.; Zerilli, F. J. Equation of State and Structural Changes in Diaminodinitroethylene under Compression. *J. Chem. Phys.* **2004**, *120*, 8060−6.
(488) Hunter, S.; Sutinen, T.; Parker, S. F.; Morrison, C. A.; Williamson, D. M.; Thompson, S.; Gould, P. J.; Pulham, C. R. Experimental and DFT-D Studies of the Molecular Organic Energetic Material RDX. *J. Phys. Chem. C* **2013**, *117*, 8062−8071.
(489) McIntosh, A. I.; Yang, B.; Goldup, S. M.; Watkinson, M.; Donnan, R. S. Terahertz Spectroscopy: A Powerful New Tool for the Chemical Sciences? *Chem. Soc. Rev.* **2012**, *41*, 2072−2082.
(490) Day, G. M.; Zeitler, J. A.; Jones, W.; Rades, T.; Taday, P. F. Understanding the Influence of Polymorphism on Phonon Spectra: Lattice Dynamics Calculations and Terahertz Spectroscopy of Carbamazepine. *J. Phys. Chem. B* **2006**, *110*, 447−456.
(491) Shen, Y.-C. Terahertz Pulsed Spectroscopy and Imaging for Pharmaceutical Applications: A Review. *Int. J. Pharm.* **2011**, *417*, 48−60.
(492) Siegrist, K.; Bucher, C. R.; Mandelbaum, I.; Hight Walker, A. R.; Balu, R.; Gregurick, S. K.; Plusquellic, D. F. High-Resolution Terahertz Spectroscopy of Crystalline Trialanine: Extreme Sensitivity to Beta-Sheet Structure and Cocrystallized Water. *J. Am. Chem. Soc.* **2006**, *128*, 5764−75.
(493) Allis, D. G.; Korter, T. M. Theoretical Analysis of the Terahertz Spectrum of the High Explosive PETN. *ChemPhysChem* **2006**, *7*, 2398−2408.
(494) Allis, D. G.; Prokhorova, D. A.; Korter, T. M. Solid-State Modeling of the Terahertz Spectrum of the High Explosive HMX. *J. Phys. Chem. A* **2006**, *110*, 1951−1959.
(495) Saito, S.; Inerbaev, T. M.; Mizuseki, H.; Igarashi, N.; Note, R.; Kawazoe, Y. First Principles Calculation of Terahertz Vibrational Modes of a Disaccharide Monohydrate Crystal of Lactose. *Jpn. J. Appl. Phys.* **2006**, *45*, L1156−L1158.
(496) Allis, D. G.; Fedor, A. M.; Korter, T. M.; Bjarnason, J. E.; Brown, E. R. Assignment of the Lowest-Lying THz Absorption Signatures in Biotin and Lactose Monohydrate by Solid-State Density Functional Theory. *Chem. Phys. Lett.* **2007**, *440*, 203−209.
(497) Oppenheim, K. C.; Korter, T. M.; Melinger, J. S.; Grischkowsky, D. Solid-State Density Functional Theory Investigation of the Terahertz Spectra of the Structural Isomers 1,2-Dicyanobenzene and 1,3-Dicyanobenzene. *J. Phys. Chem. A* **2010**, *114*, 12513−21.
(498) Pellizzeri, S.; Delaney, S. P.; Korter, T. M.; Zubieta, J. Using Solid-State Density Functional Theory and Terahertz Spectroscopy to Spectroscopically Distinguish the Various Hydrohalide Salts of 5-(4-Pyridyl)Tetrazole. *J. Mol. Struct.* **2013**, *1050*, 27−34.
(499) Pellizzeri, S.; Delaney, S. P.; Korter, T. M.; Zubieta, J. Using Terahertz Spectroscopy and Solid-State Density Functional Theory to Characterize a New Polymorph of 5-(4-Pyridyl)Tetrazole. *J. Phys. Chem. A* **2014**, *118*, 417−26.
(500) King, M. D.; Korter, T. M. Application of London-Type Dispersion Corrections in Solid-State Density Functional Theory for Predicting the Temperature-Dependence of Crystal Structures and Terahertz Spectra. *Cryst. Growth Des.* **2011**, *11*, 2006−2010.
(501) Zhang, F.; Hayashi, M.; Wang, H.-W.; Tominaga, K.; Kambara, O.; Nishizawa, J.-i.; Sasaki, T. Terahertz Spectroscopy and Solid-State Density Functional Theory Calculation of Anthracene: Effect of

DOI: 10.1021/acs.chemrev.5b00648
Chem. Rev. 2016, 116, 5567−5613

Dispersion Force on the Vibrational Modes. *J. Chem. Phys.* **2014**, *140*, 174509.
(502) King, M. D.; Korter, T. M. Modified Corrections for London Forces in Solid-State Density Functional Theory Calculations of Structure and Lattice Dynamics of Molecular Crystals. *J. Phys. Chem. A* **2012**, *116*, 6927−34.
(503) King, M. D.; Blanton, T. N.; Misture, S. T.; Korter, T. M. Prediction of the Unknown Crystal Structure of Creatine using Fully Quantum Mechanical Methods. *Cryst. Growth Des.* **2011**, *11*, 5733−5740.
(504) King, M. D.; Davis, E. A.; Smith, T. M.; Korter, T. M. Importance of Accurate Spectral Simulations for the Analysis of Terahertz Spectra: Citric Acid Anhydrate and Monohydrate. *J. Phys. Chem. A* **2011**, *115*, 11039−11044.
(505) Takahashi, M.; Ishikawa, Y.; Ito, H. The Dispersion Correction and Weak-Hydrogen-Bond Network in Low-Frequency Vibration of Solid-State Salicylic Acid. *Chem. Phys. Lett.* **2012**, *531*, 98−104.
(506) Williams, M. R. C.; Aschaffenburg, D. J.; Ofori-Okai, B. K.; Schmuttenmaer, C. A. Intermolecular Vibrations in Hydrophobic Amino Acid Crystals: Experiments and Calculations. *J. Phys. Chem. B* **2013**, *117*, 10444−10461.
(507) Kim, J.; Kwon, O.-P.; Jazbinsek, M.; Park, Y. C.; Lee, Y. S. First-Principles Calculation of Terahertz Absorption with Dispersion Correction of 2,2-Bithiophene as Model Compound. *J. Phys. Chem. C* **2015**, *119*, 12598−12607.
(508) Kim, J.; Kwon, O.-P.; Brunner, F. D. J.; Jazbinsek, M.; Lee, S.-H.; Günter, P. Phonon Modes of Organic Electro-Optic Molecular Crystals for Terahertz Photonics. *J. Phys. Chem. C* **2015**, *119*, 10031−10039.
(509) Li, R.; Zeitler, J. A.; Tomerini, D.; Parrott, E. P. J.; Gladden, L. F.; Day, G. M. A Study into the Effect of Subtle Structural Details and Disorder on the Terahertz Spectrum of Crystalline Benzoic Acid. *Phys. Chem. Chem. Phys.* **2010**, *12*, 5329.
(510) Katz, G.; Zybin, S.; Goddard, W. A.; Zeiri, Y.; Kosloff, R. Direct MD Simulations of Terahertz Absorption and 2D Spectroscopy Applied to Explosive Crystals. *J. Phys. Chem. Lett.* **2014**, *5*, 772−776.
(511) Facelli, J. C.; Grant, D. M. Determination of Molecular Symmetry in Crystalline Naphthalene using Solid-State NMR. *Nature* **1993**, *365*, 325−327.
(512) Martineau, C.; Senker, J.; Taulelle, F. NMR Crystallography. *Annu. Rep. NMR Spectrosc.* **2014**, *82*, 1−57.
(513) Portieri, A.; Harris, R. K.; Fletton, R. A.; Lancaster, R. W.; Threlfall, T. L. Effects of Polymorphic Differences for Sulfanilamide, as Seen Through ^{13}C and ^{15}N Solid-State NMR, Together with Shielding Calculations. *Magn. Reson. Chem.* **2004**, *42*, 313−320.
(514) Stueber, D. The Embedded Ion Method: A New Approach to the Electrostatic Description of Crystal Lattice Effects in Chemical Shielding Calculations. *Concepts Magn. Reson., Part A* **2006**, *28*, 347−368.
(515) Ferraro, M. B.; Facelli, J. C. Modeling NMR Chemical Shifts: Surface Charge Representation of the Electrostatic Embedding Potential Modeling of Crystalline Intermolecular Effects in ^{19}F Solid State NMR Chemical Shifts. *J. Mol. Struct.* **2002**, *603*, 159−164.
(516) Pickard, C.; Mauri, F. All-Electron Magnetic Response with Pseudopotentials: NMR chemical shifts. *Phys. Rev. B: Condens. Matter Mater. Phys.* **2001**, *63*, 245101.
(517) Charpentier, T. The PAW/GIPAW Approach for Computing NMR Parameters: A New Dimension Added to NMR Study of Solids. *Solid State Nucl. Magn. Reson.* **2011**, *40*, 1−20.
(518) Johnston, J. C.; Iuliucci, R. J.; Facelli, J. C.; Fitzgerald, G.; Mueller, K. T. Intermolecular Shielding Contributions Studied by Modeling the ^{13}C Chemical-Shift Tensors of Organic Single Crystals with Plane Waves. *J. Chem. Phys.* **2009**, *131*, 144503.
(519) Holmes, S. T.; Iuliucci, R. J.; Mueller, K. T.; Dybowski, C. Density Functional Investigation of Intermolecular Effects on ^{13}C NMR Chemical-Shielding Tensors Modeled with Molecular Clusters. *J. Chem. Phys.* **2014**, *141*, 164121.
(520) Holmes, S. T.; Iuliucci, R. J.; Mueller, K. T.; Dybowski, C. Critical Analysis of Cluster Models and Exchange-Correlation Functionals for Calculating Magnetic Shielding in Molecular Solids. *J. Chem. Theory Comput.* **2015**, *11*, 5229−5241.
(521) Flaig, D.; Maurer, M.; Hanni, M.; Braunger, K.; Kick, L.; Thubauville, M.; Ochsenfeld, C. Benchmarking Hydrogen and Carbon NMR Chemical Shifts at HF, DFT, and MP2 Levels. *J. Chem. Theory Comput.* **2014**, *10*, 572−578.
(522) Lodewyk, M. W.; Siebert, M. R.; Tantillo, D. J. Computational Prediction of ^{1}H and ^{13}C Chemical Shifts: A Useful Tool for Natural Product, Mechanistic, and Synthetic Organic Chemistry. *Chem. Rev.* **2012**, *112*, 1839−62.
(523) Blanco, F.; Alkorta, I.; Elguero, J. Statistical Analysis of ^{13}C and ^{15}N NMR Chemical Shifts from GIAO/B3LYP/6-311++G** Calculated Absolute Shieldings. *Magn. Reson. Chem.* **2007**, *45*, 797−800.
(524) Konstantinov, I. A.; Broadbelt, L. J. Regression Formulas for Density Functional Theory Calculated ^{1}H and ^{13}C NMR Chemical Shifts in Toluene-d_8. *J. Phys. Chem. A* **2011**, *115*, 12364−72.
(525) Samultsev, D. O.; Semenov, V. A.; Krivdin, L. B. On the Accuracy of the GIAO-DFT Calculation of ^{15}N NMR Chemical Shifts of the Nitrogen-Containing Heterocycles−A Gateway to Better Agreement with Experiment at Lower Computational Cost. *Magn. Reson. Chem.* **2014**, *52*, 222−30.
(526) Teale, A. M.; Lutnaes, O. B.; Helgaker, T.; Tozer, D. J.; Gauss, J. Benchmarking Density-Functional Theory Calculations of NMR Shielding Constants and Spin-Rotation Constants using Accurate Coupled-Cluster Calculations. *J. Chem. Phys.* **2013**, *138*, 024111.
(527) Auer, A. A. Quantitative Prediction of Gas-Phase ^{17}O Nuclear Magnetic Shielding Constants. *J. Chem. Phys.* **2009**, *131*, 024116.
(528) Bonhomme, C.; Gervais, C.; Babonneau, F.; Coelho, C.; Pourpoint, F.; Azais, T.; Ashbrook, S. E.; Griffin, J. M.; Yates, J. R.; Mauri, F.; et al. First-Principles Calculation of NMR Parameters Using the Gauge Including Projector Augmented Wave Method: A Chemist's Point of View. *Chem. Rev.* **2012**, *112*, 5733−5779.
(529) Bühl, M.; van Mourik, T. NMR Spectroscopy: Quantum-Chemical Calculations. *WIRES: Comput. Mol. Sci.* **2011**, *1*, 634−647.
(530) Harris, R. K.; Joyce, S. A.; Pickard, C. J.; Cadars, S.; Emsley, L. Assigning Carbon-13 NMR Spectra to Crystal Structures by the INADEQUATE Pulse Sequence and First Principles Computation: A Case Study of Two Forms of Testosterone. *Phys. Chem. Chem. Phys.* **2006**, *8*, 137−143.
(531) Kucukbenli, E.; Sonkar, K.; Sinha, N.; Gironcoli, S. D. Complete ^{13}C NMR Chemical Shifts Assignment for Cholesterol Crystals by Combined CP-MAS Spectral Editing and ab Initio GIPAW Calculations with Dispersion Forces. *J. Phys. Chem. A* **2012**, *116*, 3765−3769.
(532) Abraham, A.; Apperley, D. C.; Gelbrich, T.; Harris, R. K.; Griesser, U. J. NMR Crystallography−Three Polymorphs of Phenobarbital. *Can. J. Chem.* **2011**, *89*, 770−778.
(533) Ukmar, T.; Kaucic, V.; Mali, G. Solid-State NMR Spectroscopy and First-Principles Calculations: A Powerful Combination of Tools for the Investigation of Polymorphism of Indomethacin. *Acta. Chim. Slov.* **2011**, *58*, 425−433.
(534) Pindelska, E.; Szeleszczuk, L.; Pisklak, D. M.; Mazurek, A.; Kolodziejski, W. Solid-State NMR as an Effective Method of Polymorphic Analysis: Solid Dosage Forms of Clopidogrel Hydrogensulfate. *J. Pharm. Sci.* **2015**, *104*, 106−113.
(535) Dracinsky, M.; Budesinsky, M.; Warzajtis, B.; Rychlewska, U. Solution and Solid-State Effects on NMR Chemical Shifts in Sesquiterpene Lactones: NMR, X-ray, and Theoretical Methods. *J. Phys. Chem. A* **2012**, *116*, 680−688.
(536) Smith, J. R.; Xu, W.; Raftery, D. Analysis of Conformational Polymorphism in Pharmaceutical Solids using Solid-State NMR and Electronic Structure Calculations. *J. Phys. Chem. B* **2006**, *110*, 7766−76.
(537) Pindelska, E.; Szeleszczuk, L.; Pisklak, D. M.; Majka, Z.; Kolodziejski, W. Crystal Structures of Tiotropium Bromide and Its Monohydrate in View of Combined Solid-state Nuclear Magnetic Resonance and Gauge-Including Projector-Augmented Wave Studies. *J. Pharm. Sci.* **2015**, *104*, 2285−2292.

DOI: 10.1021/acs.chemrev.5b00648
Chem. Rev. 2016, 116, 5567−5613

(538) Tatton, A. S.; Pham, T. N.; Vogt, F. G.; Iuga, D.; Edwards, A. J.; Brown, S. P. Probing Intermolecular Interactions and Nitrogen Protonation in Pharmaceuticals by Novel ^{15}N-Edited and 2D ^{14}N-^{1}H Solid-State NMR. *CrystEngComm* **2012**, *14*, 2654.
(539) Harris, R. K.; Hodgkinson, P.; Zorin, V.; Dumez, J.-N.; Elena-Herrmann, B.; Emsley, L.; Salager, E.; Stein, R. S. Computation and NMR Crystallography of Terbutaline Sulfate. *Magn. Reson. Chem.* **2010**, *48* (Suppl 1), S103−12.
(540) Apperley, D. C.; Batsanov, A. S.; Clark, S. J.; Harris, R. K.; Hodgkinson, P.; Jochym, D. B. Computation of Magnetic Shielding to Simultaneously Validate a Crystal Structure and Assign a Solid-State NMR Spectrum. *J. Mol. Struct.* **2012**, *1015*, 192−201.
(541) Paluch, P.; Pawlak, T.; Oszajca, M.; Lasocha, W.; Potrzebowski, M. J. Fine Refinement of Solid State Structure of Racemic Form of Phospho-Tyrosine Employing NMR Crystallography Approach. *Solid State Nucl. Magn. Reson.* **2015**, *65*, 2−11.
(542) Carignani, E.; Borsacchi, S.; Bradley, J. P.; Brown, S. P.; Geppi, M. Strong Intermolecular Ring Current Influence on ^{1}H Chemical Shifts in Two Crystalline Forms of Naproxen: A Combined Solid-State NMR and DFT Study. *J. Phys. Chem. C* **2013**, *117*, 17731−17740.
(543) Salager, E.; Stein, R. S.; Pickard, C. J.; Elena, B.; Emsley, L. Powder NMR Crystallography of Thymol. *Phys. Chem. Chem. Phys.* **2009**, *11*, 2610.
(544) Braun, D. E.; Koztecki, L. H.; McMahon, J. a.; Price, S. L.; Reutzel-Edens, S. M. Navigating the Waters of Unconventional Crystalline Hydrates. *Mol. Pharmaceutics* **2015**, *12*, 3069−3088.
(545) Filip, X.; Borodi, G.; Filip, C. Testing the Limits of Sensitivity in a Solid-State Structural Investigation by Combined X-Ray Powder Diffraction, Solid-State NMR, and Molecular Modelling. *Phys. Chem. Chem. Phys.* **2011**, *13*, 17978−17986.
(546) Filip, X.; Grosu, I.-G.; Miclaus, M.; Filip, C. NMR Crystallography Methods to Probe Complex Hydrogen Bonding Networks: Application to Structure Elucidation of Anhydrous Quercetin. *CrystEngComm* **2013**, *15*, 4131.
(547) Dudenko, D. V.; Williams, P. A.; Hughes, C. E.; Antzutkin, O. N.; Velaga, S. P.; Brown, S. P.; Harris, K. D. M. Exploiting the Synergy of Powder Xray Diffraction and Solid-State NMR Spectroscopy in Structure Determination of Organic Molecular Solids. *J. Phys. Chem. C* **2013**, *117*, 12258−12265.
(548) Dudenko, D. V.; Yates, J. R.; Harris, K. D. M.; Brown, S. P. An NMR Crystallography DFT-D Approach to Analyse the Role of Intermolecular Hydrogen Bonding and π-π Interactions in Driving Cocrystallisation of Indomethacin and Nicotinamide. *CrystEngComm* **2013**, *15*, 8797.
(549) Gortari, I. D.; Portella, G.; Salvatella, X.; Bajaj, V. S.; van der Wel, P. C. A.; Yates, J. R.; Segall, M. D.; Pickard, C. J.; Payne, M. C.; Vendruscolo, M.; et al. Time Averaging of NMR Chemical Shifts in the MLF Peptide in the Solid State. *J. Am. Chem. Soc.* **2010**, *132*, 5993−6000.
(550) Dumez, J.-N.; Pickard, C. J. Calculation of NMR Chemical Shifts in Organic Solids: Accounting for Motional Effects. *J. Chem. Phys.* **2009**, *130*, 104701.
(551) Robinson, M.; Haynes, P. D. Dynamical Effects in ab Initio NMR Calculations: Classical Force Fields Fitted to Quantum Forces. *J. Chem. Phys.* **2010**, *133*, 084109.
(552) Harper, J. K.; Tishler, D.; Richardson, D.; Lokvam, J.; Pendrill, R.; Widmalm, G. Solid-State NMR Characterization of the Molecular Conformation in Disordered Methyl α-L-Rhamnofuranoside. *J. Phys. Chem. A* **2013**, *117*, 5534.
(553) Dračínský, M.; Hodgkinson, P. A Molecular Dynamics Study of the Effects of Fast Molecular Motions on Solid-State NMR Parameters. *CrystEngComm* **2013**, *15*, 8705.
(554) Exner, T. E.; Frank, A.; Onila, I.; Möller, H. M. Toward the Quantum Chemical Calculation of NMR Chemical Shifts of Proteins. 3. Conformational Sampling and Explicit Solvents Model. *J. Chem. Theory Comput.* **2012**, *8*, 4818−4827.
(555) Exner, T. E. Conformational Sampling by Ab Initio Molecular Dynamics Simulations Improves NMR Chemical Shift Predictions. *J. Chem. Theory Comput.* **2013**, *9*, 3293.
(556) Kong, X.; Shan, M.; Terskikh, V.; Hung, I.; Gan, Z.; Wu, G. Solid-State ^{17}O NMR of Pharmaceutical Compounds: Salicylic Acid and Aspirin. *J. Phys. Chem. B* **2013**, *117*, 9643−9654.
(557) Zheng, A.; Yang, M.; Yue, Y.; Ye, C.; Deng, F. ^{13}C NMR Shielding Tensors of Carboxyl Carbon in Amino Acids Calculated by ONIOM Method. *Chem. Phys. Lett.* **2004**, *399*, 172−176.
(558) Chen, X.; Zhan, C.-G. First-Principles Studies of C-13 NMR Chemical Shift Tensors of Amino Acids in Crystal State. *J. Mol. Struct.: THEOCHEM* **2004**, *682*, 73−82.
(559) Zheng, A.; Chen, L.; Yang, J.; Yue, Y.; Ye, C.; Lu, X.; Deng, F. Prediction of the ^{13}C NMR Chemical Shifts of Organic Species Adsorbed on H-ZSM-5 Zeolite by the ONIOM-GIAO Method. *Chem. Commun.* **2005**, 2474.
(560) Vila, J. A.; Scheraga, H. A. Assessing the Accuracy of Protein Structures by Quantum Mechanical Computations of $^{13}C^{\alpha}$ Chemical Shifts. *Acc. Chem. Res.* **2009**, *42*, 1545−53.
(561) Gao, Q.; Yokojima, S.; Kohno, T.; Ishida, T.; Fedorov, D. G.; Kitaura, K.; Fujihira, M.; Nakamura, S. Ab Initio NMR Chemical Shift Calculations on Proteins using Fragment Molecular Orbitals with Electrostatic Environment. *Chem. Phys. Lett.* **2007**, *445*, 331−339.
(562) Gao, Q.; Yokojima, S.; Fedorov, D. G.; Kitaura, K.; M, S.; S, N. Fragment-Molecular-Orbital-Method-Based ab Initio NMR Chemical-Shift Calculations for Large Molecular Systems. *J. Chem. Theory Comput.* **2010**, *6*, 1428−1444.
(563) Frank, A.; Onila, I.; Möller, H. M.; Exner, T. E. Toward the Quantum Chemical Calculation of Nuclear Magnetic Resonance Chemical Shifts of Proteins. *Proteins: Struct., Funct., Genet.* **2011**, *79*, 2189−202.
(564) Tang, S.; Case, D. A. Calculation of Chemical Shift Anisotropy in Proteins. *J. Biomol. NMR* **2011**, *51*, 303−12.
(565) Frank, A.; Moller, H. M.; Exner, T. E. Toward the Quantum Chemical Calculation of NMR Chemical Shifts of Proteins. 2. Level of Theory, Basis Set, and Solvents Model Dependence. *J. Chem. Theory Comput.* **2012**, *8*, 1480−1492.
(566) He, X.; Wang, B.; Merz, K. M. Protein NMR Chemical Shift Calculations Based on the Automated Fragmentation QM/MM Approach. *J. Phys. Chem. B* **2009**, *113*, 10380−8.
(567) Zhu, T.; He, X.; Zhang, J. Z. H. Fragment Density Functional Theory Calculation of NMR Chemical Shifts for Proteins with Implicit Solvation. *Phys. Chem. Chem. Phys.* **2012**, *14*, 7837−45.
(568) He, X.; Zhu, T.; Wang, X.; Liu, J.; Zhang, J. Z. H. Fragment Quantum Mechanical Calculation of Proteins and Its Applications. *Acc. Chem. Res.* **2014**, *47*, 2748−57.
(569) Flaig, D.; Beer, M.; Ochsenfeld, C. Convergence of Electronic Structure with the Size of the QM Region: Example of QM/MM NMR Shieldings. *J. Chem. Theory Comput.* **2012**, *8*, 2260−2271.
(570) Reid, D. M.; Collins, M. A. Calculating Nuclear Magnetic Resonance Shieldings using Systematic Molecular Fragmentation by Annihilation. *Phys. Chem. Chem. Phys.* **2015**, *17*, 5314−5320.
(571) Aliev, A. E.; Mann, S. E.; Rahman, A. S.; McMillan, P. F.; Corà, F.; Iuga, D.; Hughes, C. E.; Harris, K. D. M. High-Resolution Solid-State ^{2}H NMR Spectroscopy of Polymorphs of Glycine. *J. Phys. Chem. A* **2011**, *115*, 12201−11.
(572) Toan, T.; DeLuca, H. F.; Dahl, L. F. Solid-state Conformations of Vitamin D_3. *J. Org. Chem.* **1976**, *41*, 3476−3478.
(573) Spackman, M. A.; Jayatilaka, D. Hirshfeld Surface Analysis. *CrystEngComm* **2009**, *11*, 19.
(574) McKinnon, J. J.; Spackman, M. A.; Mitchell, A. S. *Acta Cryst. B* **2004**, *60*, 627−668.
(575) Spackman, M. A.; McKinnon, J. J. Fingerprinting Intermolecular Interactions in Molecular Crystals. *CrystEngComm* **2002**, *4*, 378−392.
(576) Hirshfeld, F. L. Bonded-Atom fragments for Describing Molecular Charge Densities. *Theor. Chim. Acta* **1977**, *44*, 129−138.
(577) Johnson, E. R.; Keinan, S.; Mori-Sánchez, P.; Contreras-García, J.; Cohen, A. J.; Yang, W. Revealing Noncovalent Interactions. *J. Am. Chem. Soc.* **2010**, *132*, 6498−506.
(578) Contreras-García, J.; Johnson, E. R.; Keinan, S.; Chaudret, R.; Piquemal, J.-p.; Beratan, D. N.; Yang, W. NCIPLOT: A Program for

DOI: 10.1021/acs.chemrev.5b00648
Chem. Rev. 2016, 116, 5567−5613

Plotting Noncovalent Interaction Regions. *J. Chem. Theory Comput.* **2011**, *7*, 625−632.
(579) Otero-de-la Roza, A.; Johnson, E. R.; Luaña, V. Critic2: A Program for Real-Space Analysis of Quantum Chemical Interactions in Solids. *Comput. Phys. Commun.* **2014**, *185*, 1007−1018.
(580) Otero-de-la Roza, A.; Luaña, V.; Tiekink, E. R. T.; Zukerman-Schpector, J. Unraveling Interactions in Molecular Crystals Using Dispersion Corrected Density Functional Theory: The Case of the Epoxydihydroarsanthrene Molecules. *J. Chem. Theory Comput.* **2014**, *10*, 5010−5019.
(581) Valle, M.; Oganov, A. R. Crystal Fingerprint Space−A Novel Paradigm for Studying Crystal-Structure Sets. *Acta Crystallogr., Sect. A: Found. Crystallogr.* **2010**, *66*, 507−517.
(582) Macrae, C. F.; Bruno, I. J.; Chisholm, J. A.; Edgington, P. R.; McCabe, P.; Pidcock, E.; Rodriguez-Monge, L.; Taylor, R.; Van De Streek, J.; Wood, P. A. Mercury CSD 2.0 - New Features for the Visualization and Investigation of Crystal Structures. *J. Appl. Crystallogr.* **2008**, *41*, 466−470.
(583) Gelbrich, T.; Hursthouse, M. B. A Versatile Procedure for the Identification, Description and Quantification of Structural Similarity in Molecular Crystals. *CrystEngComm* **2005**, *7*, 324−336.

DOI: 10.1021/acs.chemrev.5b00648
Chem. Rev. 2016, 116, 5567−5613